MINISTRY OF SCIENCE AND HIGHER EDUCATION OF THE REPUBLIC OF KAZAKHSTAN

Institute of Information and Computational Technologies

Mamyrbayev Orken,
Pavlov Sergii,
Momynzhanova Kymbat,
Zhanegizov Ardan

METHODS AND SYSTEMS FOR DIAGNOSING DIABETIC RETINOPATHY AND GLAUCOMA

Monography

Approved by the Academic Council of the Institute of Information and Computational Technologies of the Science Committee of the Ministry of Science and Higher Education of the Republic of Kazakhstan

Publishing house «Alash Book»
Almaty
2025

UDC 616
LBC 56.7
M22

Considered and approved by the Academic Council of the Institute of Information and Computational Technologies of the Ministry of Education and Science of the Republic of Kazakhstan (Protocol №6, 28.04.2025)

Reviewers:

M.A. Bektemesov – General Director, Academician of NIA RK, professor, doctor of physical and mathematical sciences, Institute of Information and Computational Technologies.

A.U. Kalizhanova – Professor, candidate of physical and mathematical sciences, professor of the Department of IT engineering and artificial intelligence of the Almaty University of energy and Communications named after G. Daukeev

O. Zh. Mamyrbayev, S. V. Pavlov,
K.R. Momynzhanova, **A. S. Zhanegizov**

M22 **Methods and systems for diagnosing diabetic retinopathy and glaucoma:** Monograph. – Almaty, «Alash Book», 2025 -156 p.

ISBN 978-601-311-189-6

This monograph focuses on the development of intelligent systems for the automated diagnosis of diabetic retinopathy and glaucoma using fundus image analysis. It presents advanced methods of image preprocessing, segmentation, and classification based on artificial intelligence. The study emphasizes the application of convolutional neural networks and expert systems in ophthalmic diagnostics. The proposed approaches aim to improve the accuracy and accessibility of early disease detection. The monograph was prepared within the framework of a project funded by the Science Committee of the Ministry of Science and Higher Education of the Republic of Kazakhstan. (AP19675574 Development of an intelligent system for diagnosing structural changes in pathologies based on biomedical image analysis and processing.)

UDC 616
LBC56.7

ISBN 978-601-311-189-6

CONTENTS

List of major symbols and notations

2D – 2-dimensional;
3D – 3-dimensional;
ACC – accuracy;
BT – biological tissue;
CNN – convolutional neural network;
DBMS– database management system;
DNN – deep neural networks;
DR – diabetic retinopathy;
DSS – decision support system;
FAG – fluorescence angiography;
MA – microaneurysm;
MAE – mean absolute error;
MSE – mean squared error;
NN – neyral network;
OCT – optical coherence tomography;
PDR – proliferative diabetic retinopathy;
PRE – precision;
REC – recall;
ReLU – rectified linear unit;
RGB – red, green, blue;
ROC – receiver operating characteristic curve;
SP – specificity.

Introduction

The world is witnessing a growing pandemic of diabetes, which is one of the most common chronic diseases in the world. According to the World Health Organization, at the beginning of 2020, more than 420 million people worldwide suffered from this disease [1]. Diabetes can lead to a range of serious health complications, including vision problems.

In this regard, the development of an information system for the diagnosis of diabetic retinopathy is an important task in the medical field. Such a system can greatly facilitate the diagnostic process and help doctors detect and treat diabetic retinopathy in time [2]. Normal and diabetic retinal images are illustrated in Figure 1.1.

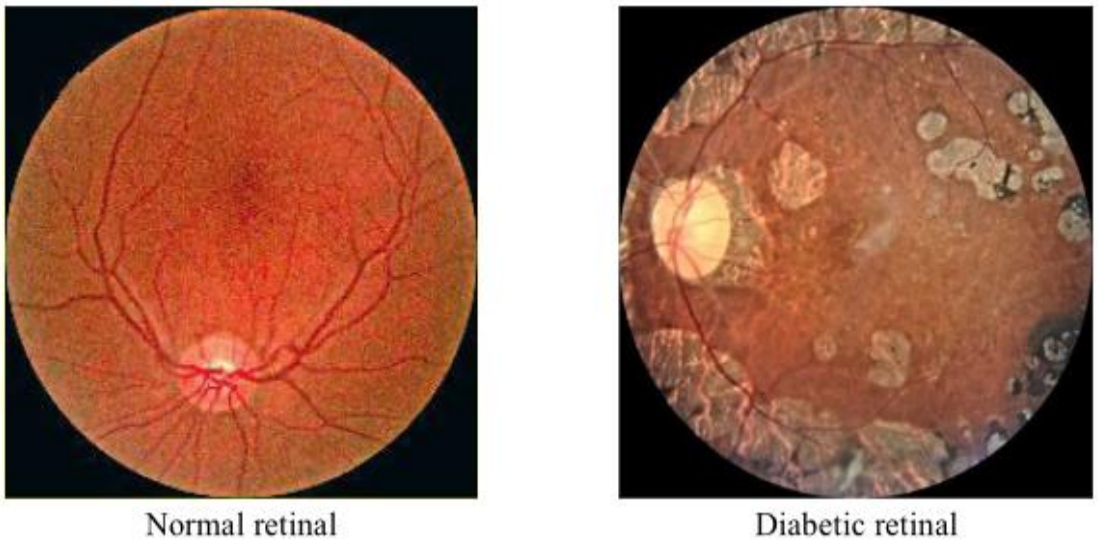

Figure 1.1. Examples of normal retinal and diabetic retinal [3]

Modern technologies make it possible to automate the process of diagnosing diabetic retinopathy [4, 5, 6, 7] and provide quick and accurate analysis. This requires the development of a special information system that would allow diagnostics using retinal images obtained with the help of various medical devices.

The application of machine learning and image processing methods can become a powerful tool in the development of such an information system [8, 9, 10, 11, 12, 13]. Machine learning is a branch of artificial intelligence that deals with the development of algorithms and models that can learn from data and make predictions based on new data. Image processing includes a number of methods that allow

you to process and analyze images for the purpose of detecting diseases and complications.

The development of an information system for the diagnosis of diabetic retinopathy is an urgent task, because such a system can be useful for doctors and patients who are faced with the problem of diabetic retinopathy [14, 15, 16, 17]. The developed system can provide fast and accurate analysis of retinal images, which will allow doctors to detect and treat diabetic retinopathy in time, preventing vision loss and blindness in patients [18, 19, 20, 21].

In addition, the development of an information system for the diagnosis of diabetic retinopathy can become the basis for further research and development in the field of medical informatics [7, 22, 23, 24, 25, 26]. An important component of such research is the search for new methods and algorithms for image processing that can be applied to the diagnosis of other diseases of the visual organs and, in general, to improve the quality of medical diagnostics [27].

In a lot of scientific studies, information systems for the diagnosis of diabetic retinopathy, which are based on methods of machine learning and image processing, have already been developed and tested [13, 28, 29, 30, 31, 32, 33]. However, more research and development is needed to improve the efficiency and accuracy of such systems and make them more accessible and user-friendly for medical personnel [9, 14, 34, 35].

Therefore, the development of an information system for the diagnosis of diabetic retinopathy is a relevant and important research that can have a significant positive impact on the practice of diabetes treatment and reduce the risk of serious complications in patients [36, 37, 38, 39, 40, 41].

Methods of image processing, machine learning and statistical data analysis will be used to implement these tasks. As part of the study, an analysis of the solutions available on the market for the diagnosis of diabetic retinopathy will be carried out, which will allow to identify their advantages and disadvantages, as well as to determine the possibilities of further improvement of the developed information system.

Therefore, the results of the study will allow to develop an effective information system for the diagnosis of diabetic retinopathy, which can become an important tool for practicing doctors and improve the quality of diagnosis and treatment of this disease [39, 42, 43, 44].

Within the framework of this study, the main aspects of the diagnosis of diabetic retinopathy will be considered, in particular, the mechanism of the development of the disease and its clinical signs [22, 45, 46, 47]. For a more detailed understanding of the problem, scientific articles and publications dedicated to the study of this issue will be analyzed [48, 49, 50, 51, 52].

In addition, basic imaging techniques that can be used to analyze retinal images and identify signs of diabetic retinopathy will be reviewed. Different approaches to image processing will be analyzed, in particular, machine learning methods that allow determining signs of retinopathy based on the analysis of a large number of images.

The work will develop software that allows automated analysis of retinal images and determination of signs of diabetic retinopathy. The developed software will be tested on the basis of retinal images obtained as a result of the diagnosis of retinopathy in patients with diabetes.

To evaluate the effectiveness of the developed information system, a comparative analysis of the results of retinopathy diagnosis, obtained using the developed system and traditional diagnostic methods, will be conducted. The results of the analysis will make it possible to draw conclusions about the effectiveness of the developed system and compare it with solutions available on the market for the diagnosis of diabetic retinopathy [53, 54].

This study is of great importance for practical medicine and may contribute to the improvement of the diagnosis of diabetic retinopathy and the development of more effective methods of treatment of this disease. The results of the study may be useful for ophthalmologists who diagnose and treat diabetic retinopathy, as well as for patients with diabetes who are at risk of developing this disease.

For image processing in this study, computer vision algorithms will be used, which allow automatic analysis of images and obtaining information from them [55, 56, 57, 58, 59]. Computer vision is already used in medicine, in particular, to diagnose cancer and other diseases.

This study will use the materials and results of previous studies in the field of diagnosing diabetic retinopathy and the application of machine learning and image processing methods in medicine [60, 61, 62, 63]. In particular, research using deep learning will be used to diagnose diabetic retinopathy based on images of patients' eyes [56, 57, 58, 64, 65]. The results of research on the development of a diabetic

retinopathy diagnostic system based on image processing and machine learning methods will also be used [66, 67, 68, 69, 70].

The dissertation work will be accompanied by relevant materials, including graphic images, tables and analytical notes. In particular, image samples will be created that can be used to diagnose diabetic retinopathy, and the results of testing the developed information system on real retinal images will also be presented.

The main contribution of this study is the development of an information system that can help doctors quickly and effectively diagnose diabetic retinopathy, which will provide more effective treatment and prevention of complications in patients with diabetes.

The dissertation will describe in detail the development of an information system for the diagnosis of diabetic retinopathy, including the analysis of existing diagnostic methods, the selection of image processing approaches and methods, the development of algorithms and software.

Experimental studies will also be conducted, which will allow to evaluate the effectiveness of the developed information system and compare it with existing diagnostic methods. For this purpose, real images of the retina of patients with diabetes will be used.

In addition, the dissertation will consider the use of artificial intelligence in the diagnosis of diabetic retinopathy, as well as possible directions for the further development of the developed information system.

Therefore, this dissertation has a significant practical contribution to the development of medical technology and will help to improve the diagnosis of diabetic retinopathy, which can reduce the number of complications in patients with diabetes and improve their quality of life.

Also, the research will use methods of identifying features that allow describing image properties associated with diabetic retinopathy. These methods include the determination of textural features that can help in recognizing changes in eye tissues, as well as geometric structure features that allow us to describe the shape and location of various structures in the eye.

Open source software and libraries for machine learning and image processing, such as TensorFlow, Keras, OpenCV and others, will be used to develop an information system for the diagnosis of diabetic

retinopathy. This will reduce development costs and allow for a system that is more accessible to doctors and patients.

In addition, the development of an information system for the diagnosis of diabetic retinopathy can have a significant impact on modern medicine. Diabetes is quite common, and diabetic retinopathy can lead to serious complications, including vision loss and permanent eye damage. Development of an effective diagnostic system can help detect this disease in time and prevent its development.

Therefore, this study is an important step in the development of an information system for the diagnosis of diabetic retinopathy using machine learning and image processing methods. The possibility of creating a more effective diagnostic system depends on the results of the study, which can have a significant impact on people's health and reduce the number of cases of vision loss and irreversible eye damage in diabetic patients.

1 Analysis of methods. Advancements in eye diagnosis: The role of AI in medical imaging

1.1 Convolutional Neural Networks

Recent advances in artificial intelligence and machine learning have opened new horizons in automating the analysis of visual data. One of the most significant areas of progress is the application of Convolutional Neural Networks (CNNs), which have proven to be a powerful tool for processing and interpreting images. CNNs have become an integral part of fields such as medical diagnostics, autonomous systems, biometrics, robotics, and intelligent video surveillance.

The popularity of CNNs is largely due to their ability to automatically extract multi-layered features from images, eliminating the need for manual feature engineering. CNN architectures are effectively used to solve tasks such as classification, segmentation, localization, and object detection in various visual environments. Thanks to their adaptability and high accuracy, CNNs have become key components in decision support systems, particularly in medicine, where precision and interpretability are of critical importance.

CNNs are especially widely used in ophthalmology for the diagnosis of diseases such as diabetic retinopathy, glaucoma, cataracts, and other eye conditions. Their implementation enables automated analysis of fundus images, improves diagnostic accuracy, and reduces the burden on healthcare professionals. In parallel, ongoing research explores the integration of CNNs with other architectures such as Vision Transformers (ViT), recurrent networks, and optimization methods, opening new prospects for developing hybrid and more precise models.

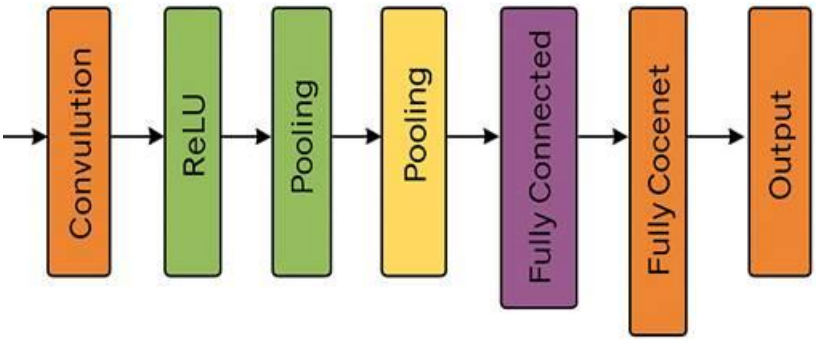

Figure 2.1. The main stages of image processing in a CNN model

In [71], a method for classifying diabetic retinopathy (DR) using a convolutional neural network (CNN) is presented, incorporating the ResNet architecture and YOLO. The model is designed to recognize three stages of DR: normal retina (NR), non-proliferative (NPDR), and proliferative (PDR) retinopathy. Fundus images undergo preprocessing through noise filtering and normalization before being fed into the CNN. The network utilizes convolutional layers, ReLU activation, max pooling, and a dropout layer to enhance generalization. YOLO provides fast and accurate localization of pathological areas. The model was trained on 5500 images and achieved high accuracy, up to 94.5% for NPDR. The method's advantages include high performance, automatic feature extraction, and potential for clinical application. However, the model is limited to three stages of the disease and does not cover, for example, macular edema. Other noted drawbacks include high hardware requirements, long training times, and relatively low specificity. Future improvements may involve optimizing computational efficiency and expanding classification capabilities.

The method presented in [72] proposes the use of pre-trained convolutional neural networks (CNNs) for classifying multiple eye diseases based on fundus images. The approach focuses on four classes: normal condition, cataract, glaucoma, and diabetic retinopathy. Before being fed into the model, images undergo preprocessing, including background removal and resizing to 224×224 pixels, which enhances feature extraction quality. InceptionV3, MobileNetV2, EfficientNetB0, and EfficientNetB1 are used as both feature extractors and classifiers. MobileNetV2 achieved the best results, with an accuracy of 98.53% and high precision and recall values. Using pre-trained models significantly reduced the number of trainable parameters and sped up the training process. The method also offers good scalability and is suitable for multi-class classification. Advantages include high accuracy, versatility, and reduced risk of overfitting. However, some misclassifications occur between visually similar conditions (e.g., glaucoma and cataract), which calls for further refinement. The method could be improved by incorporating additional clinical features, such as patient history and demographic data.

The study presents a comparative analysis of convolutional neural network (CNN) architectures, specifically VGG16, VGG19, ResNet18, and ResNet50, for automated detection of ophthalmic diseases [73]. It targets four common eye conditions: cataract, diabetic retinopathy,

glaucoma, and normal eye. The dataset, sourced from Kaggle, includes 4,217 labeled retinal images. The models were fine-tuned using transfer learning, trained for 25 epochs with hyperparameter optimization and early stopping. VGG architectures outperformed the ResNet models in all metrics, with VGG19 achieving the highest accuracy of 92%, followed by VGG16 at 91%. ResNet18 and ResNet50 achieved 87% and 85% accuracy, respectively. The system also employed Gradio UI to enable real-time diagnosis via a user-friendly web interface. Confusion matrices revealed that all models accurately identified diabetic retinopathy, but struggled to distinguish glaucoma from other conditions. VGG models showed better generalization with minimal overfitting, as evidenced by smooth training and validation curves. However, challenges such as data imbalance and limited interpretability of CNNs remain. The study concludes that VGG19 offers a robust solution for eye disease detection and recommends further enhancements through model refinement and clinical collaboration. The findings contribute to more efficient and accessible diagnostic tools in ophthalmology.

In study [74], a hybrid method for eye disease classification is proposed using Convolutional Neural Networks (CNNs) and Vision Transformers (ViT). To enhance classification performance, the authors extract features from two different pre-trained CNN models (e.g., EfficientNetB0 and VGG16), which are then concatenated and fed into a classifier. Principal Component Analysis (PCA) is applied to reduce the dimensionality of the combined features. The model is trained on a large dataset containing over 9,800 images of various eye diseases, including glaucoma, cataract, diabetic retinopathy, and others. During the classification phase, ViT is used to capture global relationships between image regions. Results show that ViT achieves the highest accuracy of 98.1%, outperforming CNN-based feature fusion models that reached up to 97.32%. Advantages of the method include high accuracy, scalability, and the ability to detect complex visual patterns. A key benefit of ViT lies in its ability to analyze spatial relationships without relying on convolution operations. However, the method demands significant computational resources and longer training time. Challenges also remain in model interpretability and in selecting the optimal architecture for specific diseases.

The [75] presents a deep learning-based framework for automated screening and diagnosis of ophthalmic diseases using convolutional

neural networks (CNNs). It focuses on classifying fundus images into four categories: normal, glaucoma, diabetic retinopathy, and cataract. The dataset used contains over 10,000 labeled retinal images with varied quality and disease severity. The architecture is based on a deep CNN with multiple convolutional and pooling layers followed by fully connected layers. The authors implemented dropout and batch normalization to reduce overfitting and improve model generalization. The model achieved an accuracy of 94.7% and an F1 score of 93.2% on the test set. Performance was evaluated using precision, recall, accuracy, and AUC metrics. Grad-CAM visualization was applied to interpret model decisions by highlighting important regions in the fundus images. The system outperformed several traditional machine learning methods and earlier shallow CNN models. One of the strengths of the method is its ability to learn hierarchical features directly from raw image data. However, the model performance declined when tested on images from different devices or datasets. The authors suggest future improvements via transfer learning, data augmentation, and domain adaptation techniques.

System [76] presents a computer-aided diagnosis approach for eye diseases based on Convolutional Neural Networks (CNN), capable of classifying images into six categories: normal, glaucoma, strabismus, eye protrusion, uveitis, and cataract. The dataset used consisted of 2,893 images collected from the Kaggle platform, which were quality-validated and divided into training and testing sets. Prior to training, the images were normalized, augmented, and resized to a uniform size of 150×150 pixels. To optimize the training process, two algorithms were compared: Adam and Stochastic Gradient Descent (SGD). The CNN model using the Adam optimizer achieved an accuracy of 94%, significantly outperforming the model with SGD, which achieved only 48%. Adam provided more stable convergence and superior precision, recall, and F1-score across all classes. Results also showed that SGD was less robust to data variability and more prone to overfitting. The CNN architecture included three convolutional layers, three pooling layers, and two fully connected layers, using ReLU and SoftMax activation functions. The authors highlighted that the choice of optimizer plays a crucial role in improving classification accuracy. Among the strengths of the method are high accuracy and diagnostic automation, making it a useful support tool in clinical practice.

Limitations include high computational requirements and the need for further clinical validation.

Method [77] proposes an approach for early detection of Autism Spectrum Disorder (ASD) using Artificial Neural Networks (ANN) and Convolutional Neural Networks (CNN). The diagnosis is based on gaze path images obtained via eye-tracking technology, which is non-invasive and child-friendly. The study uses a dataset that includes eye movement images of children with and without ASD, expanded through data augmentation to a total of 2,555 images. During preprocessing, the images were converted to grayscale and resized to 100×100 pixels. The ANN model was trained on vectorized images transformed using Principal Component Analysis (PCA), achieving an accuracy of 74.57%. In contrast, the CNN model based on a modified AlexNet architecture achieved a higher accuracy of 85.28%. CNN's main advantages include capturing spatial and temporal dependencies, reducing the number of parameters, and weight sharing. Both models employed Early Stopping, Checkpoint, and learning rate reduction techniques. Gaze trajectory visualization, including fixations and saccades, enabled interpretation of subject behavior. The results confirm the potential of deep neural networks for early ASD diagnosis. The method is particularly useful in clinical practice to accelerate diagnosis and provide timely support to children.

A method for early detection and classification of ophthalmic diseases using enhanced Convolutional Neural Networks (CNN) is presented in [78]. For the diagnosis of five classes (strabismus, cataract, chalazion, keratitis, and healthy eye), both a custom CNN model and pre-trained architectures — SqueezeNet, VGG16, and ResNet50 combined with LSTM — were used. The dataset consisted of 2,402 images gathered from open sources and was expanded through augmentation techniques such as rotation, scaling, and flipping. All images were resized to 64×64 pixels, normalized, and encoded. Training was conducted using the Adam optimizer, cross-entropy loss function, and overfitting prevention techniques such as Dropout and Early Stopping. SqueezeNet achieved the highest test accuracy of 98.16%, outperforming VGG16, the custom CNN, and ResNet50-LSTM. Evaluation based on precision, recall, and F1-score further confirmed SqueezeNet's superiority. The model showed particularly strong performance in identifying keratitis and cataract. Advantages of the method include high accuracy, stability, and classification

efficiency. However, the authors note the need to increase the number of disease classes and optimize image preprocessing. The approach is promising for clinical use, especially in resource-limited settings.

Convolutional Neural Networks (CNNs) have proven to be one of the most powerful and effective tools for image processing. Due to their ability to automatically extract and analyze multi-layered features, CNNs have found wide application across various fields, particularly in medical diagnostics and ophthalmology. CNN architectures demonstrate high accuracy, adaptability, and robustness to noise, making them indispensable for tasks such as image classification, detection, and segmentation. Although they require significant computational resources and large datasets for training, the development of optimized and hybrid models continues to expand the capabilities of CNNs in intelligent visual information analysis systems.

1.2 U-Net method

The advancement of deep learning in recent years has led to significant progress in image segmentation, particularly in biomedical applications. One of the most effective and widely used architectures for semantic segmentation tasks is U-Net - a convolutional neural network first introduced in 2015 for the segmentation of microscopic images. Due to its versatility, high accuracy, and ability to perform well with limited annotated data, U-Net quickly became a standard in medical imaging.

A distinctive feature of the U-Net architecture is its symmetric encoder–decoder structure with skip connections linking corresponding convolutional and upsampling layers. These connections enable effective restoration of spatial resolution, improving localization and segmentation accuracy. Over the years, many modifications of U-Net have been proposed, including Residual U-Net, Attention U-Net, Transformer U-Net, and others—each adapted to specific tasks and image types.

- Net has proven effective in tasks such as:
- segmentation of the pupil and iris in videonystagmography for diagnosing vestibular disorders;
- detection of pathological regions in diabetic retinopathy;

- automatic segmentation of blood vessels, optic disc, and optic cup for glaucoma diagnosis;
- identification of congenital anomalies such as eye coloboma based on OCT and fundus images.

The relevance of U-Net is also due to its robustness to noise, adaptability to various color spaces (e.g., CMYK instead of RGB), and its compatibility with transformers, autoencoders, and attention-enhancing algorithms. These features make U-Net one of the most promising approaches for developing intelligent systems for automated diagnosis in ophthalmology.

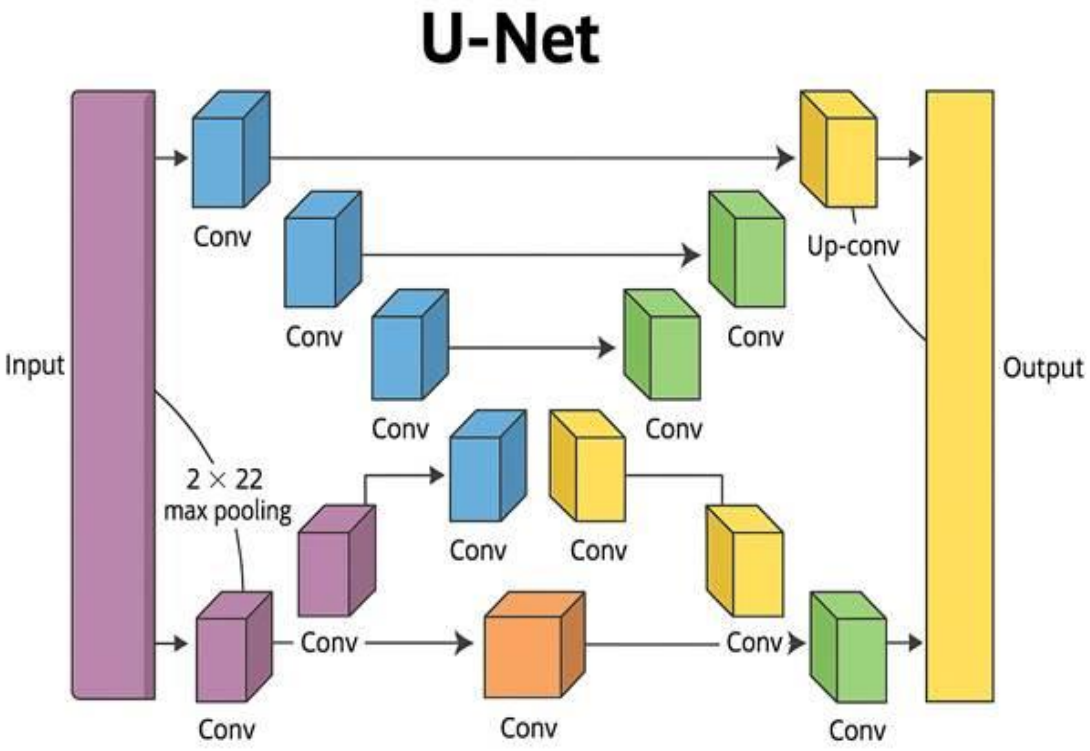

Figure 2.2. U-Net architecture for semantic image segmentation

The proposed method is aimed at pupil segmentation in videonystagmography (VNG) to improve the accuracy of diagnosing benign paroxysmal positional vertigo (BPPV) [79]. The core of the approach is a combination of the convolutional neural network U-Net and the RANSAC algorithm, which is robust to noise and outliers. The CASIA-Iris-Degradation dataset is used as the input, containing various types of noise such as eyelid and eyelash movements, glare, and camera shifts.

The image preprocessing stage includes resizing and correction of annotation coordinates. RANSAC is applied for elliptical approximation of the pupil shape, providing noise resilience, while U-Net is responsible for precise segmentation. The effectiveness of the method was evaluated using the mean squared error (MSE) metric. Experiments demonstrated that the combined approach (RANSAC + U-Net) achieves the best results on noise-free images and delivers reliable performance under different noise conditions.

The research work [80] focuses on the automatic segmentation of retinal lesions in diabetic retinopathy (DR) using an enhanced U-Net architecture. The analysis was conducted using the publicly available IDRiD dataset, which includes pixel-wise annotated images with DR features such as hard and soft exudates, microaneurysms, and hemorrhages.

A key feature of the method is the use of CMYK channels instead of RGB, as different lesions are more distinguishable in specific color components. Additionally, a residual learning unit was integrated into the U-Net structure, allowing for a deeper model and improved resistance to vanishing gradients. Further preprocessing steps included contrast adjustment, color normalization, and noise reduction, which enhance detection accuracy.

The results showed that the Enhanced U-Net outperforms the classical U-Net in metrics such as sensitivity, specificity, Dice, and Jaccard indices. For instance, sensitivity in detecting hemorrhages reached 99.22%, and the Dice coefficient was 0.97. Thus, the proposed method provides more accurate and reliable lesion segmentation, contributing to early diagnosis of DR and serving as a valuable tool in ophthalmic practice.

The method presented in study [81] is aimed at accurate segmentation of eye coloboma—a congenital ocular malformation that can lead to blindness. To address this task, an improved version of U-Net is proposed, enhanced with a Global Attention mechanism that allows the model to consider image context and better detect small yet critical features.

The GA-UNet model integrates transformer-based attention blocks to focus on affected regions while suppressing background noise. A pretrained EfficientNet is used as the encoder, which speeds up training and enhances the model’s generalization ability. The processing pipeline starts with normalization, data augmentation, and coloboma

mask generation. The model is then trained using a loss function combining Dice coefficient and binary cross-entropy.

The model was evaluated on a dataset of 500 images and achieved an accuracy of 94.3%, sensitivity of 91.5%, specificity of 96.2%, and an F1 score of 0.92. Compared to classical U-Net and other CNN-based approaches, GA-UNet showed an accuracy improvement of 5–10%. Therefore, GA-UNet demonstrates high effectiveness for automated coloboma diagnosis and can serve as a valuable tool in clinical practice.

The study by the authors [82] focuses on automatic segmentation of the retinal fundus for glaucoma diagnosis using the U-Net architecture. The primary goal is to segment the optic disc and cup regions, which enables calculation of the Cup-to-Disc Ratio (CDR), a critical indicator for assessing glaucoma progression.

The study used a dataset of over 650 color fundus images. Several preprocessing techniques were applied, including green channel extraction, histogram normalization, Gaussian filtering, and directional filtering. The U-Net architecture was implemented with parameters such as input size of 128×128, batch size of 32, filters ranging from 64 to 1024, ReLU activation function, and Adam optimizer.

Following segmentation of the optic disc and cup, the CDR was calculated: values above 0.56 indicated a suspicion of glaucoma. Additionally, a risk-level classification system was implemented using the K-Nearest Neighbors (KNN) algorithm: low (CDR < 0.3), moderate (0.3–0.6), and high (CDR > 0.6).

The method achieved high segmentation accuracy—up to 98.42%—with a loss of 0.15 after 160 training epochs. Thus, the proposed system demonstrates strong potential for clinical use in early and accurate glaucoma diagnosis.

In this study [83], an improved eye pupil detection system is presented, based on the integration of Variational Autoencoders (VAE) with the U-Net architecture. The main goal is to enhance the accuracy and robustness of pupil segmentation under challenging conditions such as glare, occlusions (eyelashes, eyelids), and anatomical variations. VAE is used to extract latent features and suppress noise, while U-Net provides high-precision pixel-level segmentation.

During preprocessing, images are normalized and enhanced using CLAHE and Gaussian filtering. Annotated datasets with diverse lighting conditions and viewing angles were used for training. Pupil

segmentation is performed by fusing VAE-derived features with the decoder part of U-Net via skip connections.

The model was trained using Binary Cross Entropy and Dice loss functions, and evaluated using metrics such as accuracy, recall, F1-score, and IoU. The proposed method achieved 97.83% accuracy and outperformed existing approaches such as elliptical fitting and CNN-based methods. The method shows strong potential for applications in ophthalmology, biometrics, and human-computer interaction, especially in real-time scenarios.

The study proposes an advanced method for retinal vessel segmentation using the Residual U-Net architecture [84]. The goal is to accurately extract the vascular structure from fundus images to aid in the diagnosis of ophthalmic and cardiovascular diseases, including glaucoma, diabetic retinopathy, and hypertension. The original dataset consisted of 100 images, which was expanded to 6,000 through augmentation techniques such as rotation, flipping, and scaling.

The model incorporates residual blocks to avoid the vanishing gradient problem and improve deep network training. Additionally, a Channel and Spatial Squeeze and Excitation (CSSE) attention mechanism is applied to focus on the most relevant features. The architecture comprises five encoder levels and four decoder levels with skip connections that preserve spatial information.

Images are normalized and converted to grayscale before being fed into the model. Evaluation metrics include accuracy (97.7%), recall, precision, and Dice coefficient (79.96%). The results demonstrate improved performance compared to previous methods. The proposed approach can be effectively used in systems for automated diagnosis and vision health monitoring.

This study presents a novel approach for the automatic detection of eye coloboma using the Transformer-Enhanced U-Net architecture combined with transfer learning [85]. The main objective is to improve the accuracy and robustness of ocular anomaly segmentation through the use of self-attention mechanisms and knowledge transfer from pretrained models (e.g., EfficientNet). The proposed model combines the strengths of U-Net and transformers, enabling effective extraction of both local and global features.

The training data included fundus and optical coherence tomography (OCT) images, which underwent normalization and augmentation. The model architecture incorporates encoders with

pretrained weights and transformer modules capable of capturing long-range dependencies and contextual relationships. Segmentation is performed using a decoder with skip connections, ensuring high-resolution output.

Model performance evaluation yielded strong results: Dice coefficient — 0.87, IoU — 0.76, sensitivity — 90%, specificity — 92%. The model effectively detects blurry or faint signs of coloboma. Clinicians confirmed its applicability in real-world settings, especially where annotated data is limited. Thus, the proposed solution demonstrates significant potential for improving early diagnosis and automating ophthalmic assessments.

The U-Net architecture has proven to be an effective and versatile tool for semantic segmentation tasks, particularly in the field of medical imaging. Thanks to its symmetric structure, skip connections, and ability to accurately restore spatial details, U-Net delivers high precision even with a limited amount of training data. Numerous modifications—such as Residual U-Net, Attention U-Net, and Transformer U-Net—further demonstrate its flexibility and relevance. This makes U-Net one of the key technologies in the development of intelligent systems for automated diagnosis.

1.3 ResNet method

In recent years, deep convolutional neural networks (CNNs) have become the primary tool for image processing tasks, including medical diagnostics. However, as network depth increases, challenges such as vanishing gradients and performance degradation arise, limiting the effectiveness of traditional architectures. To overcome these issues, the Residual Network (ResNet) architecture was introduced in 2015, bringing a revolutionary change to the design of deep models. The key feature of ResNet is the use of skip connections, which allow information to bypass certain layers and flow directly through the network, thereby facilitating the training of very deep architectures.

This innovation enables the effective extraction and preservation of complex image features, making ResNet one of the most widely used models for tasks such as classification, segmentation, and disease diagnosis in medical imaging. Among its variants, ResNet-18 is particularly popular due to its simplified structure, offering a favorable

balance between accuracy and computational efficiency. This makes it especially suitable for deployment in clinical and mobile systems for automated image analysis.

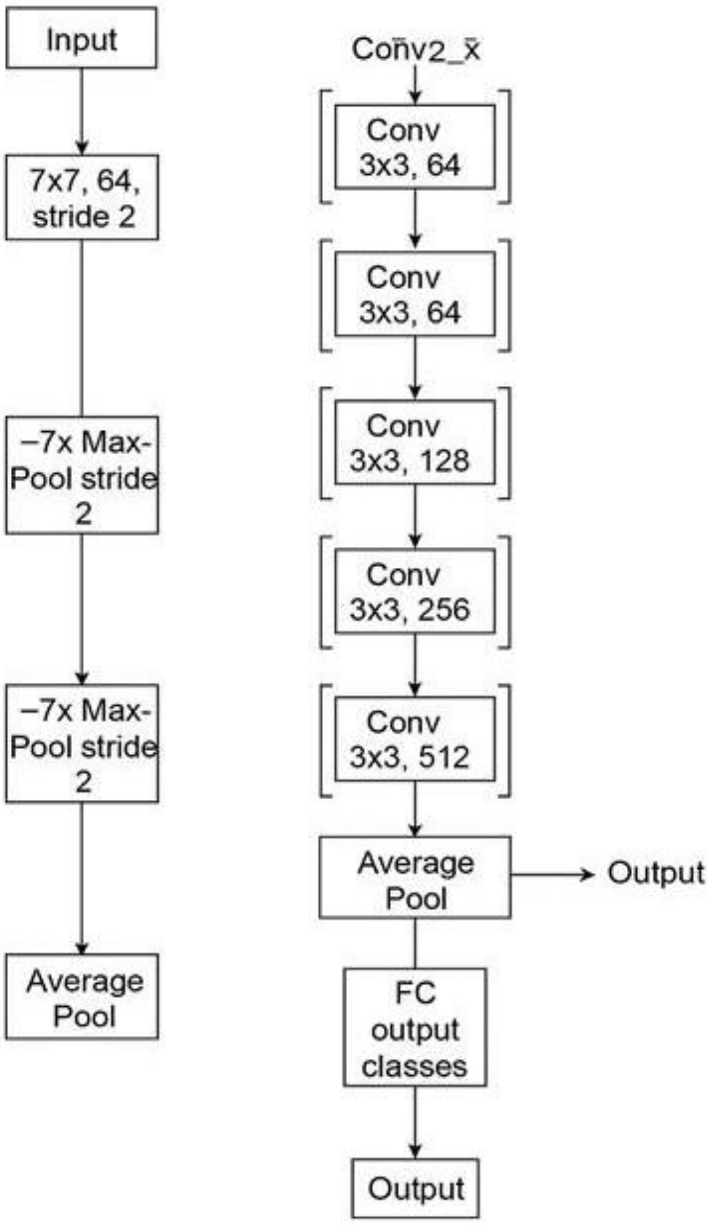

Figure 2.3. ResNet-18 architecture

The model presented in [86] is based on the use of the deep convolutional neural network ResNet-18 for the automatic detection of diabetic retinopathy. Fundus images from an open-access Kaggle dataset were used as input data. A total of 2,838 images were collected, evenly distributed between the "with retinopathy" and "without retinopathy" classes.

During the preprocessing stage, the images were resized to 224×224 pixels, in accordance with the input requirements of the ResNet-18 architecture. The dataset was split into training (80%) and testing (20%) subsets. The training process employed the Adam optimizer with a learning rate of 0.0001, over 15 epochs, and a batch size of 16.

The results demonstrated high efficiency: the model achieved an accuracy of 99.91% on the training set and 96.65% on the test set. It also achieved high values for precision (94.33%), sensitivity (98.88%), and F1-score (0.966). These performance metrics surpass those of previous studies utilizing architectures such as VGG-16, Inception-V3, and Xception.

The model was implemented and trained on the Google Colab platform, and the final version was deployed in cloud storage for future use. Thus, the proposed system can effectively complement clinical diagnosis by enabling early disease detection and reducing the risk of vision loss.

In this study [87], an automated approach for diagnosing retinal diseases based on optical coherence tomography (OCT) images is proposed. The primary architecture used was a pre-trained ResNet-18 model, further refined through transfer learning. The original dataset comprised 84,484 images classified into four categories: normal, diabetic macular edema (DME), choroidal neovascularization (CNV), and drusen. The data were split into training and validation sets in a 70:30 ratio.

Various data augmentation techniques were applied, including random rotations, flips, and adjustments in brightness and contrast. All images were resized to 224×224 pixels and normalized using ImageNet statistics. The training process was conducted in two stages: initial training and fine-tuning with unfrozen layers at a reduced learning rate.

After fine-tuning, the model achieved an accuracy of 96.61%. The confusion matrix revealed high precision and recall values across all four classes. Particularly high classification accuracy was observed for the CNV and DME classes. The use of ResNet-18 allowed for a balanced performance between architectural simplicity and classification accuracy. The developed model can serve as a valuable tool for ophthalmologists, enabling early diagnosis and reducing the burden on healthcare systems.

In study [88], a method for classifying eye diseases using transfer learning based on the ResNet50 architecture is proposed. The research focuses on four classes: normal, glaucoma, diabetic retinopathy, and cataract. The original dataset was obtained from the Kaggle platform and contains approximately 1,000 images for each class. The images were preprocessed to remove white borders and augmented using techniques such as random rotations, flips, and color adjustments.

The model architecture is based on a pre-trained ResNet50, with the original classification layers removed and replaced by two fully connected layers designed to handle four-class classification. During training, the categorical cross-entropy loss function and the Adam optimizer were employed. To prevent overfitting, an early stopping mechanism was used.

The model achieved an accuracy of 92.91% on the test set, outperforming other architectures such as VGG19, EfficientNetB0, and DenseNet121. The highest F1-score was achieved for diabetic retinopathy classification — 0.995. The confusion matrix confirmed the model's high sensitivity in detecting various fundus pathologies. This approach demonstrates the strong potential of deep learning for ophthalmic diagnostics and can serve as a supportive tool for clinical decision-making.

This study [89] presents a solution for the automatic diagnosis of eye diseases using the ResNet-18 convolutional neural network. The aim of the study is to classify fundus images into four categories: cataract, glaucoma, normal condition, and diabetic retinopathy. The model was trained using a dataset from Kaggle, comprising a total of 4,096 images. All images were preprocessed by resizing them to 224×224 pixels.

The ResNet-18 architecture was modified by removing the original final layer and replacing it with a new layer consisting of four outputs and a softmax activation function. The training process utilized the Adam optimizer and categorical cross-entropy loss function. Data augmentation techniques—such as image rotation, flipping, and brightness adjustment—were applied to improve the model's generalization capabilities. Eighty percent of the data were used for training, while the remaining 20% served as the validation set.

The final classification accuracy on the test set reached 94.3%, and the F1-score was 0.943, indicating high model performance. Compared to other methods, ResNet-18 demonstrated a superior balance between

accuracy and computational efficiency. The developed system has the potential to serve as a decision support tool in ophthalmology, facilitating early disease diagnosis.

This study [90] presents an approach to early diagnosis of eye diseases using the ResNet-18 architecture. The objective of the research is to classify images into four categories: normal, cataract, glaucoma, and diabetic retinopathy. A combined dataset was used, consisting of images from IDRiD, HRF, and other sources, with approximately 1,000 images per class.

To enhance model performance, 70% of the ResNet-18 layers were frozen, and the final layers were replaced with two newly added fully connected layers. Training was performed with differential learning rates: 5×10^{-5} for the base network and 8×10^{-4} for the newly added layers. Data augmentation techniques such as image rotation and flipping were also applied.

The final model achieved an accuracy of 86% and an F1-score of 0.86, indicating balanced performance. The best results were observed in the classification of cataract and diabetic retinopathy, with F1-scores exceeding 0.91. For glaucoma, the model achieved an accuracy of 81% and a recall of 78%, suggesting the need for further optimization.

Loss and accuracy analysis showed stable model convergence with no signs of overfitting. The confusion matrix confirmed high precision in three classes, but revealed some misclassification between glaucoma and normal cases. Overall, the study demonstrates the potential of ResNet-18 as a clinical decision support tool for automated ophthalmic diagnosis.

This study [91] presents an automatic eye disease classification system based on the ResNet-18 architecture. The research focuses on recognizing four categories: glaucoma, cataract, diabetic retinopathy, and normal condition. The experiment utilized a Kaggle dataset containing approximately 1,600 images for each class. All images were resized to 224×224 pixels and normalized.

The model was implemented using the TensorFlow framework and trained with the following parameters: 15 epochs, batch size of 32, and a learning rate of 0.0001. The Adam optimizer and cross-entropy loss function were used. Transfer learning was applied by fine-tuning a pre-trained ResNet-18 model on medical image data, replacing its final layers with new ones tailored for the classification task.

To enhance generalization and mitigate overfitting, data augmentation techniques were employed. The model achieved a test accuracy of 95.8%, confirming the high effectiveness of the proposed approach. Particularly strong performance was observed in the classification of cataract and diabetic retinopathy. The confusion matrix showed minimal misclassifications across classes.

Overall, the model demonstrated great potential as a clinical decision support tool for ophthalmologists, especially in large-scale screening and early diagnosis.

Thus, the ResNet architecture represents one of the most significant advancements in the field of deep learning, enabling the effective training of very deep neural networks. Through the use of residual connections, ResNet substantially mitigates the vanishing gradient problem and enhances the generalization capability of models. The ResNet-18 variant is particularly popular, as it combines high accuracy with low computational complexity, making it an optimal choice for medical diagnostic tasks, including automated classification of eye diseases. The reliability, flexibility, and scalability of the architecture make it a universal tool for implementation in practical intelligent image analysis systems.

1.4 VGG method

Convolutional Neural Networks (CNNs) have proven to be among the most effective methods for image processing and interpretation, particularly in the field of medical diagnostics. Among them, the VGG (Visual Geometry Group) architecture, developed by researchers at the University of Oxford, has gained significant attention. Variants such as VGG16 and VGG19 are widely used due to their structural simplicity and strong capability to extract deep and informative features from images. A distinctive feature of VGG is the use of multiple consecutive convolutional layers with small kernels (3×3), followed by pooling layers, which enables high accuracy while maintaining reasonable computational efficiency. With the ability to load pretrained weights (e.g., from ImageNet), VGG models are commonly applied in transfer learning tasks, including ophthalmology, for the automated diagnosis of eye diseases.

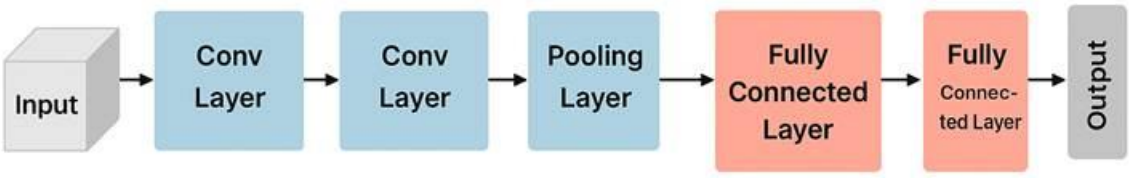

Figure 2.4 Architecture of the VGG method

In this study, a method for automatic cataract detection in fundus images is proposed using a convolutional neural network based on the VGG19 architecture and transfer learning techniques [92]. The input dataset used was ODIR5K, consisting of 1088 images (588 with cataract and 500 normal). The preprocessing steps included resizing images to 224×224 pixels, normalizing pixel values, and applying augmentation techniques such as rotation, flipping, and scaling.

A pre-trained VGG19 model was used, where convolutional layers were frozen and a new classification head was added for binary classification. The model was trained for 15 epochs using the Adam optimizer and binary cross-entropy loss function. The resulting accuracy reached 98.17%, with the model demonstrating high recall and precision in cataract detection. The confusion matrix indicated that the model exhibited strong generalization performance overall.

A method for automatic diagnosis of diabetic retinopathy (DR) is proposed based on the VGG19 convolutional neural network using transfer learning techniques. The initial dataset consisted of color fundus images divided into two classes: with DR signs and without them [93]. The images were preprocessed by resizing to 224×224 pixels, normalization, and data augmentation using shifting, scaling, and flipping to enhance the model's generalization capability.

A pre-trained VGG19 model (originally trained on ImageNet) was used as the base, with its top classification layers removed. New dense layers with ReLU and Softmax activation functions, along with Dropout layers to prevent overfitting, were added. The model was trained on 2076 images, split into training, validation, and test sets.

The results showed high classification accuracy — 95.79% on the test set. Additional evaluation was performed using precision, recall, and F1-score metrics. The model demonstrated excellent ability to distinguish between positive and negative DR cases, making it a promising tool for early disease diagnosis.

The study proposes a method for automatic classification of diabetic retinopathy (DR) stages using a convolutional neural network based on the VGG-19 architecture [94]. The APTOS dataset was used, consisting of 4851 fundus images categorized into four classes: normal (grade 0), mild (grade 1), proliferative (grade 2), and severe (grade 3).

Before training, the images underwent preprocessing steps including resizing to a standard size, region-of-interest cropping, Gaussian filtering to remove noise, and conversion to grayscale. The VGG-19 model was fine-tuned using transfer learning by loading pretrained weights (from ImageNet) and replacing the top layers with new dense layers for classification.

Training was performed using the categorical cross-entropy loss function and the Adam optimizer. The model achieved a classification accuracy of 64.5% in the four-class setup. Precision and recall were 73.9% and 64.5%, respectively. The Area Under the ROC Curve (AUC) ranged from 0.86 to 0.97, indicating a strong ability to distinguish between disease stages.

Despite the moderate overall accuracy, the proposed method shows potential for clinical application in automated screening and severity assessment of diabetic retinopathy.

The method presented in this study focuses on the automatic detection of diabetic retinopathy (DR) using an enhanced deep learning model, GSO-VGG-16, based on the VGG-16 architecture [95]. The key steps include:

1. Image preprocessing: Original fundus images from the EyePACS dataset were normalized, resized to 224×224 pixels, and denoised using a Gaussian filter to preserve important features.

2. Data balancing: Random up-sampling was applied to address class imbalance (initially: 410 DR and 1017 No-DR cases) by duplicating minority class samples.

3. VGG-16 model: The base architecture was fine-tuned by adding new fully connected layers, Dropout, and ReLU activation. The final layer used a sigmoid function for binary classification.

4. Hyperparameter optimization: Grid Search Optimization (GSO) was used to identify the best values for dropout, number of dense units, activation function, and regularization. Optimal parameters were: dropout = 0.2, dense units = 512, activation = ReLU.

5. Results:

- Without GSO and filtering: VGG-16 achieved 69.63% accuracy.

- With up-sampling: accuracy increased to 79.89%.
- With the full GSO + Gaussian method: accuracy reached 92.38%, with precision, recall, and F1-score all equal to 92%.

The authors developed a method for diagnosing dyslexia in children aged 7–13 based on the analysis of eye-tracking data using a deep convolutional neural network modified from the VGG16 architecture [96]. During the experiment, children read text in Serbian presented in 13 different color configurations, and their eye gaze coordinates (x, y) were recorded using the SMI RED-m tracker (120 Hz).

The main steps of the method include:

1. Data preprocessing: Removal of artifacts (blinks and missing points) and segmentation of each reading session into 3, 5, or 10 parts.
2. Visualization: Each sequence of gaze coordinates was transformed into a color image (64×64×3) using a color gradient to represent the velocity of eye movement.
3. Deep learning model: A modified VGG16 network was used, including 3 convolutional blocks (16, 32, and 64 filters), batch normalization, pooling, Dropout, and a final sigmoid classifier. Various convolution kernel sizes (3×3, 5×5, 7×7) and pooling window sizes (2×2, 4×4) were explored.
4. Evaluation: Classification was performed both at the segment level and subject level using leave-one-subject-out cross-validation.

Results:

- The best subject-level accuracy reached 87% with the (7×7, 2×2) configuration and 3 segments.
- The visualization approach enabled minimal preprocessing and avoided the need for handcrafted feature extraction.

In this study [97], a method for automatic cataract detection is presented using a pre-trained VGG16 convolutional neural network. The original dataset included images of eyes with and without a cataract diagnosis. All images were preprocessed by resizing them to 224×224 pixels and applying normalization. The VGG16 model, initially trained on ImageNet, was fine-tuned by replacing the top layers with custom layers designed for binary classification. The convolutional layers were frozen, and the newly added dense layers were trained using the binary cross-entropy loss function and the Adam optimizer. Transfer learning techniques were applied during the training process.

The results showed a high classification accuracy of 94.3%, along with excellent sensitivity and precision metrics. This approach enables efficient eye condition classification with minimal computational cost. The method can be implemented in automated medical diagnostic systems and has demonstrated its effectiveness even with limited medical data.

In study [98], an automated system for the recognition of ophthalmic diseases (cataract, glaucoma, diabetic retinopathy, and normal cases) was developed based on convolutional neural networks (CNN). Four models were used for classification: VGG16, VGG19, ResNet18, and ResNet50. The original dataset of 4217 images was collected from the Kaggle platform and underwent preprocessing (resizing and normalization).

Transfer learning was applied in all models, with fine-tuning of the final layers, addition of Dropout layers, and ReLU activation. Training was performed over 25 epochs using the AdamW optimizer, early stopping, and hyperparameter tuning. The best results were achieved by the VGG19 and VGG16 models, with classification accuracies of **92%** and **91%**, respectively. The models were evaluated using accuracy, precision, recall, and F1-score metrics.

Additionally, a Gradio-based interface was implemented, allowing users to upload images and receive real-time diagnostic predictions.

Thus, the VGG architecture is a powerful and versatile tool for computer vision tasks, offering structural simplicity, high accuracy, and strong potential for transfer learning. Owing to these qualities, VGG models are widely used in medical diagnostics, including the automated detection of ophthalmic diseases.

1.5 You Only Look Once

YOLO (You Only Look Once) is one of the most well-known and effective architectures for object detection tasks, including applications in ophthalmology. In particular, an improved version of YOLOv5 with integrated attention modules and an enhanced feature network demonstrates high accuracy in detecting ocular surface pathologies from smartphone-acquired images. This modification employs the CBAM (Convolutional Block Attention Module), embedded within the CBAMC3 module, which helps the model focus on affected areas

while ignoring background noise. Additionally, the architecture incorporates a BiFPN (Bidirectional Feature Pyramid Network), which enables deeper and more efficient feature integration across multiple scales. This combination of modules enhances localization and segmentation accuracy, especially for small or irregular lesions. The model was trained on an annotated dataset of 953 ocular surface images, and data augmentation techniques were applied to mitigate overfitting. Results showed that the enhanced YOLOv5 achieved a mAP@0.5 of up to 97.9%, outperforming classical versions of YOLO and SSD. Its high processing speed and precision make YOLOv5 with CBAMC3 and BiFPN a powerful tool for automated diagnostics, particularly in resource-limited settings such as mobile devices. The method provides accurate localization even in complex backgrounds and can be integrated into clinical decision support systems [99].

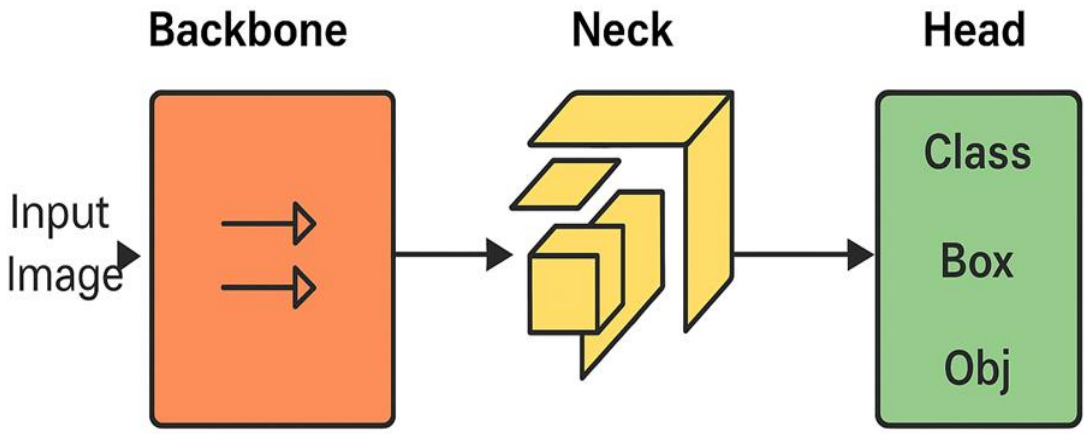

Figure 2.5. Architecture YOLO

1.6 Deep Neural Network

The Deep Neural Network (DNN) method, implemented in the form of a modified YOLO v2 with ResNet-50 as the feature extraction backbone, demonstrates high accuracy in the task of eye region localization in infrared thermal images. By leveraging anchor boxes, prior clustering of object sizes, and optimization based on the ImageNet dataset, the model achieves a mean Average Precision (mAP) of up to 98.07% and an Intersection over Union (IoU) of up to 68.98%, surpassing traditional approaches. This makes the YOLO v2-based DNN an effective tool for ophthalmological diagnostics.

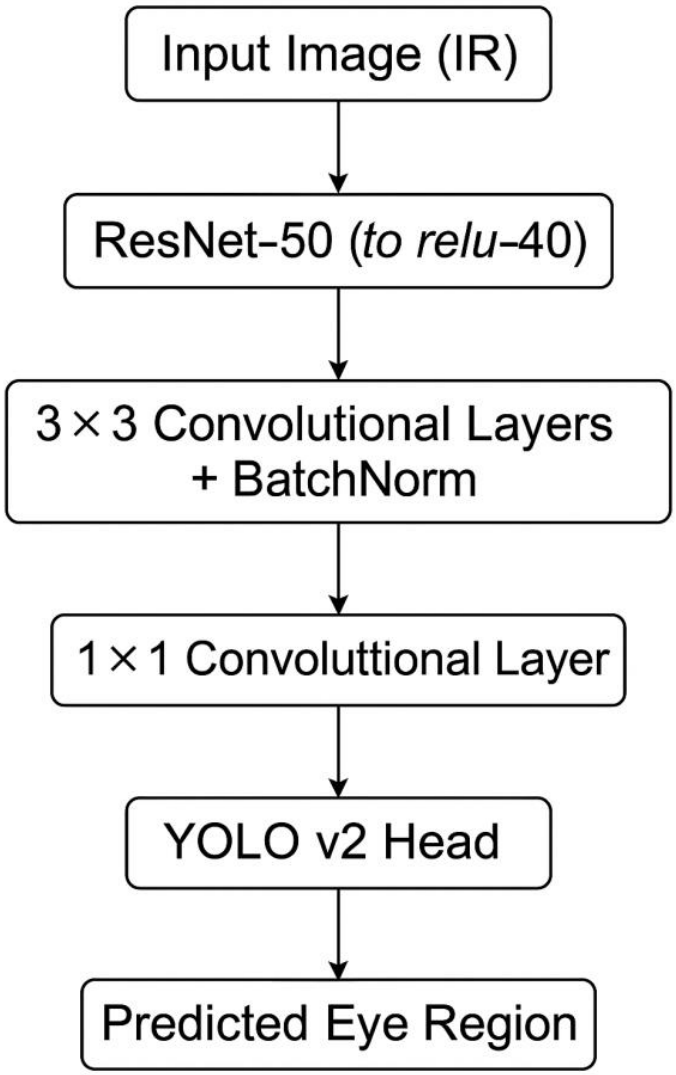

Figure 2.6. Architecture of the DNN for eye region localization in infrared thermal images

Thus, the proposed DNN model based on YOLO v2 and ResNet-50 demonstrates high accuracy and speed in localizing the eye region in infrared thermal images. By leveraging a pre-trained network and anchor boxes, the model achieves a high mAP and outperforms traditional approaches. This makes it a promising tool for automated ophthalmic disease diagnosis.

Modern artificial intelligence methods based on deep neural networks (CNNs and DNNs) have revolutionized the diagnosis of ophthalmic diseases. Architectures such as VGG, ResNet, EfficientNet, YOLO, and U-Net have demonstrated high performance in tasks such as classification, segmentation, and localization of eye pathologies. Their key advantages include automatic feature extraction, the ability to work with limited data via transfer learning, and high diagnostic

accuracy across various tasks [100]. Hybrid approaches combining CNNs with Vision Transformers (ViT), autoencoders, and attention mechanisms significantly improve sensitivity and robustness to noise, which is critical when analyzing low-quality medical images. Despite the high computational requirements and the need for clinical validation, these methods represent a promising foundation for the development of intelligent decision support systems in ophthalmology.

2 Analysis of methods and systems for diagnosing diabetic retinopathy and Glaucoma

2.1 Research problems and consequences of diseases of the fundus

Addressing the causes and consequences of ocular diseases holds significant medical and public health importance in clinical practice. Specifically, pathological conditions affecting the retina and optic nerve can arise from a variety of neurosurgical and cardiovascular disorders, as well as endocrine abnormalities. These complex cases often necessitate a collaborative approach to diagnosis and treatment, involving coordinated care between ophthalmologists and specialists from other medical fields [101].

Changes in the fundus are of significant diagnostic and prognostic value, as the majority of patients with ocular diseases require not only surgical interventions but also therapeutic treatment. This underscores the necessity for a comprehensive understanding of retinal pathology and the development of effective treatment strategies for combined patient care [102].

According to the International Diabetes Federation, approximately 537 million adults worldwide are living with diabetes, equating to one in ten individuals affected by this condition. Projections indicate that by 2030, this number could rise to between 643 million and 700 million [1, 102, 103, 104, 105, 106]. Diabetes is associated with complications affecting the retina, heart, kidneys, and nerves. Diabetic retinopathy (DR) is a leading cause of blindness in developed countries [107, 108, 109]. This serious retinal condition arises as a consequence of diabetes and can result in damage to the ocular blood vessels, as illustrated in Figure 3.1, ultimately leading to vision loss [110, 111, 112, 113, 114]. Diabetic retinopathy accounts for 2.6% of all cases of blindness [101], and individuals with diabetes are 25 times more likely to experience blindness compared to the general population. Therefore, it is imperative to develop effective treatment and prevention strategies for DR to preserve vision in diabetic patients, as visual impairment is observed in over 10% of this population.

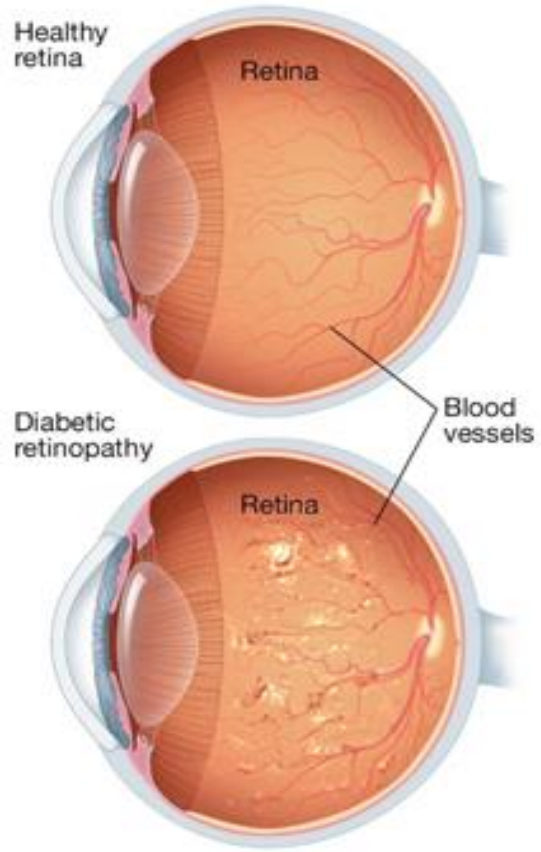

Figure 3.1. Schematic example of healthy and diabetic retina [115]

Retinal vascular complications are prevalent in patients with both type I and type II diabetes, making them a significant concern in the field of diabetology. The vascular complications associated with diabetes have profound implications for disease prognosis, patient productivity, and overall life expectancy. In individuals with diabetes, the vascular system is particularly susceptible to damage, affecting critical areas such as the retina, kidneys, lower extremities, brain, and heart.

Ophthalmologists often play a crucial role in the early detection of diabetic retinopathy (DR), as they may be the first healthcare professionals to observe characteristic changes in the fundus during examinations. Patients frequently present with symptoms such as diminished vision or the perception of floaters, often unaware of their underlying diabetic condition.

The likelihood of developing DR increases with the duration of diabetes, underscoring the importance of regular retinal screening for diabetic patients. Early diagnosis and intervention are essential to manage DR effectively and mitigate the risk of severe complications, including blindness. Therefore, implementing routine retinal

assessments is critical in the comprehensive care of individuals with diabetes, facilitating timely treatment and improving patient outcomes [2].

Risk factors are [21, 116, 117, 118, 119, 120]:

1. The duration of diabetes is important. When diabetes is detected in patients under the age of 30, the probability of developing DR after 10 years is 50%, and after 30 years - 90% of cases. DR is rarely manifested in the first 5 years of the disease and during puberty, but occurs in 5% of patients with type 2 diabetes [101, 121].

2. Insufficient control over metabolic processes in the body is a fairly common cause of the development and progression of DR.

3. Pregnancy often contributes to the rapid progression of DR. Contributing factors include insufficient control of the underlying disease before pregnancy, or suddenly started treatment in the early stages of pregnancy and the development of preeclampsia and fluid imbalance.

4. Hypertension with insufficient control leads to the progression of DR and the development of proliferative diabetic retinopathy in type 1 and type 2 diabetes.

5. Nephropathy with an acute course leads to worsening of the course of DR. Conversely, the treatment of renal pathology (for example, kidney transplantation) may be accompanied by a worsening of the condition and an excellent result after photocoagulation.

6. Other risk factors are smoking, obesity, hyperlipidemia [101].

Diabetic retinopathy (DR) is a microangiopathy characterized by primary damage to pre-capillary arterioles, capillaries, and post-capillary venules, with the potential for involvement of larger vessels. The clinical manifestations of DR include microvascular occlusion and leakage. It can be classified into three distinct stages: (a) background (non-proliferative) retinopathy, where pathological changes are confined to the intraretinal space; (b) proliferative retinopathy, in which pathological changes extend to the retinal surface or beyond; and (c) pre-proliferative retinopathy, which is characterized by changes that predict the onset of proliferative forms [101].

The pathogenesis of DR is primarily driven by two key mechanisms [122, 123]:

1. **Increased vascular permeability**, which results in the accumulation of edema, hard exudates, and retinal hemorrhages.

2. **Formation of microthrombi and capillary occlusion**, leading to ischemic and hypoxic areas within the retina. These regions subsequently produce vascular endothelial growth factors (VEGF), which stimulate the process of neovascularization.

A significant challenge in the management of DR is the difficulty in detecting the disease during its early stages, when therapeutic interventions are most likely to be effective. Early-stage DR often presents asymptomatically, complicating timely diagnosis. To facilitate detection, specialized diagnostic techniques such as ophthalmoscopy, fluorescein angiography, and optical coherence tomography are employed [124, 125, 126, 127].

The consequences of untreated DR can be severe, potentially leading to significant visual impairment or blindness. Chronic hyperglycemia, hypertension, and other risk factors are known to exacerbate the development of DR [128]. Therefore, upon diagnosis of DR, it is imperative to implement strategies aimed at preventing disease progression. These strategies may include effective diabetes management, blood pressure control, and regular monitoring of the fundus to ensure timely intervention and preserve visual function.

The pathogenic changes associated with diabetic retinopathy are summarized in Table 3.1.

Table 3.1.

Pathogenic changes occurring in diabetic retinopathy [101, 129]

	Diabetes		
	angiopathy	common retinopathy	proliferative retinopathy
The optic disc is pink	+	+	+
Swelling, increasing in size	-	-	-
The boundaries of the optic disc are clear	+	+	+
Arteries are narrowed	-	-	-
The caliber of the vessels is not uniform	+	-	+

Corkscrew and tortuosity of small venous vessels in the area of the macula	-	-	-
Copper and silver wire symptom	-	-	-
Symptom of Salus-Gunn II-III centuries.	-	-	-
Whitish-yellow spots in the retina	-	+	+
Hemorrhages in the retina and its swelling	-	+	+
The shape of a "star" in the area of the macula	-	-	
Newly formed vessels	+	+	+
Proliferation	-	-	+

2.2 Methods of researching eye diseases, in particular diabetic retinopathy

There are various methods for investigating eye diseases, tailored to the specific symptoms and pathological processes involved. Some of the more common diagnostic techniques include:

1. **Comprehensive Eye Examination**: This initial assessment is typically conducted by an ophthalmologist or optometrist. During the examination, the clinician evaluates visual acuity, visual fields, refractive errors, and the overall condition of the eyes, including the assessment of the anterior and posterior segments.
2. **Computer Spheroperimetry**: This advanced ophthalmological technique allows for precise measurement of the visual fields and detection of even minor deviations from established norms at early stages of disease. The results are documented in the form of diagrams, graphs, and three-dimensional images, providing a comprehensive view of the patient's visual field status (see Figure 3.2) [130].

These methods are essential for accurate diagnosis and management of various ocular conditions, enabling timely intervention and improved patient outcomes.

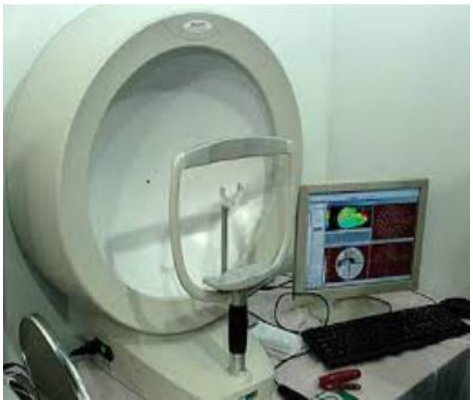

a) Computer perimeter

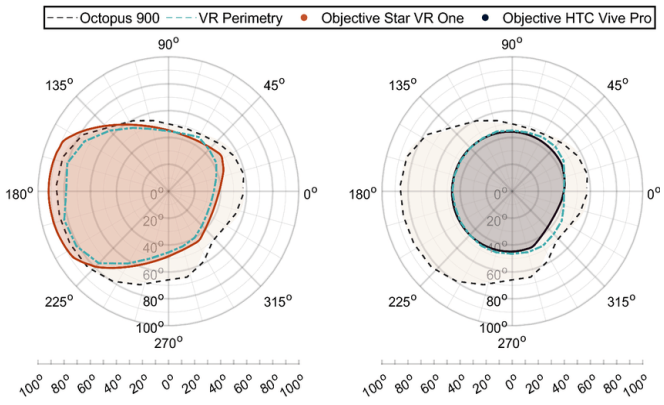

b) Kinetic visual field test

Figure 3.2. Computer perimeter (a) and example of a kinetic visual field test performed on an Octopus 900 (b) [131]

The analyzer of hydro- and hemodynamics of the eye, commonly referred to as a tonograph, is a specialized instrument designed to assess intraocular pressure as well as the parameters related to the circulation of intraocular fluid and blood within the eye.

The tonograph (see Figure 3.3) calculates a comprehensive set of tonometric, tonographic, and sphygmometric indicators that are essential for the early diagnosis of conditions associated with disturbances in ocular hydro- and hemodynamics. These conditions include various forms and stages of glaucoma, ocular hypertension, and other related disorders [132]. By providing detailed measurements, the tonograph plays a crucial role in the timely identification and management of these potentially sight-threatening diseases.

Figure 3.3. Tonograph [133]

Optical coherence tomography (OCT) (see Figure 3.4) is a contemporary, non-invasive, and non-contact imaging technique that enables high-resolution visualization of various ocular structures, achieving resolutions ranging from 1 to 15 microns. This advanced imaging modality functions as a form of optical biopsy, allowing clinicians to obtain detailed cross-sectional images of the retina and other eye tissues without the need for tissue removal or subsequent microscopic examination.

OCT is particularly valuable in diagnosing and monitoring a range of ocular conditions, including diabetic retinopathy, age-related macular degeneration, and glaucoma, as it provides critical information about the structural integrity of the eye and facilitates timely intervention [134].

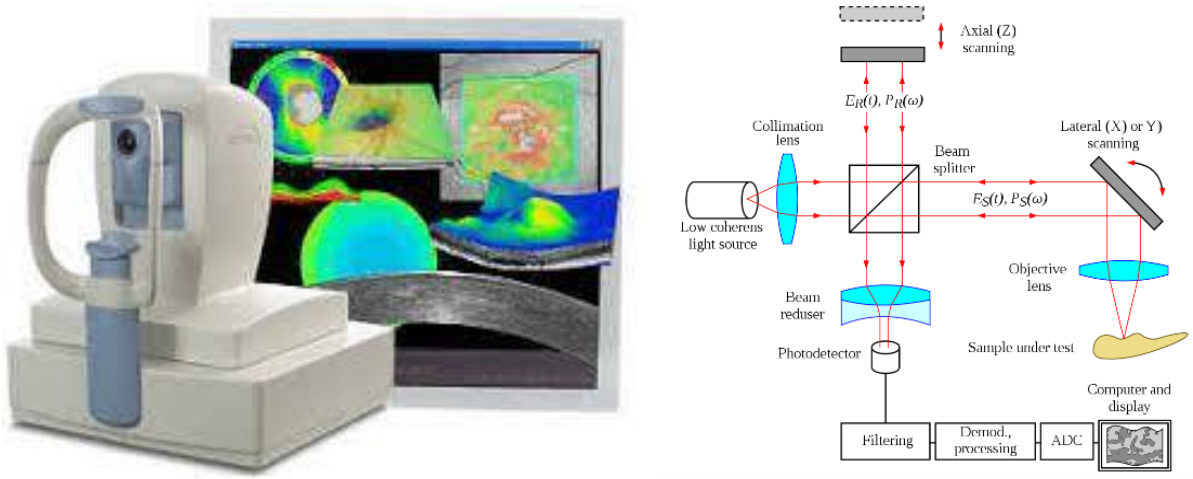

Figure 3.4. Typical optical setup of single point OCT. Scanning the light beam on the sample enables non-invasive cross-sectional imaging up to 3 mm in depth with micrometer resolution [135]

Fluorescence angiography (FAG) (see Figure 3.5 a, b), first introduced by Novotny and Alvis in 1961, is a valuable and informative technique for the in vivo examination of the retinal vasculature. This method involves the intravenous injection of a fluorescent dye, which allows for the visualization of blood flow in the retinal vessels.

While the retina can be assessed using direct and indirect ophthalmoscopy as well as biomicroscopy, fluorescence angiography serves as a crucial complement to these clinical techniques. It provides a wealth of additional information that is essential for the accurate diagnosis and management of various pathological conditions affecting the retina and optic nerve, including diabetic retinopathy, retinal vein

occlusions, and choroidal neovascularization [136]. By enhancing the understanding of vascular dynamics and pathology, FAG plays a critical role in guiding treatment decisions and monitoring disease progression.

a) Image of vessels b) Angiograph

Figure 3.5. Image of vessels during fluorescence angiography [137] (a) and angiograph (b) [138]

Ophthalmobiomicroscopy is a specialized technique that enables the assessment of the relationship between the retina and the vitreous body, as well as the evaluation of the condition and qualitative changes in the retina, allowing for precise localization of any abnormalities. This examination is performed using a conventional slit lamp (biomicroscopy) in conjunction with a high-powered collecting lens, typically ranging from 70 to 80 diopters or higher (see Figure 3.6) [132].

It is essential that ophthalmobiomicroscopy is conducted with accompanying photography and thorough documentation of the obtained data. This practice facilitates the accurate recording of the state of pathological foci on the fundus, providing reliable information regarding the effectiveness of the prescribed treatment and enabling ongoing monitoring of disease progression. By systematically documenting findings, clinicians can enhance the quality of patient care and make informed decisions regarding therapeutic interventions.

Figure 3.6. Ophthalmobiomicroscopy [139]

Computer topography of the cornea (see Figure 3.7) is a non-contact imaging technique used to analyze the structure and shape of the cornea. This method employs a specialized device that generates a detailed three-dimensional map of the corneal surface, providing valuable information about its curvature, thickness, and overall topography.

The resulting topographic maps are essential for diagnosing and managing various corneal conditions, including keratoconus, astigmatism, and preoperative assessments for refractive surgery. By offering precise measurements and visual representations of corneal irregularities, computer topography enhances the clinician's ability to tailor treatment plans and monitor changes in corneal health over time [140, 141].

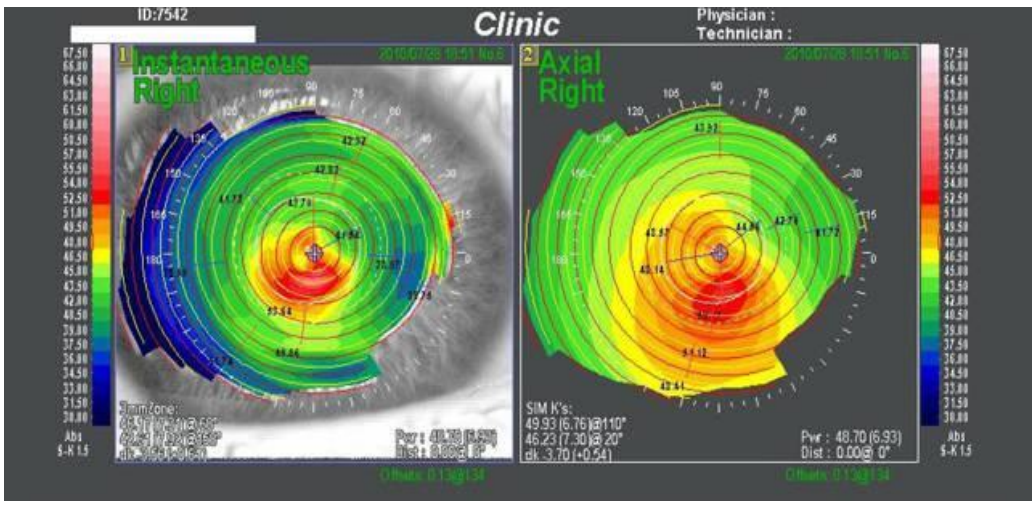

Figure 3.7. Computer topography of the cornea [142]

Ocular tomography is a diagnostic method employed to investigate the structural integrity of the eyes. This technique is particularly useful for identifying disorders affecting the meridional and collecting vessels, the optic disc, and conditions such as macular retinitis. By providing detailed cross-sectional images of the ocular structures, ocular tomography aids in the early detection and management of various ocular pathologies.

In addition to ocular tomography, electrophysiological studies are utilized to assess the functionality of different components of the eyes and the visual system. For instance, an electroretinogram (ERG) (see Figure 3.8) is a valuable tool for detecting retinal pathologies by measuring the electrical responses of the retina to light stimuli. Similarly, an electroencephalogram (EEG) can be employed to evaluate disorders related to the processing of visual information in the brain. Together, these diagnostic methods enhance the understanding of ocular health and facilitate timely intervention for visual impairments.

Figure 3.8. Electroretinogram [143]

Ocular angiography (see Figure 3.9) is a diagnostic method used to study blood circulation within the eyes. This technique involves the intravenous injection of a contrast dye, which allows for the visualization of the retinal and choroidal blood vessels through imaging. Ocular angiography is particularly valuable for diagnosing

diseases associated with impaired blood circulation in the eyes, such as diabetic retinopathy, retinal vein occlusions, and age-related macular degeneration.

By providing detailed images of the vascular structures and blood flow dynamics, ocular angiography aids clinicians in identifying pathological changes, assessing the severity of ocular conditions, and guiding treatment decisions. This method is essential for monitoring disease progression and evaluating the effectiveness of therapeutic interventions.

Figure 3.9. Ocular angiograph [144]

These diagnostic methods play a crucial role in enabling healthcare professionals to establish accurate diagnoses and select effective treatment strategies for various eye diseases, as illustrated in Figure 3.10. By providing detailed insights into the structural and functional aspects of the eye, these techniques facilitate early detection of conditions, allowing for timely intervention. The comprehensive information obtained from these assessments not only aids in understanding the underlying pathology but also enhances the ability to monitor disease progression and evaluate treatment outcomes. Ultimately, the integration of these advanced diagnostic tools into clinical practice significantly improves patient care and visual health outcomes.

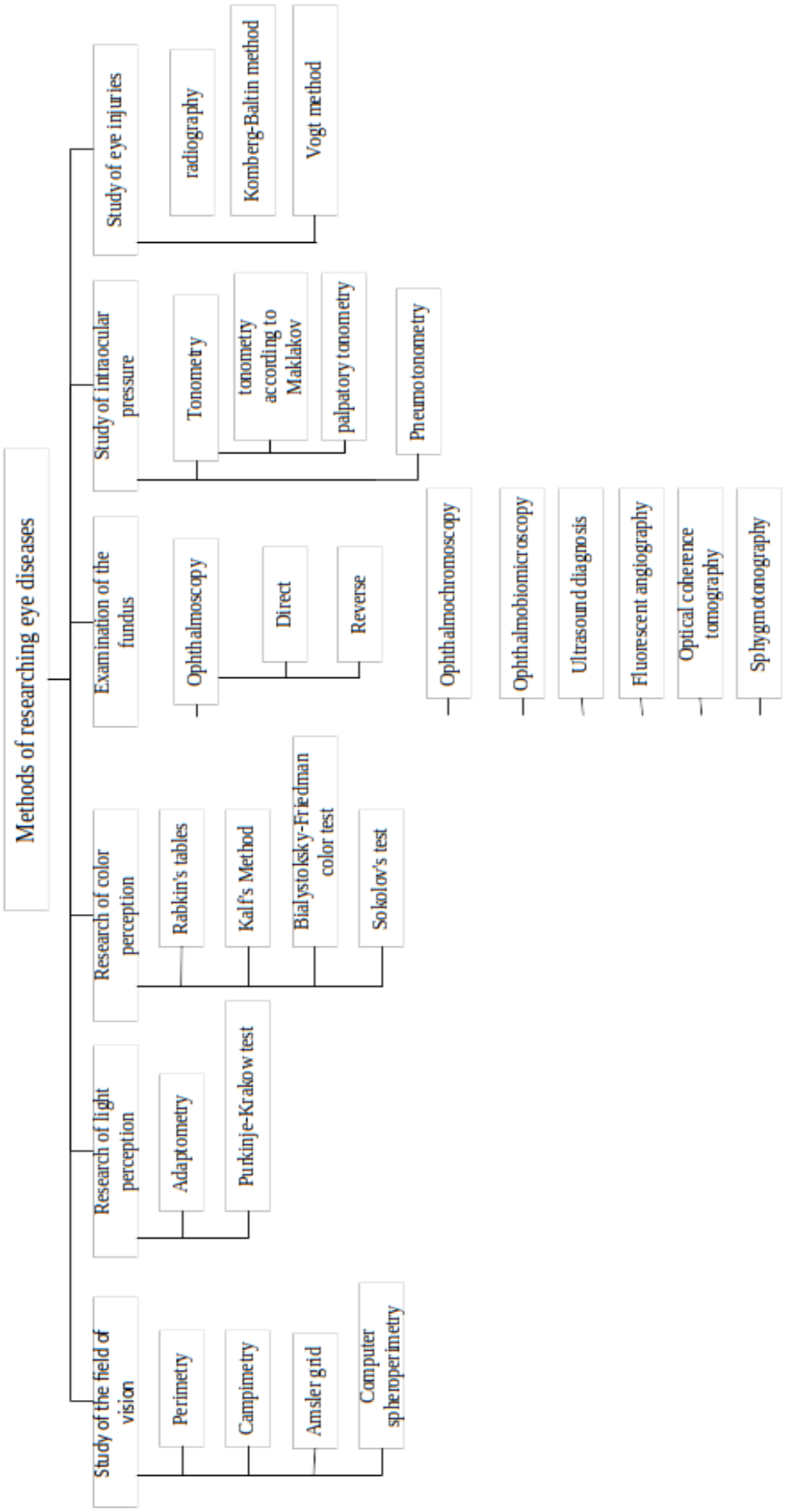

Figure 3.10. Classification of methods of research of eye diseases

2.3 Analysis of diagnostic systems for diabetic retinopathy

Diabetic retinopathy is one of the most prevalent complications of diabetes and can result in significant eye health issues, including vision loss. Various systems have been developed for diagnosing diabetic retinopathy, employing different research methods and data analysis techniques.

One of the most widely used diagnostic methods is ophthalmoscopy (or funduscopy) [145]. This technique allows for a thorough examination of the eyes and the retina, enabling clinicians to identify structural changes in the retinal vessels and surrounding tissues. Through ophthalmoscopy, it is possible to detect abnormalities such as hemorrhages, exudates, and microaneurysms, which are indicative of diabetic retinopathy.

Ophthalmoscopy can be performed using either a direct ophthalmoscope or an indirect ophthalmoscope. The direct ophthalmoscope provides a magnified view of the retina, while the indirect ophthalmoscope offers a wider field of view, facilitating a more comprehensive assessment of the blood vessels and retinal condition. This versatility makes ophthalmoscopy an essential tool in the early detection and management of diabetic retinopathy.

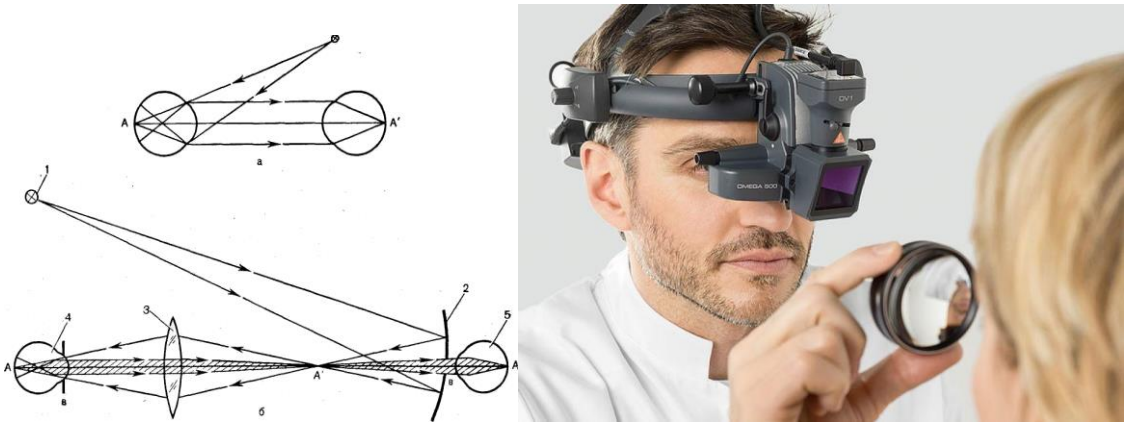

Figure 3.11. Reverse ophthalmoscopy scheme [146, 147]

The reverse ophthalmoscopy scheme represents the fundamental optical configuration of a manual mirror ophthalmoscope, which is widely utilized in clinical practice. In this setup, light from a source (see Figure 3.11) is directed onto a concave mirror (2) featuring an aperture (B). The concave mirror reflects the light and directs it toward a lens (3). As the light rays pass through the lens, they illuminate the fundus of the examined eye (4) through the optical system. In the case

of an emmetropic eye, the rays reflected from the fundus exit as a parallel beam and enter the lens (3). This configuration allows for the formation of a reverse image of the fundus in the focal plane of the lens, which can then be viewed through the aperture in the concave mirror (2) by the observer's eye (5). In this arrangement, point A on the fundus corresponds to image point A in the air. For the observer to accurately view this point, they must accommodate such that point A' aligns with point A''. To ensure that the pupil (B') does not limit the field of vision, the magnifying lens must produce an image of the aperture in the pupil (B') of the examined eye. Consequently, the pupil (B') is imaged by the lens into the aperture (B) of the mirror, positioned behind which is the observer's eye. This optical arrangement facilitates a detailed examination of the fundus, allowing for the identification of various ocular conditions.

Another important diagnostic method is fluorescence angiography (see Figure 3.12), which is utilized to study blood circulation within the retinal vessels. This technique is based on the property of fluorescein, a dye that absorbs blue light and emits a yellow-green fluorescence. Fluorescein fluoresces intensely at normal blood pH, making it a valuable tool for vascular imaging. It is considered non-toxic and is generally safe for most patients. During the procedure, fluorescein is injected into the bloodstream, allowing for a gradual contrast of the retinal vessels, which can be captured photographically. Various models of fundus cameras equipped with high-speed photography capabilities are employed for this purpose. In the resulting images, vessels that are contrasted with fluorescein appear as bright bands against the background of the fundus, while the relationship is reversed in negative photographs. This imaging technique enables clinicians to assess the condition of the retinal blood vessels, identify the presence of pathological changes, and evaluate their severity. By providing detailed visual information about the vascular status of the retina, fluorescence angiography plays a crucial role in the diagnosis and management of various ocular conditions, including diabetic retinopathy and retinal vascular diseases [148].

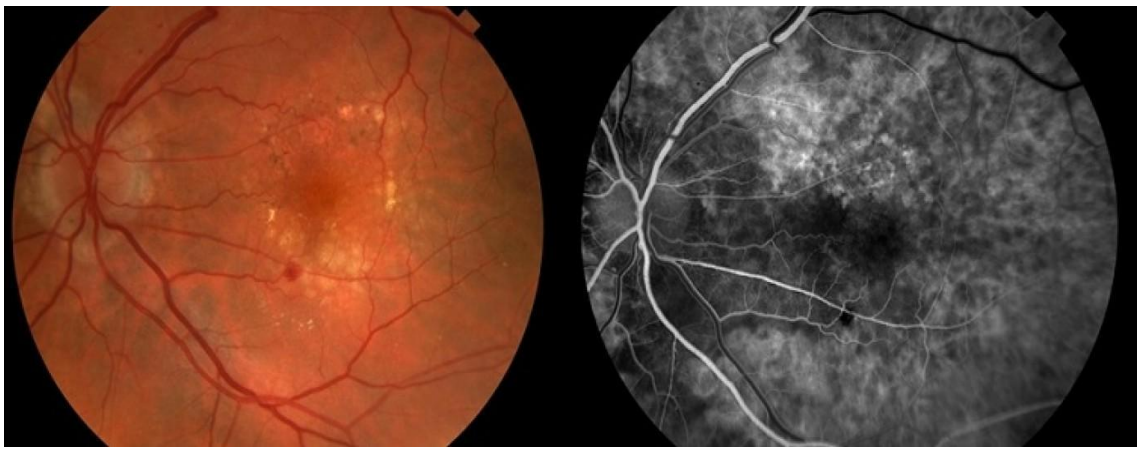

Figure 3.12. Fluorescent angiography [149]

Diabetic retinopathy [150, 151] is a significant complication of diabetes that can lead to impaired vision and, in severe cases, blindness. To effectively diagnose diabetic retinopathy, healthcare professionals can utilize a variety of research methods, including:

1. **Optical Coherence Tomography (OCT)**: This advanced imaging technique provides detailed three-dimensional images of the retinal structure, allowing for the assessment of changes in retinal thickness and the identification of abnormalities.
2. **Electrophysiological Studies**: These methods evaluate the functional integrity of the retina and the visual system. For instance, an electroretinogram (ERG) and electrooculogram (EOG) can detect early visual disturbances, providing insights into retinal function.
3. **Tonometry**: This method measures intraocular pressure, which is crucial for detecting glaucoma—a condition that can arise as a complication of diabetic retinopathy. Monitoring eye pressure is essential for preventing further vision loss.
4. **Ultrasound Examination**: Ultrasound imaging can reveal changes in the blood vessels of the eye and the retina, which may indicate the presence of diabetic retinopathy. This non-invasive technique aids in visualizing structural abnormalities.
5. **Refractometry**: This method assesses visual acuity and helps correct refractive errors that may occur as a result of diabetic retinopathy. Accurate measurement of visual function is important for comprehensive patient care.

Each of these diagnostic methods has its own advantages and limitations, and they can be employed individually or in combination to provide a more comprehensive understanding of the state of the eyes and associated vascular structures. For example, combining

ophthalmoscopy with fluorescein angiography can enhance the assessment of vascular and retinal damage, while optical coherence tomography can complement these findings by measuring retinal thickness and other critical parameters. This multifaceted approach is essential for accurate diagnosis and effective management of diabetic retinopathy.

One of the most progressive diagnostic methods currently being utilized is machine learning, which facilitates the automated analysis of images of blood vessels and the retina [40, 152]. By training on a large dataset of images, machine learning systems can automatically identify the presence of pathological changes in the structure of the vessels and retina, assess their severity, and evaluate the risk of complications.

However, like any diagnostic system, machine learning has its limitations and potential for errors. For instance, certain changes in the structure of blood vessels and the retina can be subjective and may depend on the ophthalmologist's experience. Additionally, there is a risk of false diagnoses when relying solely on automated systems. Therefore, it is always advisable to employ multiple diagnostic methods and conduct a thorough analysis of the results to ensure accuracy [153, 154, 155].

Overall, the early detection and diagnosis of diabetic retinopathy are crucial for preventing vision loss and other serious complications. Various diagnostic methods provide detailed information about the condition of the eyes and blood vessels, enabling healthcare providers to initiate timely treatment and monitor disease progression. It is essential to recognize that diagnosing diabetic retinopathy is a complex, multi-stage process that requires a highly qualified and experienced physician.

Moreover, prevention remains the most effective strategy for avoiding the development of diabetic retinopathy. Key preventive measures include maintaining a healthy lifestyle, controlling blood sugar levels, and undergoing regular ophthalmological examinations to detect any potential changes in the structure of the blood vessels and retina. By prioritizing prevention and early intervention, patients can significantly reduce their risk of developing diabetic retinopathy and its associated complications.

When diabetic retinopathy is diagnosed, healthcare providers typically employ a comprehensive treatment approach that may include laser therapy, intraocular drug injections, surgery, and other

interventions. The primary goal of treatment is to reduce the risk of complications and preserve vision [156, 157, 158].

Consequently, the diagnosis of diabetic retinopathy is a critical component of diabetes management, focusing on the early detection of pathology and the prevention of vision loss. A variety of diagnostic methods, encompassing both traditional and automated techniques, enable clinicians to obtain a complete understanding of the condition of the eyes and blood vessels, thereby facilitating more effective treatment and complication prevention.

One of the most promising methods for managing diabetic retinopathy is telemedicine, which allows healthcare providers to remotely monitor patients' eye health and conduct online consultations and examinations. This approach is particularly beneficial for individuals living in remote or hard-to-reach areas, as well as those with mobility limitations, advanced age, or health issues that restrict their ability to travel.

In many countries, the development of telemedicine is still in the formative and testing stages. However, there are already platforms available that enable effective remote monitoring of ocular health, such as the EyeArt AI System from Eyenuk [159]. This system utilizes artificial intelligence for the automated diagnosis of diabetic retinopathy, enhancing the efficiency and accessibility of care.

Overall, diagnostic systems for diabetic retinopathy are continually evolving and improving, allowing healthcare professionals to detect and treat the disease more effectively. By integrating advanced technologies and telemedicine into clinical practice, the management of diabetic retinopathy can be significantly enhanced, ultimately leading to better patient outcomes and reduced risk of vision loss.

2.4 Analysis of decision support systems

In many medical diagnostic systems, the reliability of results can be compromised, particularly due to the absence of a decision support system (DSS). The interpretation of images of biological structures by diagnosticians often requires significant time and effort, and this process may not always yield optimal outcomes [104, 113, 160, 161].

To enhance the reliability and efficiency of assessing pathological conditions in diabetes, particularly through the analysis of retinal

images, the development of a robust decision support system is essential. A well-constructed expert DSS can significantly improve diagnostic accuracy.

To effectively build such a system, it is crucial to select and define a sufficient number of informational parameters that will ensure the accuracy and reliability of the diagnosis when analyzing polarimetric images. Commonly employed methodologies for this purpose include statistical, correlational, and fractal approaches. However, these methods alone may not provide the high reliability required for diagnostic systems. Therefore, integrating informative indicators, such as statistical metrics alongside other types of expert systems, can enhance the overall reliability of the DSS.

The next step involves selecting the appropriate rule type for the DSS. Various established methods can be utilized, including those based on statistical decision theory [162], fuzzy logic [163, 164, 165], decision tree algorithms [166], and neural network technologies [167, 168, 169, 170, 171]. The choice of method may vary depending on the specific conditions and diagnostic techniques employed. By carefully considering these factors, a more effective and reliable decision support system can be developed, ultimately improving the diagnosis and management of diabetic retinopathy and other related conditions.

2.4.1 Discriminant analysis

Discriminant analysis [162, 168, 172] is used to make decisions about which variables distinguish two or more groups. The basic idea of discriminant analysis is to determine whether the populations differ on the mean of any variable (or linear combination of variables) and then use that variable to predict for new members whether they belong to one or another group [172].

Discriminant analysis is based on the assumption that the description of objects of each kth class is the implementation of a multidimensional random variable distributed according to the normal law $N_m(\mu_k; \Sigma_k)$ with means μ_k and the covariance matrix:

$$C_k = \frac{1}{n_k - 1} \sum_{i=1}^{n_k} (x_{ik} - \mu_k)^T (x_{ik} - \mu_k); \qquad (3.1)$$

(The index m indicates the dimensionality of the feature space).

Within the statistical (probabilistic) approach, the Bayesian method is used [172].

According to the Bayes formula, the reliability of the conclusion about the presence of this or that pathology is determined $P(Y_j / X_i)$ [168, 172]:

$$P(Y_j / X_i) = \frac{P(Y_j)P(X_i / Y_j)}{P(X_i)} \qquad (3.2)$$

Taking into account the set of features, $X_1,...,X_K$, the Bayes formula takes the form [23]:

$$P(Y_j / X_1,..., X_K) = \frac{P(Y_j)P(X_1,..., X_K / Y_j)}{P(X_1,..., X_K)} \qquad (3.3)$$

The decisive rule according to the Bayesian method is to find the maximum of the conditional posterior probability $P(Y_j / X_1,..., X_K)$ [173].

Figure 3.13 illustrates the division of the population into two distinct classes through the application of a discriminant function, which effectively separates the groups based on their characteristic features."

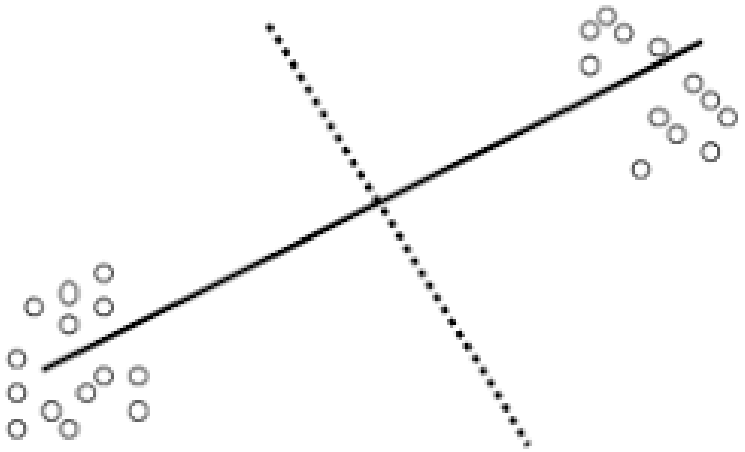

Figure 3.13. Division of the population into two classes using a discriminant function [173]

The Bayesian method presents a distinct advantage in its flexibility to incorporate a wide array of features that may stem from various physical origins. This approach is particularly beneficial because it relies on probability estimates of feature occurrences rather than solely on the raw dimensional values. By focusing on the likelihood of different outcomes, the Bayesian method can effectively integrate diverse types of information, allowing for a more comprehensive analysis of the data.

Despite its strengths, the Bayesian method has a significant limitation: it requires a substantial amount of prior information to be effective. This reliance on prior knowledge can pose challenges, especially in situations where such information is scarce or difficult to obtain. Consequently, the effectiveness of the Bayesian approach may be compromised if the prior distributions are not well-informed or accurately represent the underlying phenomena.

On the other hand, discriminant analysis is characterized by its high sensitivity to the distribution of input data. This sensitivity means that even minor changes in the data can lead to significant variations in classification results. Such fluctuations can undermine the reliability of the analysis, making it crucial to ensure that the input data is representative and stable. This inherent vulnerability to data distribution highlights a critical limitation of discriminant analysis, as it may yield inconsistent results in the presence of slight perturbations in the dataset.

In summary, while the Bayesian method offers the advantage of integrating diverse features through probability estimates, it is constrained by its dependence on prior information. Conversely, discriminant analysis, although useful, is highly sensitive to input data distribution, which can lead to substantial variations in classification outcomes. Understanding these strengths and limitations is essential for selecting the appropriate analytical method for a given research context.

2.4.2 Decision tree

Decision trees [166, 172, 174, 175, 176] are a powerful and widely used method for partitioning the space of objects based on a systematic set of splitting criteria. These criteria are articulated as logical

statements concerning specific variables, which can evaluate to either true or false. The effectiveness of decision trees can be understood through three fundamental aspects:

1. **Sequential Dichotomous Segmentation**: The rules governing the decision tree allow for a sequential process of dichotomous segmentation of the dataset. This means that at each node of the tree, the data is split into two distinct groups based on the outcome of a specific condition related to a variable. This iterative process continues until a stopping criterion is met, such as reaching a predefined depth of the tree or achieving a minimum number of samples in a node. This stepwise refinement enables the model to capture complex patterns and interactions within the data, leading to more accurate classifications.

2. **Similarity and Grouping**: Within the framework of decision trees, two objects are considered similar if they are located within the same segment of the partition. This segmentation is crucial as it establishes a basis for grouping objects that share common characteristics, thereby facilitating the identification of patterns and relationships within the data. The ability to classify objects into homogeneous groups enhances the interpretability of the model, allowing for insights into the underlying structure of the data.

3. **Information Gain and Feedback**: A key feature of decision trees is the increase in information regarding the target variable at each step of the partitioning process. This is often quantified using metrics such as information gain or Gini impurity, which measure the effectiveness of a split in terms of its ability to reduce uncertainty about the target variable. As the tree grows, each split ideally leads to a more homogeneous grouping of the target variable, thereby enhancing the model's predictive accuracy. This feedback mechanism is essential for refining the decision-making process, as it allows the model to adaptively learn from the data and improve its performance over time.

Decision trees provide a robust framework for data classification through their ability to perform sequential dichotomous segmentation, establish similarity among objects, and enhance information gain at each partitioning step. These characteristics make decision trees a valuable tool in various fields, including machine learning, data mining, and statistical analysis. Figure 3.14 graphically presents an example of a decision tree.

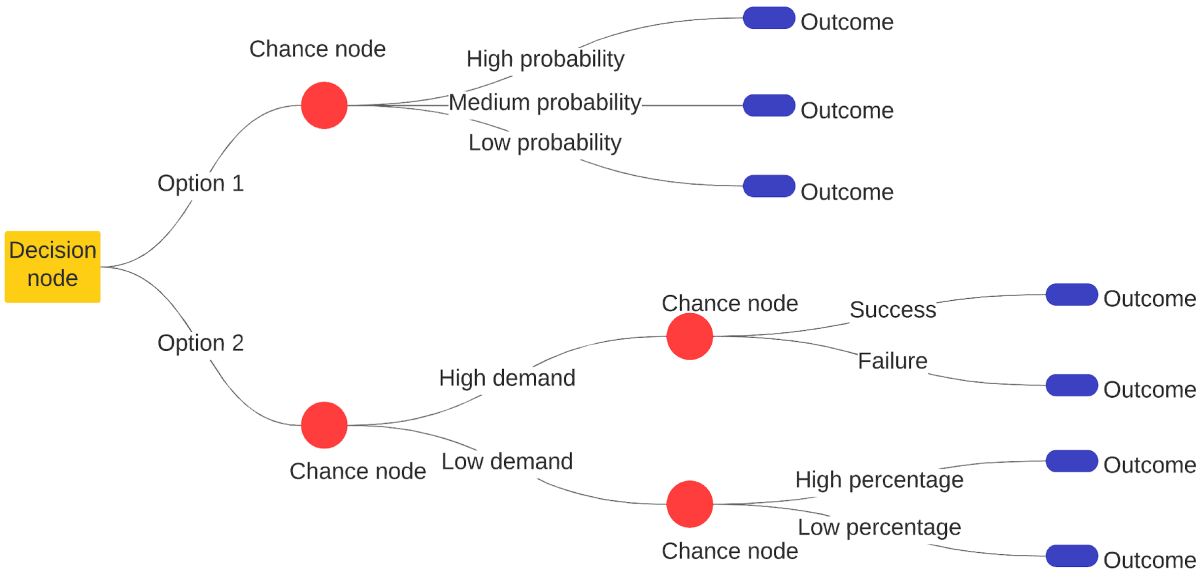

Figure 3.14. Example of a typical decision tree [177]

Decision trees are a widely utilized technique for addressing classification problems [175, 176], owing to several notable advantages:

1. **Simplicity and Interpretability**: The decision tree model is inherently straightforward, making it easy to understand and interpret. It operates on a set of rules structured in the form of "if ..., then ...," which allows users to follow the decision-making process intuitively. The clear, tree-like structure further facilitates interpretation, enabling stakeholders to grasp the rationale behind predictions.
2. **Minimal Data Preparation**: Unlike many other modeling techniques, decision trees do not require extensive data preprocessing, such as normalization or logarithmic transformations. This characteristic simplifies the modeling process and makes decision trees accessible for practitioners with varying levels of expertise.
3. **"White Box" Model**: Decision trees function as "white box" models, meaning that the decision-making process can be explicitly explained using Boolean logic. This transparency is advantageous in applications where understanding the rationale behind predictions is crucial, such as in healthcare or finance.
4. **Versatility**: Decision trees can be applied to both quantitative and qualitative dependent variables, making them versatile tools for a wide range of classification tasks. This adaptability allows researchers to utilize decision trees across diverse fields and datasets.
5. **Statistical Evaluation**: The ability to evaluate decision tree models using statistical tests enhances their reliability. This feature

allows practitioners to assess the robustness of the model and its predictions, providing confidence in the results obtained.

6. **Efficiency with Large Datasets**: Decision trees are computationally efficient and can handle large datasets effectively. Their speed in processing data makes them suitable for real-time applications and scenarios involving substantial amounts of information.

Despite these advantages, decision trees also present several disadvantages [176]:

1. **Complexity in Initial Structure Formation**: The process of forming the initial structure of a decision tree can be complex and may require careful consideration of various factors, including the selection of splitting criteria and the depth of the tree.

2. **Instability to Training Data Variations**: Decision trees are sensitive to changes in the training data. Even minor adjustments to the training sample can lead to significant alterations in the tree structure and the resulting predictions. This instability can pose challenges in ensuring consistent model performance.

3. **Limitations of Dividing Boundaries**: The nature of the dividing boundaries in decision trees imposes certain limitations, which can result in inferior classification quality compared to other methods. This is particularly evident in cases where the underlying relationships in the data are complex and not easily captured by the tree structure.

4. **Risk of Overfitting**: There is a high probability of generating overly complex trees during the training process, which can lead to overfitting. Such trees may perform well on the training data but fail to generalize effectively to unseen data.

Considering the aforementioned shortcomings, particularly in the context of classifying distributions of parameters of biological tissues represented in image form, the use of decision trees may be impractical. The complexity of the structures involved in such applications often exceeds the capabilities of decision trees, suggesting that alternative modeling approaches may be more suitable for achieving reliable and accurate classifications.

2.4.3 Fuzzy logic

Fuzzy logic is grounded in the concept of fuzzy sets, which extend traditional set theory by allowing for degrees of membership rather than a binary classification of belonging or not belonging to a set. In classical set theory, an element either belongs to a set or does not, represented by a membership value of 1 or 0, respectively:

$$\tilde{A} = \{(x, \mu_A(x)) \mid x \in \mathbf{X}\}, \tag{3.4}$$

where the membership function quantifies the membership of the elements of the fundamental set to the fuzzy set.

In contrast, fuzzy sets are characterized by a membership function that can assign any value within the continuous range of [0, 1]. This flexibility enables a more nuanced representation of uncertainty and vagueness, which is often encountered in real-world scenarios [165, 174, 178, 179].

The membership functions for the corresponding fuzzy terms L, LM, M, HM, H on the interval $[P_1;\ P_1 + 4h]$ have the following form:

$$\mu^L(p) = \begin{cases} -\frac{0.5}{h}p + 1 + \frac{0.5}{h}P_1, p \in [P_1;\ P_1 + h], \\ -\frac{1}{6h}p + \frac{P_1}{6h} + \frac{4}{6}, p \in [\ P_1 + h;\ P_1 + 4h], \end{cases} \tag{3.5}$$

$$\mu^{LM}(p) = \begin{cases} \frac{1}{2h}p + 0.5 - \frac{1}{2h}P_1, p \in [P_1;\ P_1 + h], \\ -\frac{1}{2h}p + 1.5 + \frac{P_1}{2h}, p \in [\ P_1 + h;\ P_1 + 2h], \\ -\frac{1}{4h}p + 1 + \frac{P_1}{4h}, p \in [\ P_1 + 2h;\ P_1 + 4h], \end{cases} \tag{3.6}$$

$$\mu^{M}(p) = \begin{cases} \frac{1}{2h}p - \frac{1}{2h}P_1, p \in [P_1;\ P_1 + 2h], \\ -\frac{1}{2h}p + 2 + \frac{P_1}{2h}, p \in [\ P_1 + 2h;\ P_1 + 4h], \end{cases} \tag{3.7}$$

$$\mu^{HM}(p) = \begin{cases} \frac{1}{4h}p - \frac{1}{4h}P_1, p \in [P_1;\ P_1 + 2h], \\ \frac{1}{2h}p - 0.5 - \frac{P_1}{2h}, p \in [\ P_1 + 2h;\ P_1 + 3h], \\ -\frac{1}{2h}p + 2.5 + \frac{P_1}{2h}, p \in [\ P_1 + 3h;\ P_1 + 4h], \end{cases} \quad (3.8)$$

$$\mu^{H}(p) = \begin{cases} \frac{1}{6h}p - \frac{1}{2h}P_1, p \in [P_1;\ P_1 + 3h], \\ \frac{1}{2h}p - 1 - \frac{P_1}{2h}, p \in [\ P_1 + 3h;\ P_1 + 4h]. \end{cases} \quad (3.9)$$

Figure 3.15 shows a graphical view of the membership function.

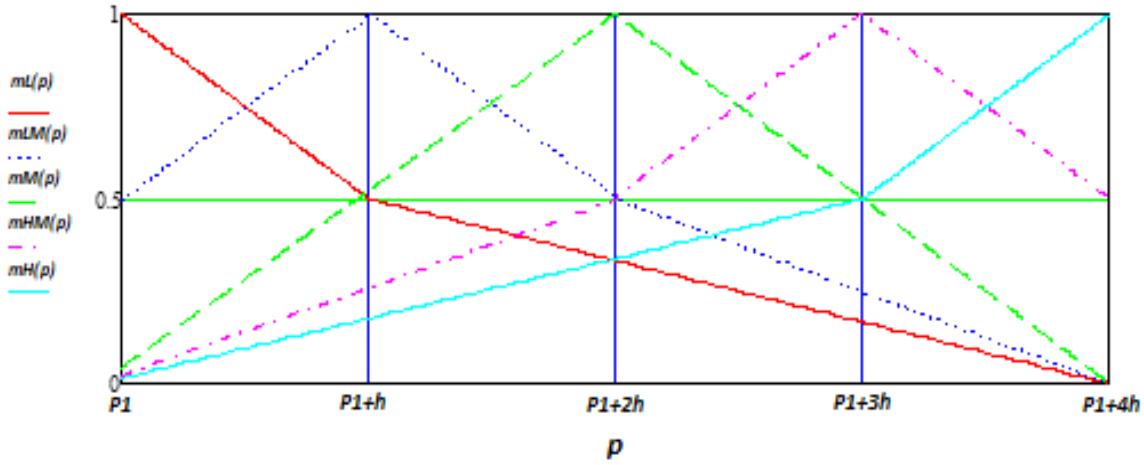

Figure 3.15. Graphic view of the membership function [180]

The membership function in fuzzy sets quantifies the degree to which an object belongs to a particular set. For instance, in a fuzzy set representing "tall people," an individual who is 180 cm tall might have a membership value of 0.8, indicating a high degree of membership, while someone who is 160 cm tall might have a membership value of 0.3. This approach allows for the modeling of concepts that are inherently imprecise, reflecting the complexity of human reasoning and decision-making processes.

Fuzzy logic systems utilize these fuzzy sets to handle reasoning that is approximate rather than fixed and exact. This is particularly

useful in situations where information is incomplete or uncertain, as it allows for the incorporation of human-like reasoning into computational models. Fuzzy logic has found applications across various domains, including control systems, decision-making, artificial intelligence, and expert systems, where it can effectively manage the ambiguity and variability of real-world data.

Moreover, fuzzy logic provides a framework for formulating rules that govern the behavior of systems. These rules are typically expressed in the form of "if-then" statements, which can capture the relationships between different variables in a way that reflects human reasoning. For example, a rule might state, "If the temperature is high, then the fan speed should be increased." Such rules can be combined and manipulated to create sophisticated models that can adapt to changing conditions and provide robust solutions to complex problems.

Fuzzy logic, grounded in the principles of fuzzy sets and characterized by the use of membership functions, provides a robust framework for modeling uncertainty and imprecision. Its capacity to represent degrees of membership allows for a more nuanced understanding of complex phenomena, facilitating human-like reasoning in decision-making processes. This makes fuzzy logic an invaluable approach across various fields, including control systems, artificial intelligence, and data analysis, where it enhances the effectiveness of decision-making and operational control in intricate systems.

However, when considering the application of fuzzy logic in the context of large databases of input polarization images, it is essential to evaluate the efficiency and practicality of different decision support system (DSS) methodologies. While fuzzy logic offers significant advantages in handling uncertainty, alternative approaches, such as neural network technologies, may provide superior performance with less computational effort. Neural networks, particularly deep learning models, excel in processing large datasets and can automatically learn complex patterns and features from the data without the need for explicit rule formulation.

Thus, in scenarios involving extensive and intricate datasets, the selection of a decision support system may favor neural network technologies over fuzzy logic, particularly when the goal is to optimize performance and reduce the effort required for model development and implementation. This consideration underscores the importance of

choosing the appropriate methodology based on the specific characteristics of the data and the requirements of the application.

2.4.4 Decision support systems based on neural network technologies

Decision support systems (DSS) that leverage neural network technologies have gained significant traction due to their ability to model complex relationships and patterns within data. Neural networks, inspired by the biological neural networks of the human brain, are particularly adept at handling non-linear relationships, making them suitable for a wide range of applications in decision-making processes.

A neural network is a computational model composed of interconnected nodes, or neurons, which process information in a manner analogous to the way human neurons operate. These networks can perform various tasks, including recognition, classification, processing, and visualization of data [181, 182, 183]. The architecture of a neural network typically consists of an input layer, one or more hidden layers, and an output layer, allowing for the transformation of input data into meaningful outputs.

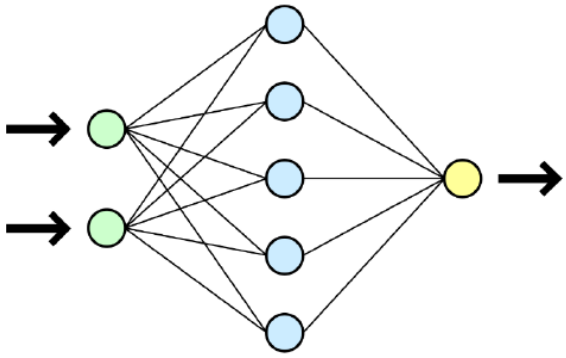

Figure 3.16. Structural diagram of a simple neural network [184]

Figure 3.16 illustrates the structural diagram of a simple neural network, showcasing the flow of information through the various layers [184]. The primary building block of this architecture is the artificial neuron, which applies an activation function to its inputs to produce an output. Figure 3.17 depicts the structure of an artificial neuron alongside various activation functions that can be employed to introduce non-linearity into the model [185, 186, 187].

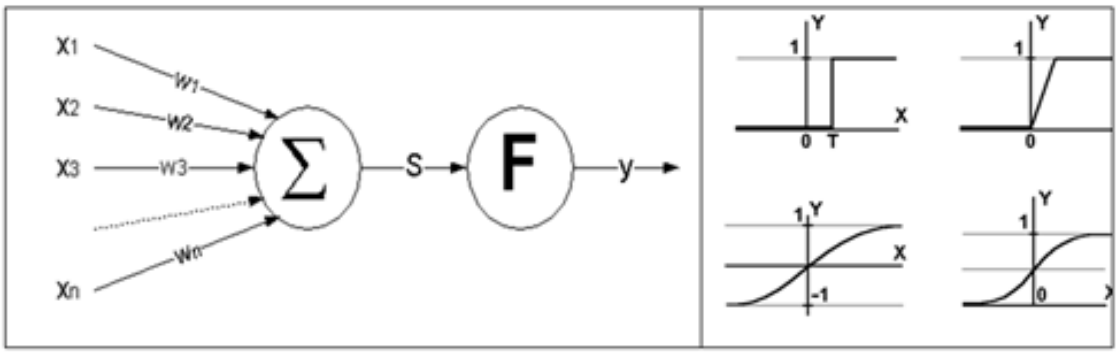

Figure 3.17. The structure of an artificial neuron (left) and a view of some activation functions (right) [188]

When designing a decision support system based on neural network technologies, it is essential to consider the different types of neural networks available, each with its unique characteristics and advantages:

1. **Multilayer Perceptron (MLP)**: The multilayer perceptron is one of the most widely used neural network architectures. It consists of multiple layers of neurons arranged in a feedforward manner: an input layer, one or more hidden layers, and an output layer. MLPs are particularly effective for static processes and can handle large datasets, making them suitable for various classification and regression tasks [187, 189]. Their ability to learn complex mappings from inputs to outputs makes them a popular choice for decision support systems in fields such as finance, healthcare, and marketing.

2. **Recurrent Neural Network (RNN)**: Recurrent neural networks are designed to process sequential data by incorporating feedback connections. Unlike traditional feedforward networks, RNNs allow their outputs to be fed back into the network, enabling them to maintain a memory of previous inputs. This characteristic makes RNNs particularly well-suited for tasks where the order of inputs is significant, such as time series forecasting, natural language processing, and speech recognition [189, 190, 191, 192]. In decision support systems, RNNs can analyze trends over time and provide insights based on historical data.

3. **Associative Memory Networks**: This category includes networks such as Hopfield networks, which consist of a single layer of neurons with feedback connections. These networks evolve over time, changing their states until they reach a stable equilibrium. The properties of the weight matrix are designed to ensure convergence to a

steady state, which can be useful in applications requiring pattern recognition and retrieval of stored information. Associative memory networks can enhance decision support systems by providing quick access to relevant information based on partial inputs.

4. **Spike Networks**: Spike networks represent a specialized class of neural networks where the signal is conveyed not by numerical values but by a series of discrete pulses, or spikes, that share the same amplitude and duration. In this framework, information is encoded in the timing and intervals between these spikes, rather than their amplitude. Spiking neurons at the output generate single spikes or bursts, closely mimicking the processes occurring in the human brain. This approach allows for a rich representation of temporal information, making spike networks suitable for applications that require real-time processing and dynamic input handling.

5. **Convolutional Neural Networks (CNNs)** are a specialized class of neural networks designed primarily for processing structured grid data, such as images. A CNN typically consists of one or more convolutional layers, which may be combined with pooling layers and fully connected layers, often utilizing variations of multilayer perceptrons. The primary function of the convolutional layers is to apply a convolution operation to the input data, which effectively extracts features while reducing the dimensionality of the data [115, 174].

In a convolutional neural network, the convolution operation employs a small, limited matrix of weights known as the convolution kernel or filter. This kernel is systematically "slid" or convolved across the input layer, producing an activation signal for the corresponding neuron in the next layer at each position. This process allows the network to capture local patterns and spatial hierarchies within the data. Importantly, the same weight matrix is applied across different regions of the input, which significantly reduces the number of parameters that need to be learned. This weight-sharing mechanism not only enhances computational efficiency but also improves the network's ability to generalize across various inputs [190].

The architecture of CNNs typically includes several key components:

- **Convolutional Layers**: These layers perform the convolution operation, extracting features from the input data. Each convolutional

layer can have multiple filters, allowing the network to learn different features at various levels of abstraction.

- **Activation Functions**: After the convolution operation, an activation function (commonly the Rectified Linear Unit, or ReLU) is applied to introduce non-linearity into the model. This step is crucial for enabling the network to learn complex patterns.
- **Pooling Layers**: Pooling layers are often employed to down-sample the feature maps produced by the convolutional layers. This process reduces the spatial dimensions of the data, helping to decrease computational load and mitigate overfitting. Common pooling techniques include max pooling and average pooling.
- **Fully Connected Layers**: At the end of the network, one or more fully connected layers are typically used to combine the features extracted by the convolutional and pooling layers. These layers produce the final output of the network, which can be used for classification or regression tasks.

Convolutional neural networks leverage the convolution operation to efficiently process and analyze structured data, particularly images. By utilizing small weight matrices and applying them across different regions of the input, CNNs can achieve deeper architectures with fewer parameters, making them highly effective for a variety of applications, including image recognition, object detection, and video analysis.

In conclusion, decision support systems based on neural network technologies provide powerful tools for modeling complex data relationships and enhancing decision-making processes. By selecting the appropriate neural network architecture—whether it be a multilayer perceptron, recurrent neural network, associative memory network, spike network, or convolutional neural network—practitioners can optimize the performance of their DSS to meet specific application needs. The adaptability and learning capabilities of neural networks make them invaluable across various domains, enabling more informed and effective decision-making. Table 3.2 summarizes the key advantages and disadvantages of the main types of neural networks.

Table 3.2

Advantages and disadvantages of the main types of neural networks [174]

Network type	Advantages	Disadvantages
Multilayer perceptron	well studied, works well with simple tasks	inability to work with dynamic processes, the need for a large training sample
Recurrent perceptron	works well with dynamic processes	the difficulty of finding errors obtained in the process of training or network operation
Associative memory	a very fast learning process, since a system of equations is used instead of gradient descent; the ability to remove an image from memory without disturbing others	a rather narrow class of problems to which it can be applied, the inability to generalize examples, the maximum amount of memory is strictly tied to the dimension of the vector
Spike networks	interesting for studying biological networks	almost any practical use seems unreasonable, as other types of networks do just as well
Convolutional neural networks	one of the best algorithms for image recognition and classification; much less weight; parallelization of calculations; relative resistance to image rotation or shift	too many network variables; it is not clear for which task and computing power which settings are required. All these parameters significantly affect the result, but are chosen empirically by researchers

3 Method and architecture of information system for diagnosis of diabetic retinopathy

3.1 Method of pre-processing of the obtained images of the affected areas of the eye

Diabetic retinopathy can progress through four stages: (i) Mild non-proliferative retinopathy, which is associated with microaneurysms (MA) and is considered an early stage. (ii) Moderate non-proliferative retinopathy, in which the blood vessels supplying the retina may become deformed and swollen as the disease progresses, losing their ability to transport blood. (iii) Severe non-proliferative retinopathy leads to impaired retinal blood supply due to occlusion of a large number of blood vessels, thereby signaling the retina to grow new vessels. (iv) Proliferative diabetic retinopathy (PD) is an advanced stage in which growth signals released by the retina activate the proliferation of new blood vessels that grow along the inner lining of the retina into a vitreous gel that fills the eye. Newly formed blood vessels are loose, due to which they bleed and leak more often. Moreover, the associated scar tissue can contract, causing retinal detachment, resulting in permanent vision loss [123, 130].

To explore and overcome these challenges, the paper focuses on obtaining the optimal model using machine learning, which will include classical neural networks (NN), deep neural networks (DNN), and convolutional neural networks (CNN). Neural networks follow the concept of the biological brain. The results are often difficult to achieve because biological neurons are more complex than these artificial ones, and researchers have also succeeded on some levels. Neural networks worked well, but due to the increased complexity and size of data, there was a need for advanced methods, which led to the emergence of deep learning concepts. Hierarchical approaches to learning attributes appeared before deep learning, but due to problems such as vanishing gradients, they began to lose their aura, as it often becomes difficult to obtain the desired results when tracking features. Deep learning models such as DNN and CNN have provided a solution to overcome this gradient lift problem. This also shows clustering of the fuzzy C-means if the data had any missing labels when the image classification is performed at later stages. So, to predict labels, Fuzzy C-Means [193] is applied to find clusters.

The dataset we used is a FUNDUS image [194] of the human retina with a pixel size of over 2000x3000. The dataset is downloaded from kaggle.com [141, 166, 172, 173, 195, 196, 197], it is freely available on the website, the dataset contains more than 35000 training images and 15000 testing images. The problem with the dataset is that its resolution varies for different images, and the image itself contains noise, so proper filtering is required to get the correct dataset.

It is worth noting that a very important stage in the preparation and construction of an informational automated decision support system is the correct selection of informative parameters, as well as image processing for analysis.

One of these steps is to remove noise from the images to improve the selection of informative features of this or that diagnostic group.

For further work, these mechanisms are followed by image pre-processing and classification to improve the accuracy of the next steps. Pre-processing of the image begins with the conversion of the given characteristics of the image into a gray scale for further analysis. The image classification steps work to classify the images according to the listed features, which allows you to get the desired results.

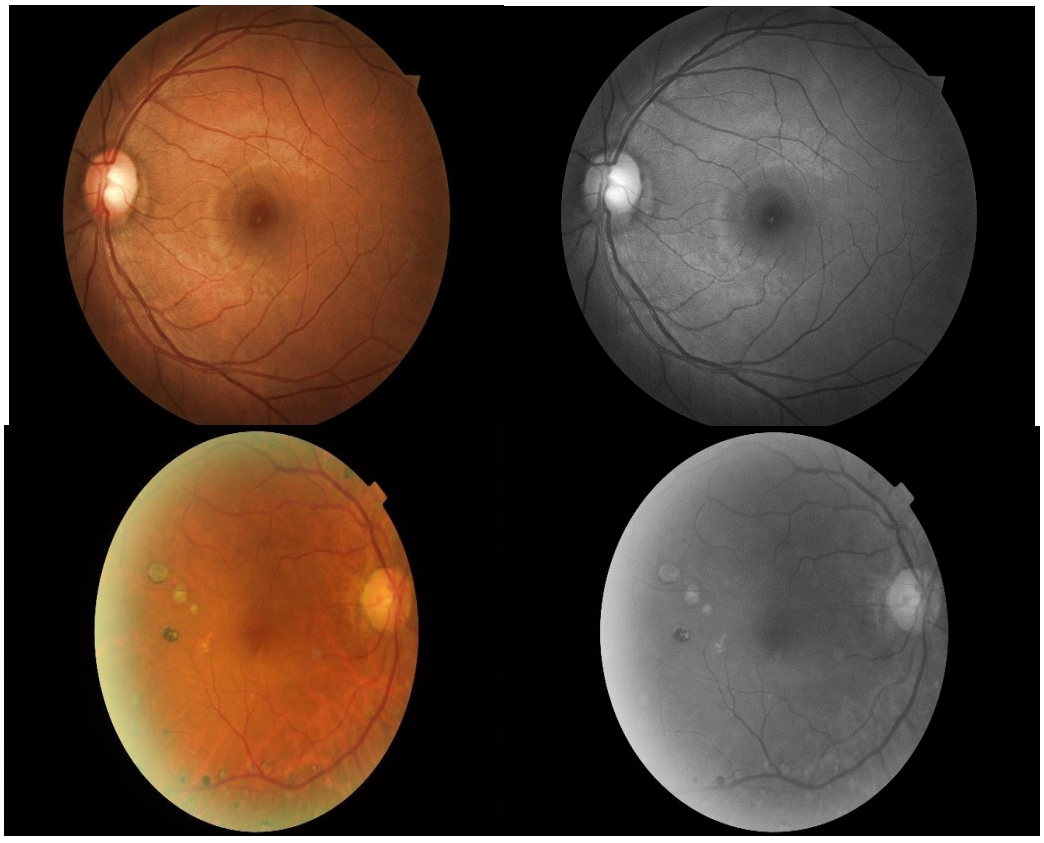

Figure 4.1. Conversion to grayscale

For work on diabetic retinopathy, for [103] image-based tactics, a given retinal image can be divided into several small sub-images. The work also includes noise reduction, as well as obtaining an improved image and accurate data. The paper uses a median filter, a non-linear digital filtering procedure used to remove noise for improved results. This method is better because under certain conditions the filter preserves edges while removing noise. The key idea behind a median filter is to work with the signal from one record followed by another, switching each record with the median of the neighboring records. If a window (ie, a neighbor sample) has an odd number of entries, then the median is the mean when all the entries in the window are numerically sorted, whereas for a given even number of entries there may be more than one median. That is, despite replacing the pixel value with the average value (as in the median filter method for image processing noise reduction) of neighboring pixels, it is replaced with the median value. The work included edge detection, among other things, because edge detection aims to detect points in an image where there is a sharp change in image brightness or some discontinuities. Existing edge detection methods can be grouped into two broad categories: the gradient method and the Laplace method. The gradient method detects edges by observing the minimum and maximum in the first derivative image, while the Laplace method looks for zero crossings present in the second derivative image to find the edges. These concepts complete the work done in image processing

Median filter is quite a convenient method of information processing, especially for noisy images. The filter works with matrices of different sizes, but unlike the convolution matrix, the size of the matrix affects only the number of pixels under consideration.

The median filter algorithm is as follows: for the current pixel, the pixels that "fall" into the matrix are sorted, and the average value from the sorted array is selected. This value is the output for the current pixel.

Below is the performance of the median filter for a kernel size of three (Figure 4.2).

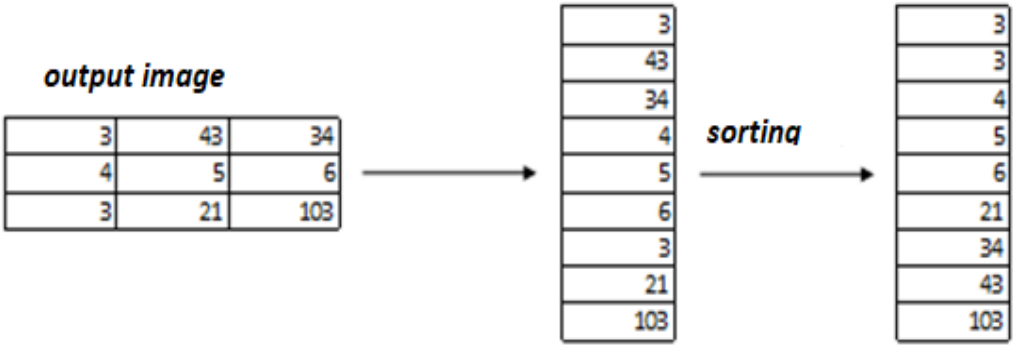

Figure 4.2. The median filter

The figure shows an example of the results of the median filter, which does an excellent job of removing noise (Figure 4.3).

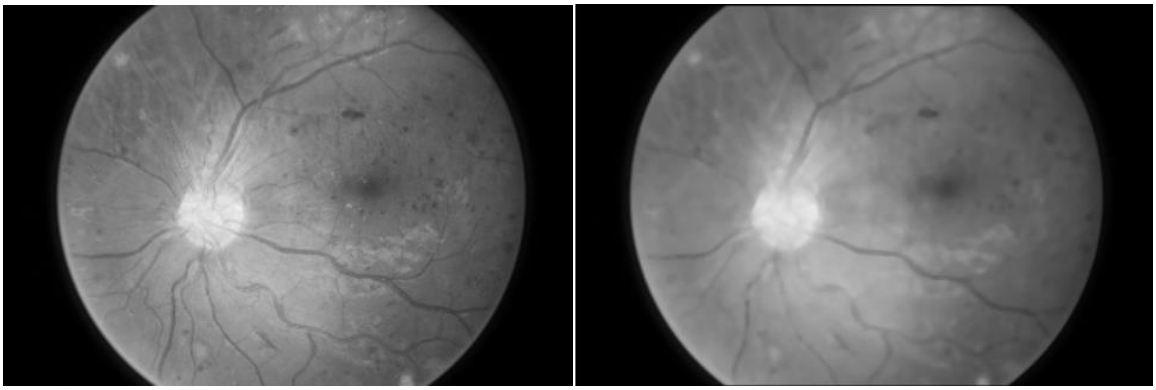

Figure 4.3. Median filter performance results

Also, to facilitate work with data, it is worth cutting off non-informative parts of images, such as black background outside the retina. This will help to save the computing power of the system, and also help to work more accurately with the informative indicators of the images for different nosologies. Since we have a fairly significant amount of researched data, it was decided to automate the process as follows:

- taking into account the fact that the image of the retina is in most cases located in the center of the investigated element, it is worth searching for the middle of the horizontal and vertical sides of the image;

- after that, alternately shift one pixel down and to the left, respectively (for the horizontal and vertical sides) and check the pixel value of the image;

- if the values of several, for example, three pixels in a row are different from zero (their color is not black), then it is worth taking these coordinates for cropping the image (Fig. 4.4 a, b)

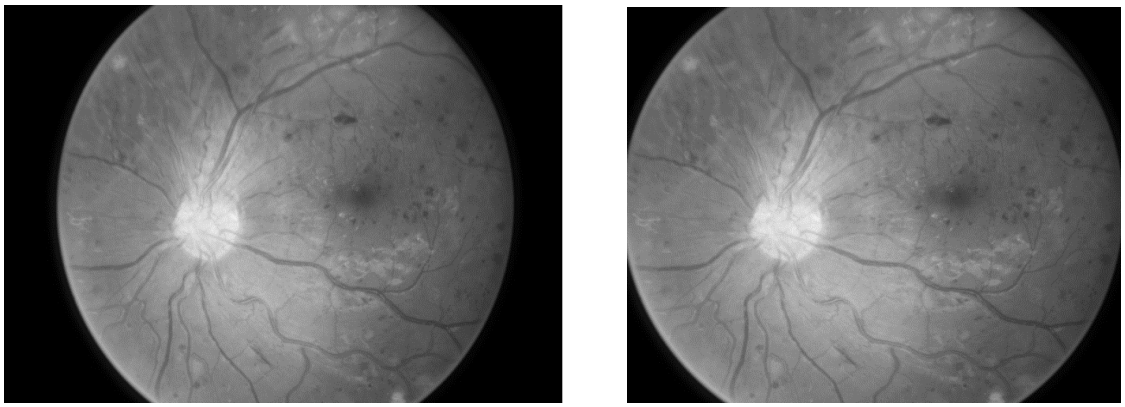

a) b)

Figure 4.4. Cropping the image

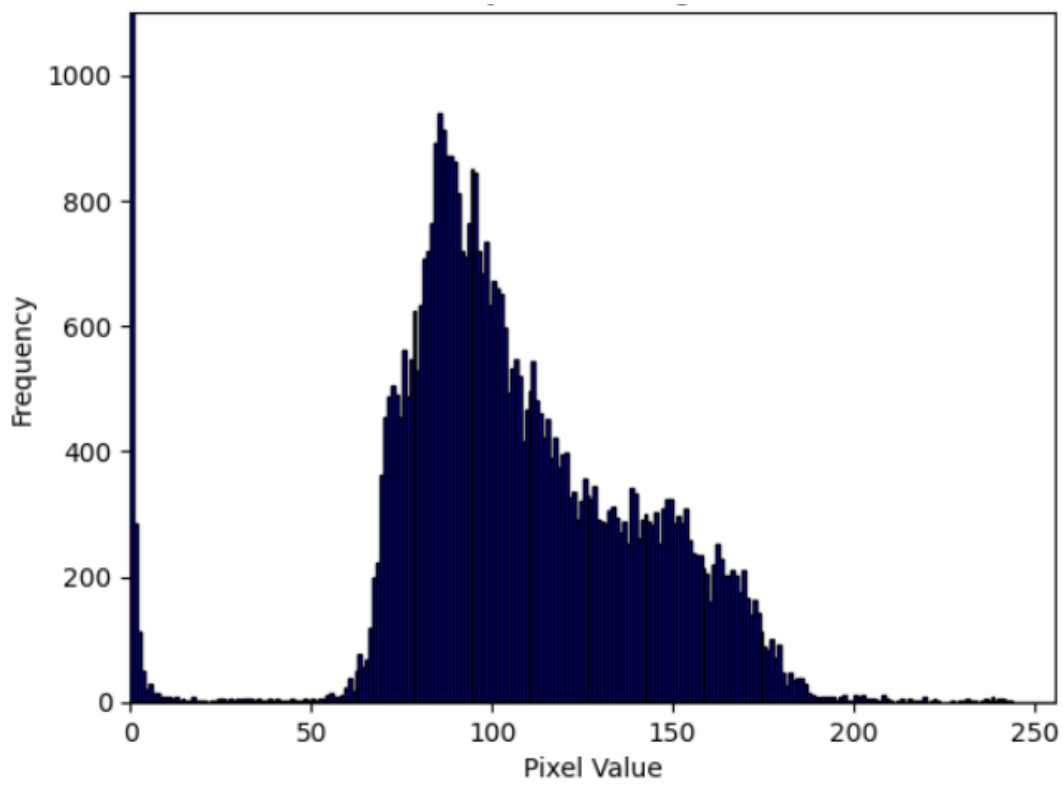

Figure 4.5. Histogram of the retinal image before processing

It is also worth noting that in order to significantly save computing resources, it is worth significantly reducing the resolution of images, since processing high-resolution images takes quite a lot of time, and with a large training base for this machine learning system, it will use an unreasonably large amount of computer computing resources.

In this case, the oversampling procedure was decided using the pixel area ratio, which allows to significantly reduce the size of the image without losing its informativeness. Listing 4.1 shows the code of

the program for automatically reducing the size of the image to save computer computing resources.

Listing 4.1. Python program code for reducing image size

```
import numpy as np

# Create a numpy array
arr = np.array (cv2.imread(image_path))

# The function to find the index of the element value in the specified row or column
def find_element_index(row, col, element):
    if row is not None:
        index = np.where(arr[row, :] == element)[0]
        if index.size == 0:
            return None
        else:
            return row, index[0]
    elif col is not None:
        index = np.where(arr[:, col] == element)[0]
        if index.size == 0:
            return None
        else:
            return index[0], col

# The path to the image
image_path = '10_left.jpeg'

# An example of using the function
element_index = find_element_index(row=1, col=None, element=6)
print(element_index)  # (1, 2)
```

Figure 4.6 Reducing image resolution

Edge detection: This is one method of feature extraction in which feature boundaries are extracted (i.e., edges of blood clots, white lesions, veins) are detected based on the sudden change of pixel values with the neighboring pixel. intensity. Then the detected pixels will be assigned the value "1" and the remaining pixels of the image or the entire matrix will be assigned the value "0". With this method, the features can be properly identified. The detected edges of the images are a 2D matrix, which in turn can be transformed into a corresponding single array or 1D array vector. The transformation of the matrix takes place in such a way that all the values of the array of rows are located next to each other from the initial to the final position without changing the sequence. A method adapted to edge detection Detection. careful edge method This method detects any abnormal changes in pixel weights (intensity values), such as crusts, depressions, color changes, etc.

$$H_{ij} = \frac{1}{2\pi\sigma^2} exp\left(\frac{\left(i-(k=1)\right)^2+\left(j-(k+1)\right)^2}{2\sigma^2}\right); 1 \le i,j \le (2k+1). \qquad (4.1)$$

The image intensity gradient can be calculated using the following formula

$$G = \sqrt{G_x^2 + G_y^2}, \qquad (4.2)$$

$$\theta = atan2\left(G_y, G_x\right). \qquad (4.3)$$

Listing 4.2. Python program code for calculating and outputting an image histogram

```
import matplotlib.pyplot as plt
import cv2
import numpy as np

def plot_histogram_gray(image_path):
    # Download image using OpenCV
    image = cv2.imread(image_path)

    # Convert the image to grayscale
    gray_image = cv2.cvtColor(image, cv2.COLOR_BGR2GRAY)

    # Calculation of the histogram
    hist, bins = np.histogram(gray_image.flatten(), bins=256, range=[0,256])

    # Output of a bar histogram
    plt.figure()
    plt.title('Grayscale Histogram')
    plt.xlabel('Pixel Value')
    plt.ylabel('Frequency')

    # Output of a bar histogram divided into columns
    plt.hist(gray_image.flatten(), bins=256, range=[0, 256], color='blue', edgecolor='black')
    plt.ylim([0, 100000])  # scale
    plt.xlim([0, 256])
    plt.show()
# The path to the image
image_path = '10_left.jpeg'

# Call the function to display a bar histogram
plot_histogram_gray(image_path)
```

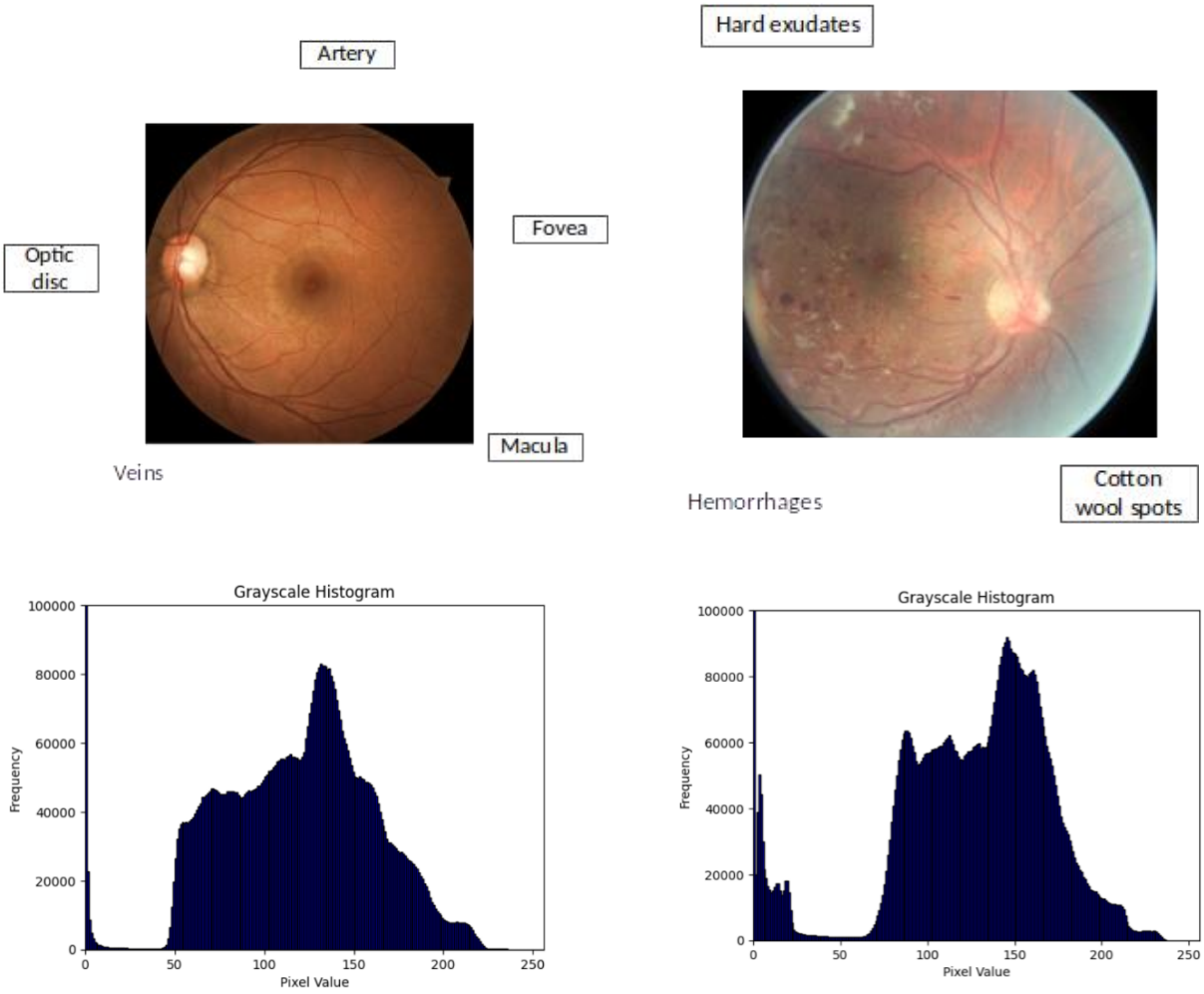

Figure 4.7. Comparison of proliferative diabetic retinopathy (PD) and healthy retina imaging

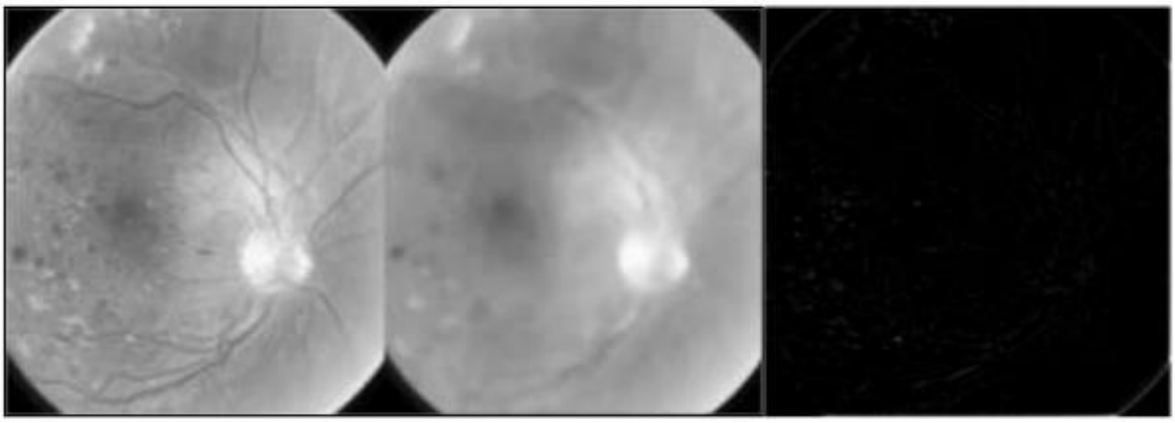

Figure 4.8. Unfiltered image, median-filtered image, and detected image noise

Figure 4.9. Contour detection method levels

Therefore, in this section, software was developed for the analysis and preprocessing of images necessary for the automated diagnosis of diabetic retinopathy.

The input data for the correct operation of the program are images, some of which are given in the appendix, formed and reproduced using the experimental system, the architecture of which is shown in the figure.

An example of fundus images, images after preprocessing, their 2-D histograms and image with selected characteristic features are shown in the figure 4.10 (Listing 4.2).

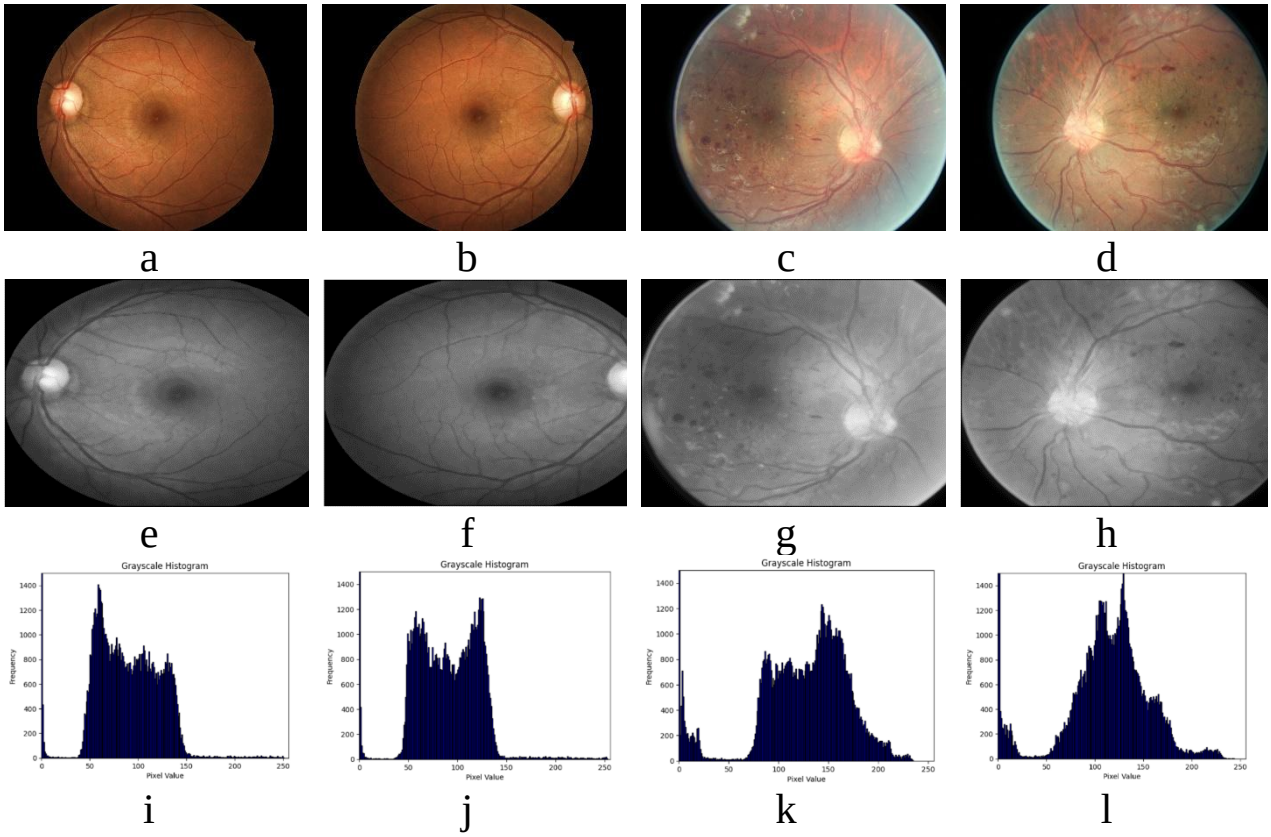

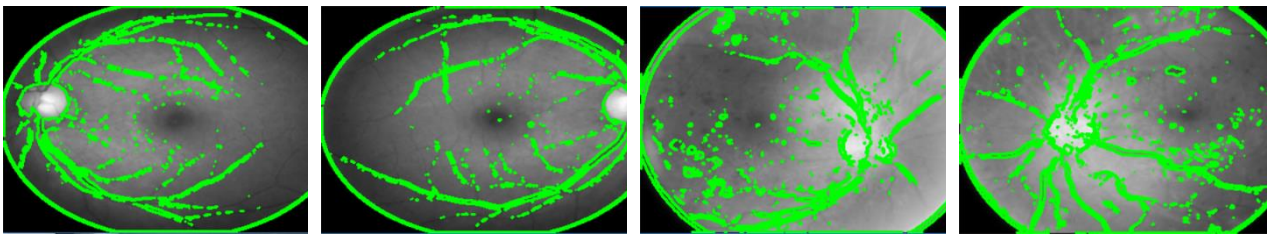

m n o p

Figure 4.10. An example of images of a healthy and diseased retina before processing (a, b, c, d), after processing (e, f, g, h), and their two-dimensional 2*D* distribution histograms (i, j, k, l) and image with selected characteristic features (m, n, o, p)

The method of morphological heterogeneous illusion helps to improve the characteristics of the studied image by removing the bright background of the image to better determine the informative indicators of the object (Figure 4.11).

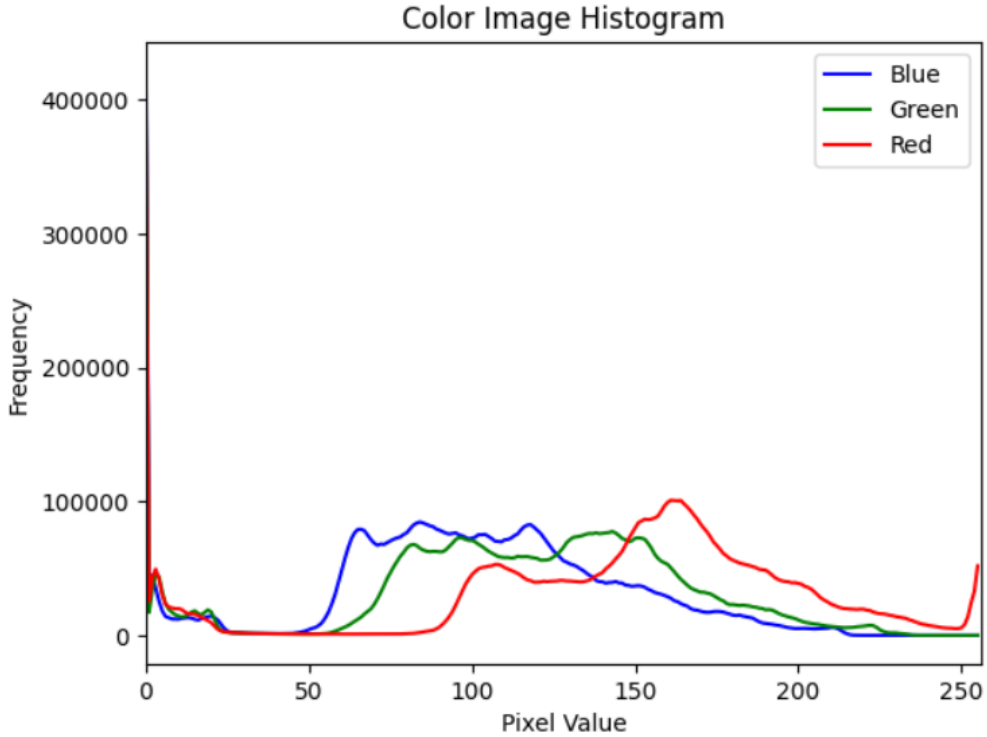

Figure 4.11. Three-dimensional histogram of a three-channel image

By removing the background lighting from the input image, one can observe the noisy features of the object. After removing the image contrast adjustment and its subsequent binarization, the images are converted to RGB, where all functions are quite clearly visible.

3.2 Architecture and algorithm of the diagnostic system

Figure 4.12 presents the extended algorithmic and software architecture of the block for processing and analyzing polarization images, it contains the following main blocks and modules:

–image capture module;

–image saving module;

–the module for forming microcommands for the unit of automatic control of system operation;

–unit for determining the images;

–a unit for reproducing the parameters of the images;

–an analysis unit for determining informative features of coordinate distributions of two-dimensional images;

– user interface module to facilitate operation and system management;

– block of the decision support system.

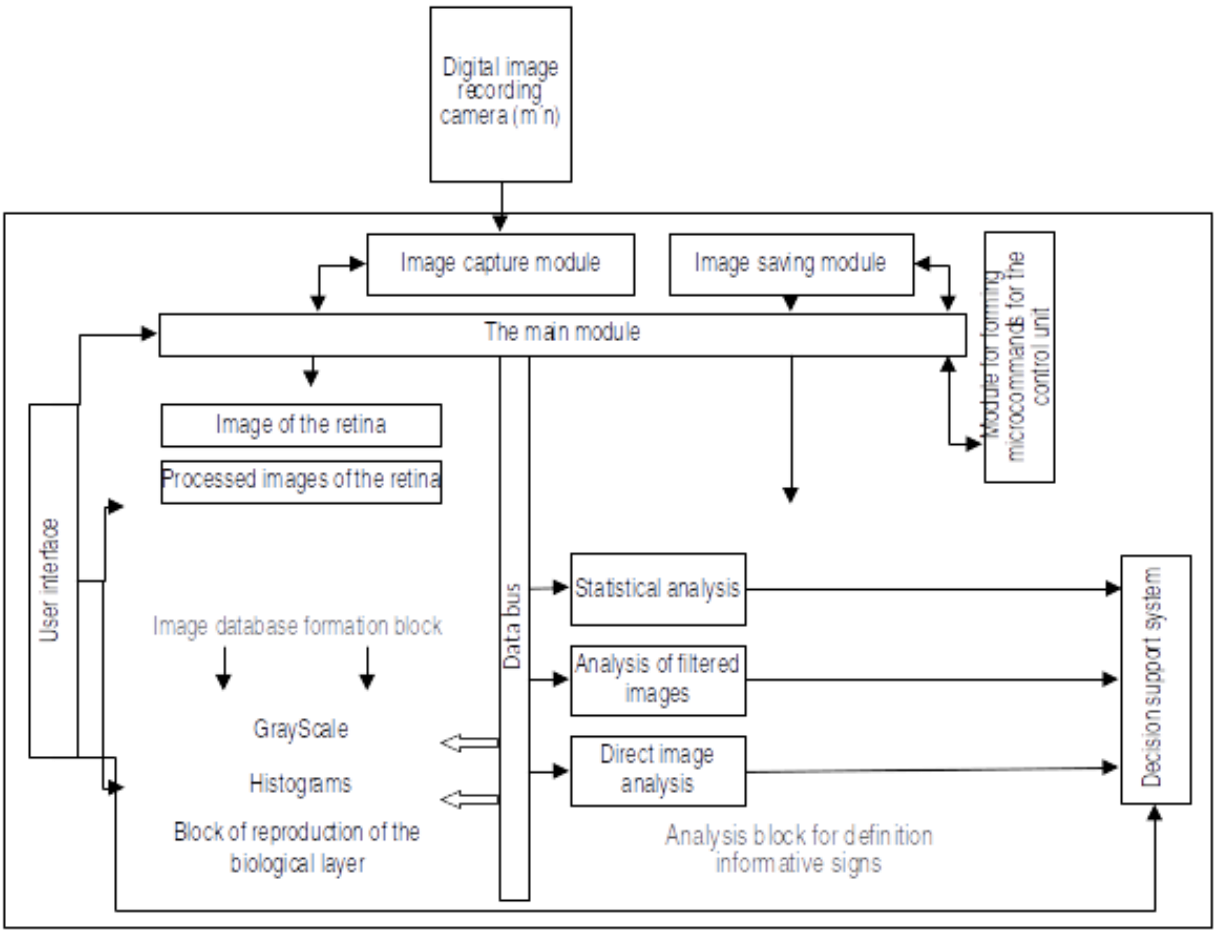

Figure 4.12. Algorithmic and software architecture

Figure 4.13 shows a generalized model architecture of diabetic retinopathy analysis.

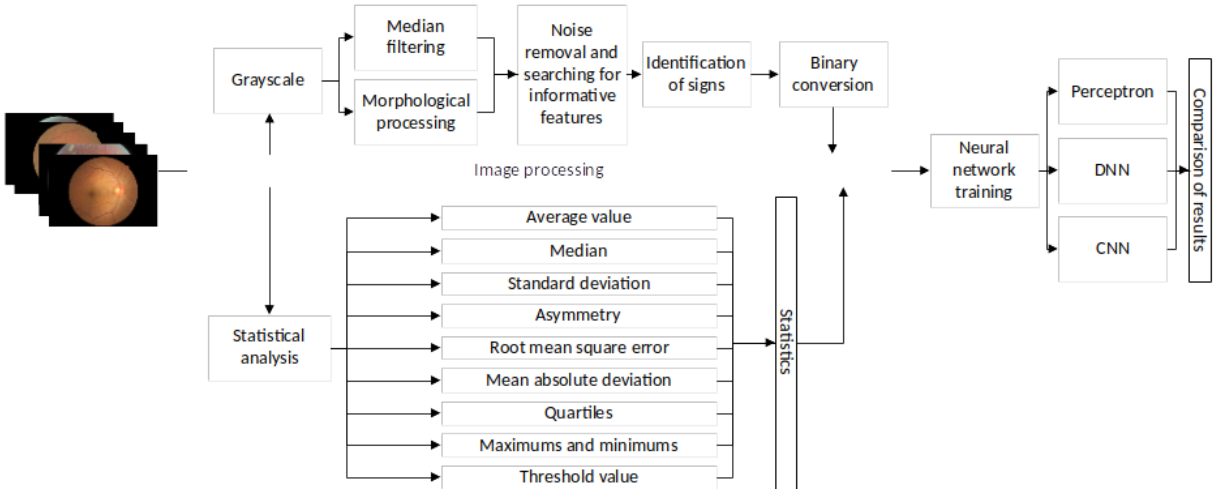

Figure 4.13. Algorithm of the method

3.3 Formation of a database of informative indicators for the diagnosis of the disease

Table 4.1.

Functions selected as statistical indicators

Characteristics	The relationship of each feature to images
Average value	Is a value that provides information about the central tendency of the given data
Median	In a given range of values, the median divides the entire data set, which can also be called the center of all data
Standard deviation	This provides details of how the values vary or differ from the average or mean
Asymmetry	Asymmetry is used to account for the lack of symmetry in the probability distribution of random variables. It is measured as positive, negative and normal
Mean squared error	It was used to determine the difference between the intensity value or values of a pixel in an image
Mean absolute deviation	This is the average distance between the values of each pixel data set from the mean
Quartiles	For the range of pixel values, it is divided into 4

	levels of groups according to the distribution of pixel values
Maximum	This is the maximum value or the largest value in the entire set of pixels
Minimum	This is the minimum value or the smallest value in the entire set of pixels
Threshold	A numeric value that segments the image and is responsible for converting the original or grayscale image to a binary image

Table 4.1 shows the statistical indicators necessary for the calculation and formation of the database for the further classification process.

Therefore, the parameters given in the table were used to form informative features for neural network training. We will give some formulas for calculating data statistical indicators of data arrays.

The statistical moment of the first order characterizes the average value of the coordinate distributions of the measured values; the second - data dispersion, i.e. deviation from the mathematical expectation of values; by the statistical moment of the third order we will understand the value that characterizes the deviation from the normal distribution of the studied data; and the fourth measures the magnitude of the "peak" of the distribution of the matrix element.

$$M_1 = \frac{1}{N}\sum_{k=1}^{N}(|x|)_k\,; \tag{4.4}$$

$$M_2 = \sqrt{\frac{1}{N}\sum_{k=1}^{N}(|x^2|)_k}\,; \tag{4.5}$$

$$M_3 = \frac{1}{M_2^3}\frac{1}{N}\sum_{k=1}^{N}(|x^3|)_k\,; \tag{4.6}$$

$$M_4 = \frac{1}{M_2^4}\frac{1}{N}\sum_{k=1}^{N}(|x^4|)_k. \tag{4.7}$$

where N is the number of elements of the orientation map;

x is the value of the pixel intensity of the k-th pixel of the image.

4 Development of decision-making support technology based on neural network

4.1 Neural network with multilayer perceptron

The first neural network model to be considered is a multilayer perceptron. This is a basic, well-studied model that has several levels of computing units connected to each other by direct communication.

The activation function of this neural network is a sigmoid function with inverse error propagation:

$$f(x) = \sigma(x) = \frac{1}{1+e^{-x}}. \quad (5.1)$$

The error backpropagation algorithm for a multilayer perceptron consists of the following steps and is shown in the Figure 5.1 [4, 31]:

Step 1: Initialize the weights with small random values.

Step 2: If the stop condition is not met, perform steps 3-10.

Step 3: For each training pair, complete steps 4-9.

Direct passage:

Step 4: Each input neuron $x_i = 1 \ldots n$ receives the input signal and propagates it to all neurons in the hidden layer.

Step 5: Each hidden layer neuron $q_i = 1 \ldots q$ sums its weighted input signals:

$$h_j = \sum_{i=1}^{n} w_{ij} * x_i, \quad (5.2)$$

applies the activation function to the received sum, forming the output signal: $v_j = f(h_j)$, which is sent to all neurons of the output layer.

Step 6: Each output neuron y_k, k = 1…m sums the weighted signals:

$$h_k = \sum_{j=1}^{k} w_{jk} * x_j, \quad (5.3)$$

forming, after applying the activation function, the output signal of the network: $y_k = f\ (h_k)$.

Error Backpropagation:

Step 7: Each output neuron compares its output value with the desired objective function and calculates $\delta_k = (t_k - y_k) * f\ (h_k)$, after which the correcting term of the weights is determined: $\Delta w_{jk} = \eta * \delta_k * v_j$, and parameters$\delta_k$ are sent to the neurons of the hidden layer.

Step 8: Each hidden layer neuron v_j sums its $\delta-$ inputs from the output layer neurons:

$$h_k = \sum_{k=1}^{m} \delta_k * x_j, \qquad (5.4)$$

the result is multiplied by the derivative of the activation function to determine δ_i:

$$\delta_i = f\left(h_j\right) * \sum_{k=1}^{m} \delta_k * x_{jk}, \qquad (5.5)$$

and the correcting term is calculated:

$$\Delta w_{jk} = \eta * \delta_k * w_{jk}, \qquad (5.6)$$

Weight adjustment:

Step 9: The weights between the hidden and output layers are modified as follows:

$$w_{jk}(new) = w_{jk}(old) + \Delta w_{jk}, \qquad (5.7)$$

Similarly, the weights between the input and hidden layers are adjusted:

$$w_{ij}(new) = w_{ij}(old) + \Delta w_{ij}, \qquad (5.8)$$

Step 10: The stopping condition is checked: minimizing the error between the desired and actual network output.

With the help of a block diagram, the presented algorithm is depicted in the appendix A, the neural network training program is shown in Listing 5.1.

Listing 5.1. A fragment of Python code for creating and training a perceptron-type neural network

```
import pandas as pd
from keras.models import Sequential
from keras.layers import Dense
from keras.optimizers import Adam

# Loading data from files
input_data = pd.read_csv("Training.csv")
target_data = pd.read_csv("trainLabels.csv")

# Conversion of data into NumPy arrays
X_train = input_data.values
y_train = target_data["Label"].values

# Number of characters in the input data
num_features = X_train.shape[10]

# Number of unique tags in the raw data
num_classes = len(target_data["Label"].unique())

# Creating a multilayer perceptron
model = Sequential()
model.add(Dense(64, activation='relu', input_dim=num_features))
model.add(Dense(32, activation='relu'))
model.add(Dense(num_classes, activation='softmax'))

# Compile the model
model.compile(loss='sparse_categorical_crossentropy',
optimizer=Adam(lr=0.001), metrics=['accuracy'])

# Training the model
model.fit(X_train, y_train, epochs=50, batch_size=8)

# Saving the trained model
model.save('trained_model.h5')

# Completion of training
print("Training is complete")
```

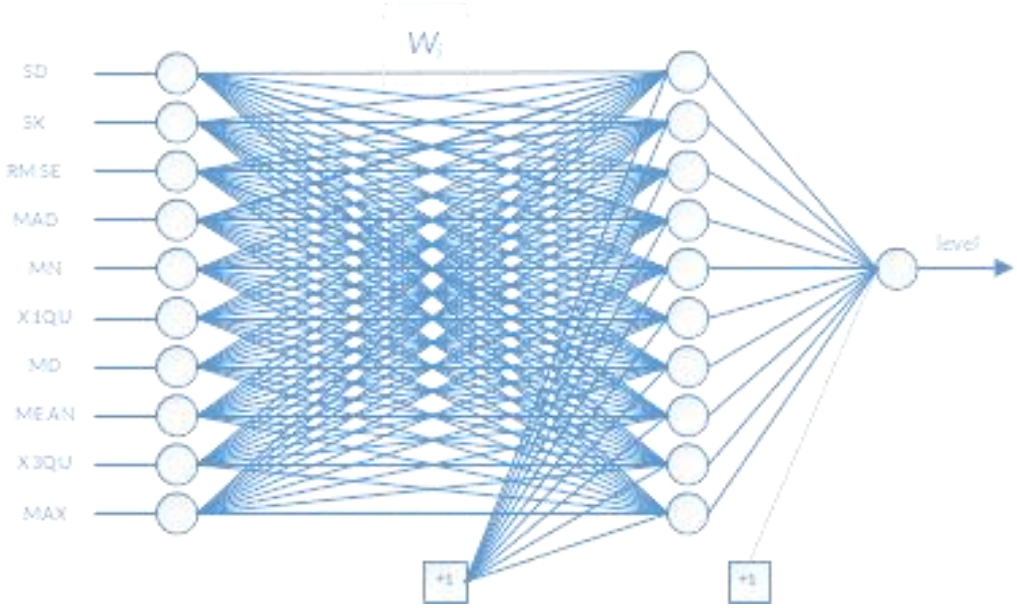

Figure 5.1. Perceptron-type neural network model for statistical data processing

4.2 Deep neural network

A deep neural network (DNN, deep neural network) is a type of NN with many layers of data processing, which transforms input data into output, hierarchically extracting and aggregating features, increasing the level of data abstraction in the direction from inputs to outputs (Figure 5.2).

Compared to shallow NNs, due to the increase in the number of neuroelements and connections, DNDs receive greater computing power and the ability to model more complex dependencies, and due to the specialization of layers and high hierarchical data processing, they become more convenient for human perception and analysis. At the same time, the specialization of data processing layers in DNd makes them more suitable for integration into the network model of a priori information about the subject area. However, as a rule, specific DND paradigms have more limited application in specific tasks (for example, some architectures can only be used for image recognition and are not suitable for other tasks).

With the help of this type of neural network, we will check the accuracy of using this technique. The accuracy of the model should vary due to the use of multiple hidden layers in relation to input-output.

Multi-layering should increase the potential of a small neural network, but it will increase the use of computing resources, so you

should be careful about the number of hidden layers of the neural network used.

The backpropagation method will also be used as a learning algorithm. The weight of neural connections will be updated using the "stochastic gradient descent" algorithm.

$$w_{ij}(t+1) = w_{ij}(t) + \eta \frac{\partial \mathrm{c}}{\partial w_{ij}} + \varepsilon(t), \qquad (5.9)$$

where η is the learning rate,
C is the cost function,
ε(t) is a type of stochastic function,
Algoritm:
Input:
X^n – is a training sample
η is the learning rate
λ is the smoothing parameter of the functional Q
Output:
Weights vector w
Body:

1. Initiate weights $w_i, (j = 0, \dots, k, wherek - dimensionalityofthefeaturespace)$;
2. Initiate the current evaluation of the functionality:

$$Q = \sum_{i=1}^{n} L\,(a(x_i, w), y_i); \qquad (5.10)$$

3. Repeat:

a. Calculate the object x_i from X^n (for example randomly);

b. Calculate the output value of the algorithm$a(x_i, w)$ and error:

$$\varepsilon_i = L(a(x_i, w), y_i); \qquad (5.11)$$

c. Take a gradient descent step:

$$w = w - \eta L_a(a(x_i, w), y_i)\varphi\,(\langle w, x_i \rangle)x_i; \qquad (5.12)$$

d. Evaluate the value of the functional:

$$Q = (1 - \lambda)Q + \lambda_{\varepsilon_i}. \quad (5.13)$$

4. Until the value of Q stabilizes and/or the weights w stop changing.

Listing 5.2. A fragment of Python code for creating and training a deep neural network

```
import pandas as pd
import numpy as np
from keras.models import Sequential
from keras.layers import Dense
from keras.optimizers import Adam

# Download data from files
input_data_file = "Training.csv"
target_data_file = "trainLabels.csv"

input_data = pd.read_csv(input_data_file).values
target_data = pd.read_csv(target_data_file).values

# Data dimensionality check
print("The dimensionality of the input data:", input_data.shape)
print("The size of the labels:", target_data.shape)

# Data normalization
input_data = (input_data - input_data.mean()) / input_data.std()

# Number of functions (number of columns in the input data)
num_features = input_data.shape[1]

# Number of classes (number of unique labels)
num_classes = len(np.unique(target_data))

# We divide the data into training and validation samples
split_ratio = 0.8
split_index = int(split_ratio * len(input_data))
```

```
    x_train, x_val = input_data[:split_index], input_data[split_index:]
    y_train, y_val = target_data[:split_index], target_data[split_index:]

    # Building a DNN model
    model = Sequential()
    model.add(Dense(128, activation='relu',
input_shape=(num_features,)))
    model.add(Dense(64, activation='relu'))
    model.add(Dense(num_classes, activation='softmax'))

    # Compile the model
    optimizer = Adam(lr=0.001)
    model.compile(optimizer=optimizer,
loss='sparse_categorical_crossentropy', metrics=['accuracy'])

    # Training the model
    epochs = 50
    batch_size = 32

    model.fit(x_train, y_train, epochs=epochs, batch_size=batch_size,
validation_data=(x_val, y_val))

    # Assessment of model accuracy on test data
    test_loss, test_accuracy = model.evaluate(x_test, y_test)
    print("Accuracy on test data:", test_accuracy)
```

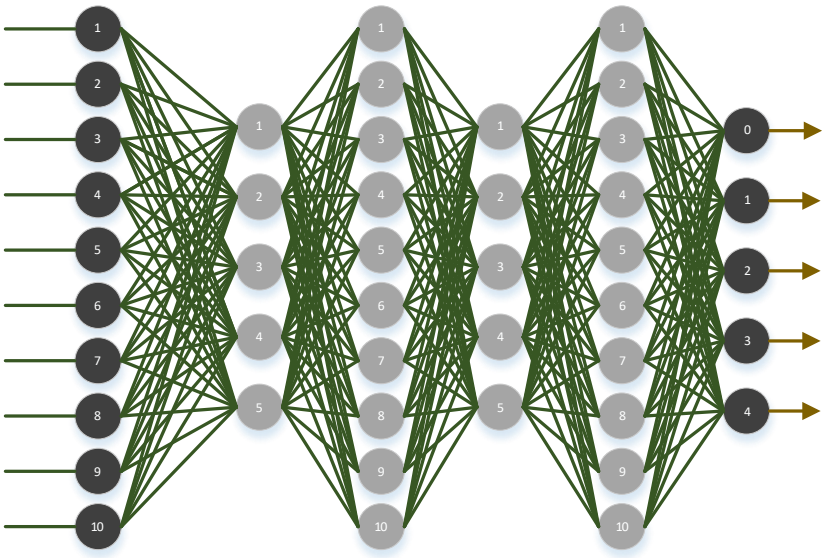

Figure 5.2. The structure of a deep neural network

This program uses the TensorFlow library to build and train a DNN neural network (Listing 5.2). The model has three layers: two layers with 64 neurons and the ReLU activation function, and an output layer with one neuron (no activation for regression). The mean squared error (MSE) as the loss function and the mean absolute error (MAE) as the model evaluation metric are used. The model is trained on 1000 examples with 10 inputs and responses for 50 epochs.

4.3 Convolutional neural network

Convolutional neural networks (CNN, ConvNet) are deep direct propagation ANNs. In fact, they are a type of BNN adapted to image processing. Convolutional networks (Figure 5.3) are inspired by the organization of the visual cortex of animals, where individual cortical neurons respond to stimuli only in a limited area of the visual field (receptive field). The receptive fields of different neurons partially overlap in such a way that they cover the entire visual field.

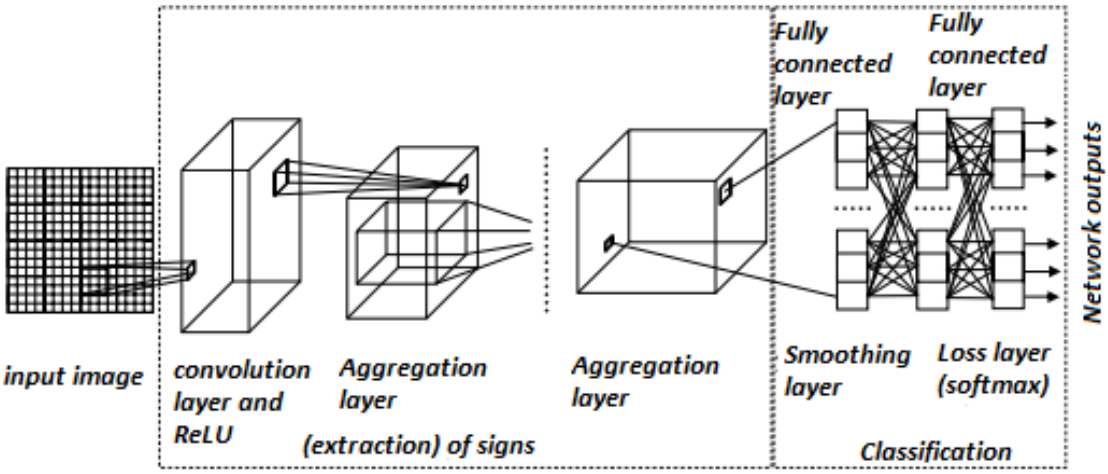

Figure 5.3. Scheme of a convolutional neural network [198]

The CNN consists of input and output layers, as well as several hidden layers. In contrast to the general BNN paradigm, the hidden layers of CNN are usually specialized and consist of convolutional layers, aggregation layers, fully connected layers, and normalization layers.

Only image data is used for the CNN training model. Processed single-channel images are fed to the input of the neural network.

Listing 5.3. A fragment of Python code for creating and training a convolutional neural network

```
import numpy as np
import tensorflow as tf
from tensorflow.keras import layers, models

# Loading data and labels
images = np.load("images.npy")
labels = np.load("trainLab.npy")

# Normalize images to range [0, 1]
images = images.astype("float32") / 255.0

# Separation of data into training and validation sets
split_ratio = 0.8
split_idx = int(len(images) * split_ratio)
train_images, val_images = images[:split_idx], images[split_idx:]
train_labels, val_labels = labels[:split_idx], labels[split_idx:]

# Creation of convolutional neural network architecture
model = models.Sequential()
model.add(layers.Conv2D(32, (3, 3), activation='relu',
input_shape=(height, width, channels)))
model.add(layers.MaxPooling2D((2, 2)))
model.add(layers.Conv2D(64, (3, 3), activation='relu'))
model.add(layers.MaxPooling2D((2, 2)))
model.add(layers.Conv2D(64, (3, 3), activation='relu'))

# Adding a fully connected layer for classification
model.add(layers.Flatten())
model.add(layers.Dense(64, activation='relu'))
model.add(layers.Dense(num_classes, activation='softmax')) #
num_classes - the number of classes to classify

# Compile the model
model.compile(optimizer='adam',
              loss='sparse_categorical_crossentropy',
              metrics=['accuracy'])
```

```
# Training the model
batch_size = 32
epochs = 10
model.fit(train_images, train_labels, batch_size=batch_size,
epochs=epochs, validation_data=(val_images, val_labels))

# Model evaluation on test data
test_loss, test_accuracy = model.evaluate(val_images, val_labels)
print(f"Test accuracy: {test_accuracy}")
```

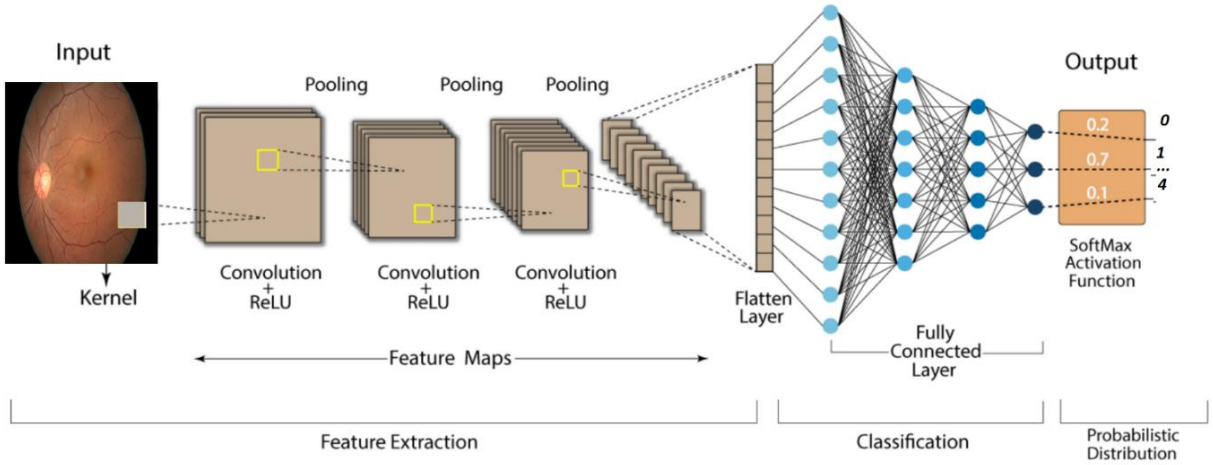

Figure 5.4. The CNN model for image classification [199]

This program uses a convolutional neural network with one convolutional layer, a pooling layer, a flat layer, and two fully connected layers. The convolutional layer has 32 filters with kernel size (3, 3) and ReLU activation function. After the convolution layer, a pooling layer with size (2, 2) is applied, which helps reduce the size of the image. The plane layer is then used to transform the raw data into a vector before passing it to the fully connected layers. When using the "MNIST" dataset with 35,000 retinal images containing 28x28 pixels, training will take much longer (Figure 5.4).

4.4 Development of a graphical user interface

Since the final product of this research involves its use by a doctor without the involvement of an additional specialist in setup and operation, it is necessary to develop a simple, intuitive user interface.

In order for the entire system to function in one program package, and it was distributed under a free license, Python programming language tools were also used to develop the graphical interface. We will use the Tkinter library in Python to create the graphical interface of the system for the diagnosis of diseases of the fundus, as indicated. To load and display images, we will use the Pillow library.

One of the important advantages is that Python is a platform-independent language, which allows software development to be abstracted from the settings of a specific operating system. Using Python to develop a software product allows you to reduce a number of requirements for the user's computer, on which the software will be installed.

Python also has a wide range of libraries and frameworks that can be used in software development to greatly simplify its structure. So, in this programming language, there are, for example, libraries for reading and converting images of various formats into numerical arrays, which is a necessary step for performing image analysis.

Given that Python is distributed under an open license, is an object-oriented programming language, has the necessary tools to implement all software functionality, in particular, libraries for working with images, technology for working with various DBMS, technology for creating graphical interfaces, this language was chosen for the implementation of the software.

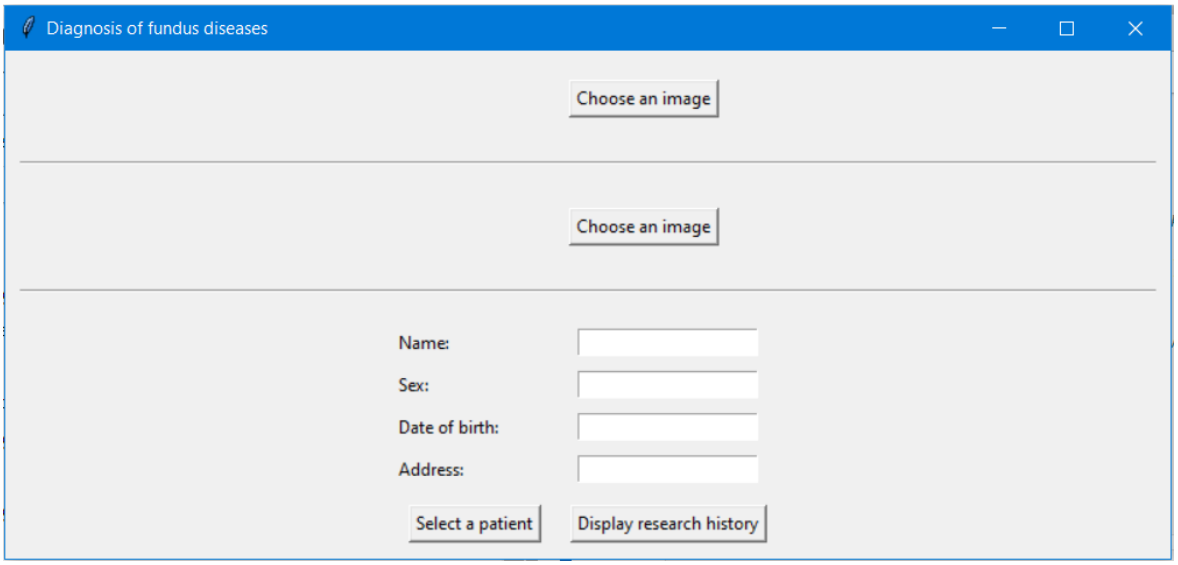

Figure 5.5. The main window

If necessary, it is possible to download already measured images of the human retina. After the user uploads an image or takes new

measurements called from the created panel, the selected maps will be loaded and displayed on the main application window. Also, in further studies, it is planned to combine the created database with work with different DBMS.

The appearance of the main window at the initial stage of work is shown in Figure 5.5. This program includes the ability to select ready-made images of the retina and further work with them. It is also possible to search by patient and display the research history of this patient.

It is possible to save data and diagnoses for further search and work with them. The methods of image processing and statistical analysis discussed in the previous sections have already been added to the logic of the graphical interface program.

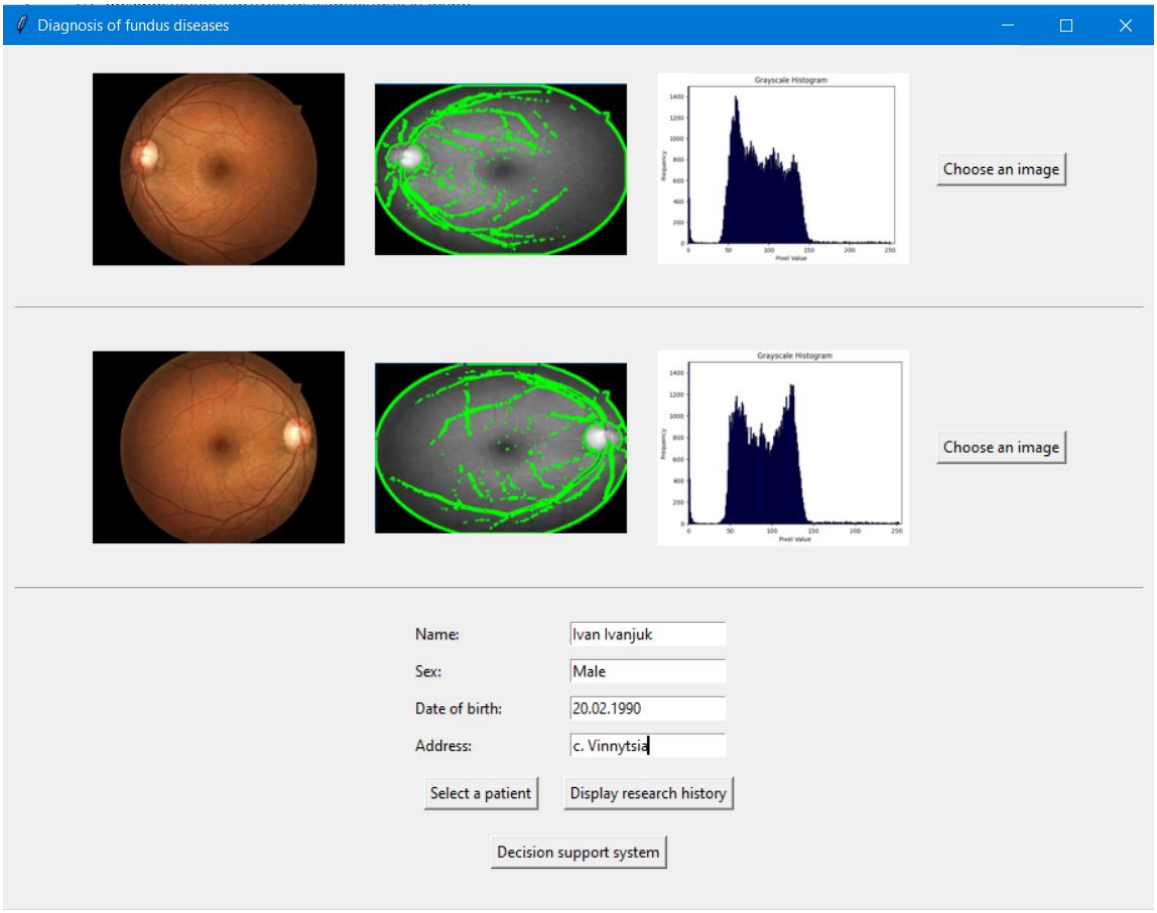

Figure 5.6. The main window with all activated functions

The analysis unit is completely abstracted from the graphical interface and data visualization and outputs formed arrays of statistical and correlation moments, which are then displayed to the user and used as informative features in the decision-making process based on neural network technology methods. At this stage of the research, there is an

opportunity to choose a method that will support decision-making (multilayer perceptron, DNN, CNN).

Clicking the "choose image" button activates the ready image selection window. In order to choose an image, you need to highlight the desired row of the table by clicking on it and click the "select" button. After that, the main window will display the selected image itself, the processed image with informative parameters highlighted, the distribution histogram and the recommended diagnosis. In order not to overload the main program window with digital data, calculated statistical indicators are not displayed. You can familiarize yourself with them in the created database of measurement histories.

Clicking on the button "Display history of studies" displays a table with pre-recommended diagnoses.

The main window with all activated functions looks as shown in Figure 5.6.

4.5 Assessment of classification reliability and discussion of results

After the diagnostic system is trained on the training data, it is tested using the data that was excluded from the training process. Thus, it is possible to compare the predictions of the trained model with the actual values. The Confusion Matrix is a means of assessing the quality of the classification model and the location of errors (Figure 5.7).

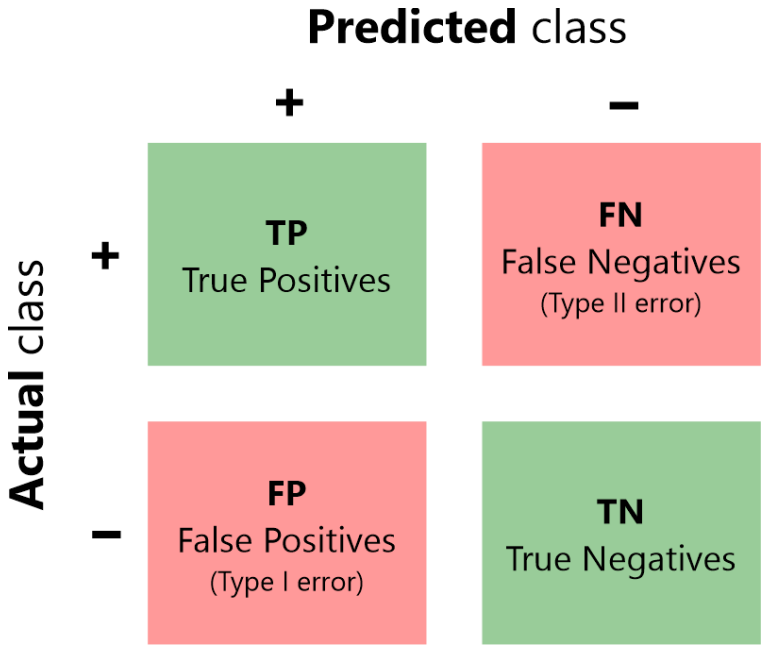

Figure 5.7. Confusion Matrix

In this figure, the notation is:

● TP - true positive: the classifier correctly assigned the object to the considered class;

● TN - true negative: the classifier correctly states that the object does not belong to the considere d class;

● FP - false positive: the classifier incorrectly assigned the object to the considered class (Type I error);

● FN - false negative: the classifier incorrectly states that the object does not belong to the class in question (Type II error).

To assess the reliability of the classification of the considered information system for image analysis, we will use the classic characteristics of the informativeness of diagnostic medical systems [147]:

● *Accuracy (Acc*) – the proportion of correct results (TP+TN) of the test among all examined patients (TP+TN+FP+FN), this indicator characterizes the probability of correctly diagnosing the functional state of a person:

$$Acc = \frac{TP+TN}{TP+TN+FP+FN}100\%; \quad (5.14)$$

● *Precision (PRE)* is the destiny of the forecasters positive results that are recognized with really true-positive results for all positively predicted objects. In other words, accuracy gives us the answer to vopros "Of all the objects that are classified as belonging to the class, how many are actually does it belong to him?"

$$\text{PRE}= \frac{TP}{TP+FP}100\%; \quad (5.15)$$

● *Recall (sensitivity) (REC)* is the proportion of all correctly-positively predicted objects to the total number of truly positive ones. That is, completeness shows how many samples from all positive examples were classified correctly. The higher the fullness, the fewer positive examples are omitted in classifications.

$$REC = \frac{TP}{TP+FN}100\%; \quad (5.16)$$

● *Specificity (SP)* is the proportion of correct negative results (TN) of the method among a group of healthy patients, this indicator characterizes the probability of a negative diagnostic result when the disease is absent:

$$SP = \frac{TN}{TN+FP}100\%;; \qquad (5.17)$$

Another informative and generalizing metric is the area under the error curve, which literally means the area under the ROC curve (Receiver Operating Characteristic) shown on figure 5.8.

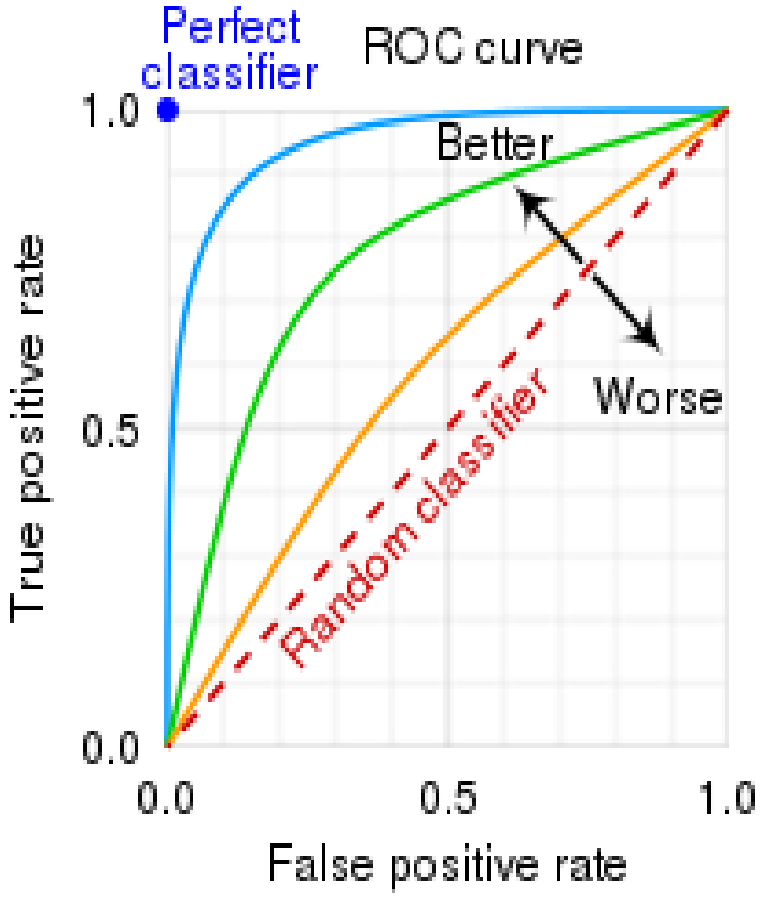

Figure 5.8. ROC curve

The above characteristics should be calculated for an information system for the analysis of retinal images in the evaluation of eye pathologies. In Table 5.1 detailed parameter utilization have been listed. The results of the analysis of the diagnostic reliability indicators of this system (*Accuracy*, *Precision*, *Recall*, *Specificity*) according to Formulas 4.21-4.23 are given in Tables 5.2-5.5 and Figures 5.9-5.12 show graphical representations of these indicators.

Table 5.1.

Parameter used for Training of Neural Network Models

	BNN	DNN	CNN (VGGnet)
Activation Function	Sigmoid	ReLU	ReLU
Fully Connected Layer	-	3	3
Convolution Layer	-	-	16
Learning Rate	0.2	0.2	0.5
Epoches	200	200	200
Image Resolution	300×300	300×300	300×300

Table 5.2

Accuracy Percentages of Each Algorithm for Processed Image Classification Image

	TRAINING	TESTING
BNN	60	61.2
DNN	90.1	87.7
CNN (VGGNET)	83.3	81.1

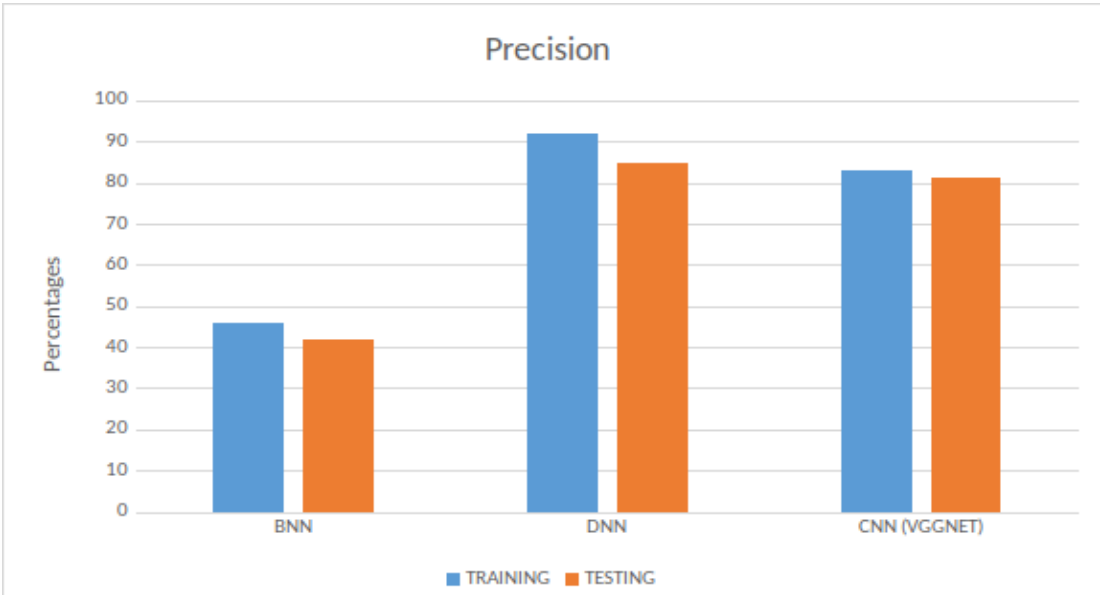

Figure 5.9. Graphical representation of the measured accuracy for three types of neural networks

Table 5.3

Precision Percentages of Each Algorithm for Processed Image Classification Image

	TRAINING	TESTING
BNN	46	55.7
DNN	92	84.6
CNN (VGGNET)	83	81.4

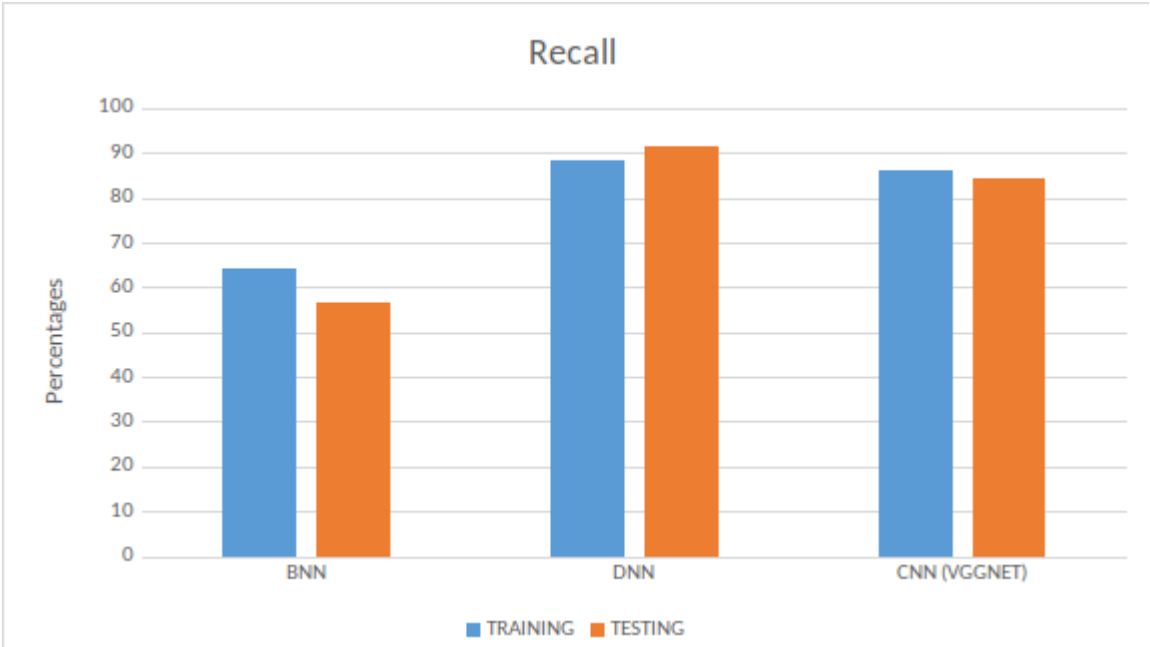

Figure 5.10. Graphical representation of the measured Precision for three types of neural networks

Table 5.4

Recall Percentages of Each Algorithm for Processed Image Classification Image

	TRAINING	TESTING
BNN	64	63.4
DNN	88.4	91.6
CNN (VGGNET)	85.9	83

Figure 5.11. Graphical representation of the measured Recall for three types of neural networks

Table 5.5

Specificity Percentages of Each Algorithm for Processed Image Classification Image

	TRAINING	TESTING
BNN	57	57.1
DNN	91.6	84
CNN (VGGNET)	80.3	79.1

Figure 5.12. Graphical representation of the measured Specificity for three types of neural networks

As we can see according to Tables 5.2-5.5 and Figures 5.9-5.12, DNN showed the best classification results. It is also worth noting that the results of CNN are slightly smaller, so with some improvement of the method or better cleaning of the data, a higher result can be achieved.

Also, the accuracy and other informative indicators of the classification results of the system are reduced due to the noisy data set, the taking of images with different lighting and different devices, as well as the erroneous pre-labeling of images by specialists.

The high quality of classification is also proven by figure 5.13, which shows three ROC curves for the studied classification systems. Again, we can make sure that the results of DNN and CNN are quite close and under different conditions can show themselves at a sufficiently high level for medical classification of diagnoses. According to the graphs, DNN and CNN approach the point with coordinates (0, 1) much closer than BNN, which is an indicator of an ideal classifier. In further research, it is planned to develop algorithms that have achieved the best results, test new ones, and test bad BNN results for a better understanding of the classification problem and its complexities.

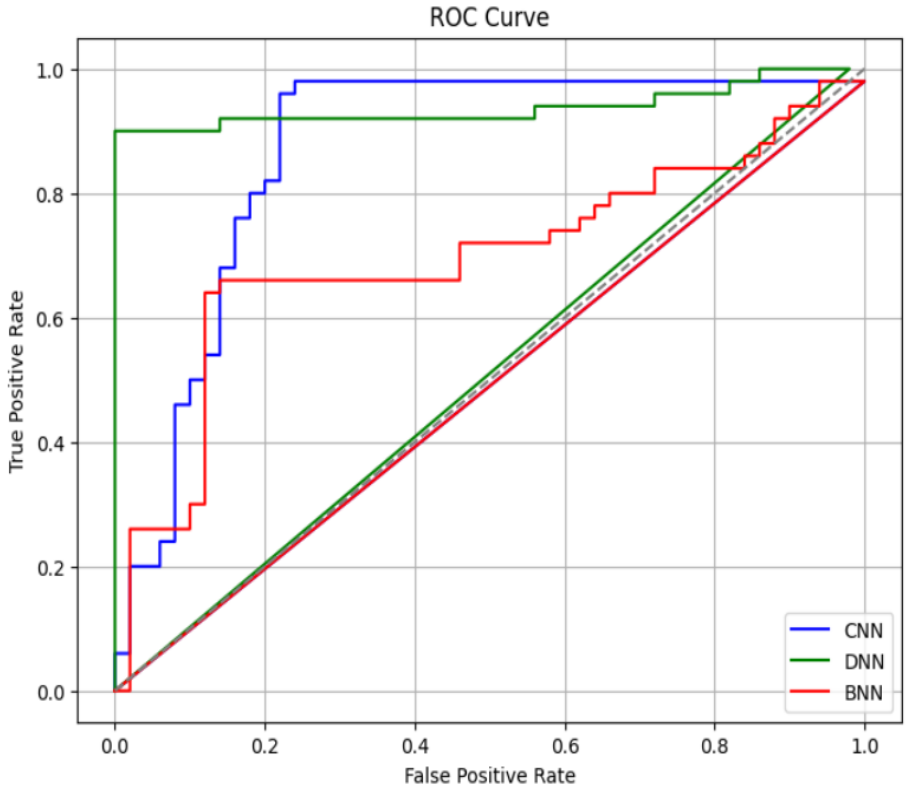

Figure 5.13. ROC curves of BNN, DNN and CNN

It is worth noting that in the case of CNN, when a new image is loaded into the diagnostic system to predict the diagnosis, it gives results in probabilistic characteristics, in fact, it shows the probability of classifying the image into different classes. Figure 5.14 shows the results of system diagnostics for different stages of diabetic retinopathy and their morbidities.

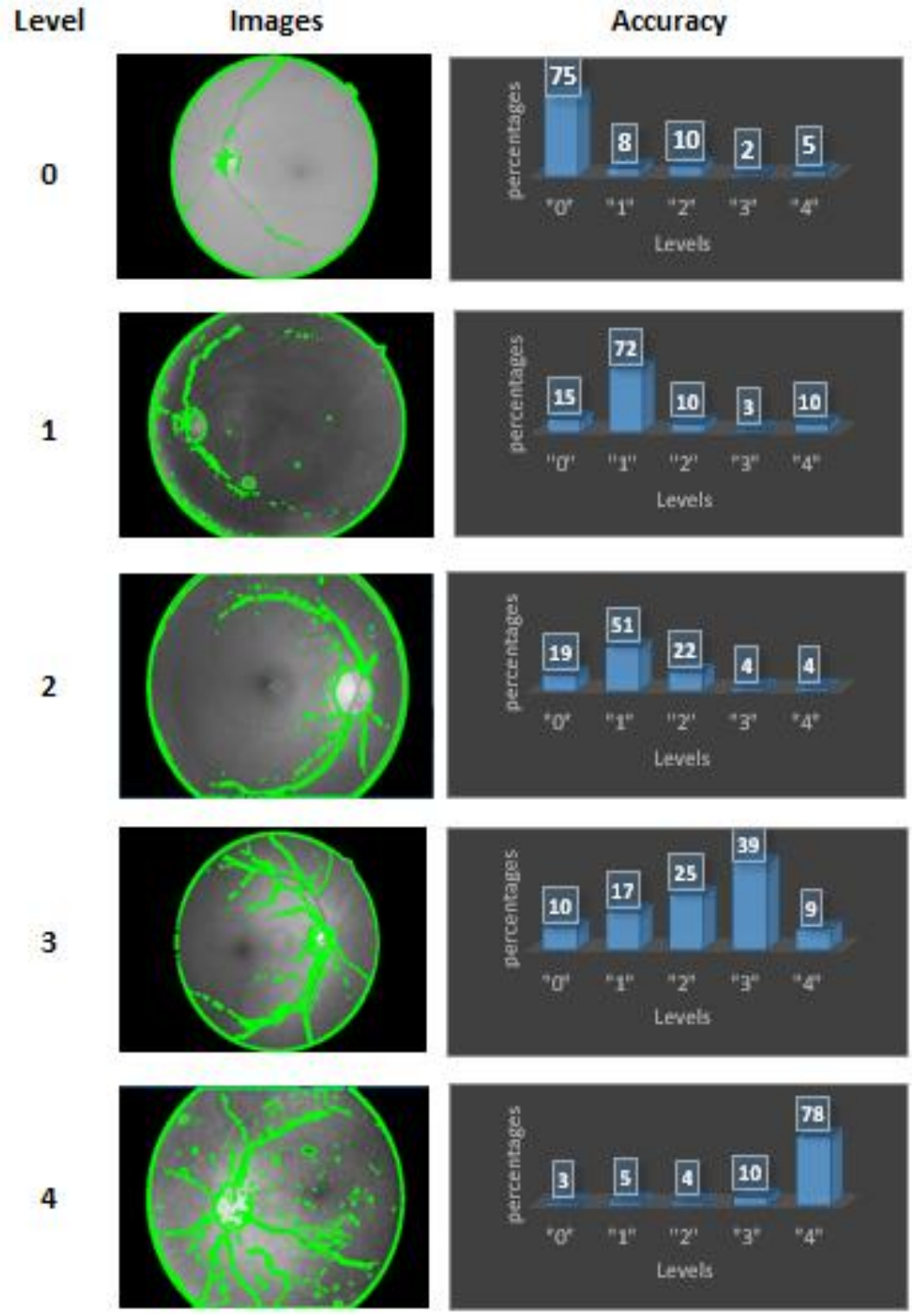

Figure 5.14. Probabilistic Result of Image Class Identification

According to the given data, we can observe that for levels 0, 1, 4, the probability of a correct prediction is more than 50%, while the rest of the points are distributed among the remaining classes. And at level 2 and 3, the probability values are less than 50%, and they are also quite equal to each other, which is the main drawback in the classification of these two classes and the main reason for reducing the accuracy of model diagnostics. At the same time, it should be noted that the binary classification according to the two nosologies "Normal" or "Pathology" shows much better results than the classification with a defined level.

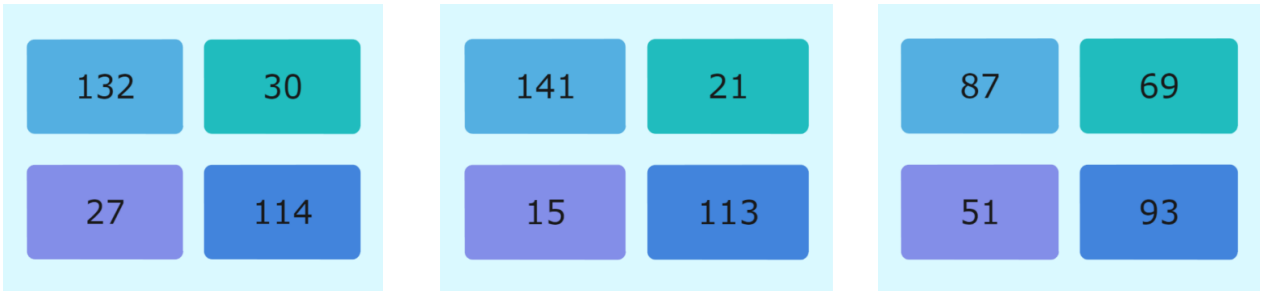

a) **b)** **c)**

Figure 5.15. Confusion matrixes

Figure 5.15 shows confusion matrixes, which are built based on the results of the studied algorithms (CNN – a, DNN – b, BNN – c). It is worth noting that the test sample of the investigated images is quite weighted, that is, the number of samples with "Normal" and "Pathology" is comparable.

4.6 Study of Cardiovascular Diseases in the Retina, Obtained by Optical Coherence Tomography

With the rapid development of artificial intelligence technology, the degree of integration of medicine and artificial intelligence is increasingly strengthened, and in the medical field, due to the aggravated aging of population in China, the impact of cardiovascular risk factors on the residents' health has become more and more significant. In our country, diseases of the cardiovascular system are the main cause of death every year, almost on a par with the consequences of COVID-19, cardiovascular diseases annually claim

the lives of more than 2.5 million people a year. This number is steadily growing every year. The negative upward trend in the incidence of the cardiovascular system increases the relevance of the proposed work. For this reason, the object of study of the proposed article was the study of pathologies of the cardiovascular system. The main object of the research is an automated artificial intelligence system for the study of three types of cardiovascular diseases (CVD) in the retina (hypertensive retinopathy, retinal artery occlusion, ischemic neuropathy), obtained by photographing the fundus using modern artificial intelligence algorithms (Deep Neural Networks (DNN). This paper aimed to develop an intelligent system for the study of cardiovascular pathologies (hypertensive retinopathy, retinal artery occlusion, ischemic neuropathy) based on images of the retina of the fundus with the possibility of diagnosing some complications. As a result, the study of three types of cardiovascular diseases based on images of optical coherence tomography, implemented with a machine learning module for predicting the risk of developing the disease with diagnostic and consulting functionality. The model showed an accuracy of 92% which obtained results are good performance indicators of the system.

AI refers to Information technology created by humans to simulate the human thinking process, extend and expand the characteristics of human thinking. However, due to the complexity of clinical problems, it is difficult to establish such a large database, and the development of expert systems has encountered a bottleneck, so machine learning (ML), an AI system that can automatically learn through data accumulation and then complete automatic recognition, came into being. In addition, on the basis of ML, experts in the field of computer science combined with artificial neural networks to further develop a deep learning (DL) system, so that the DL system has the ability to directly extract its data characteristics from a large amount of raw data. It is precisely with this efficient identification and classification ability that AI has been widely used in the medical field and has provided great help to medical research. The rapid development of medical and healthcare big data, AI algorithms and innovations in various visual, speech and tactile recognition and understanding technologies have brought broad application prospects for medical AI products, making medical activities less costly and more efficient. If we turn to the statistics of CVD in Western countries, with the use of early diagnosis

and methods for determining heart disease, a decrease in patients is observed [200]. Timely access to a specialist, diagnosis, treatment and prevention increases life by another 10-15 years. In our country, despite a significant improvement in the quality of medical care, there are still high rates of mortality from CVD. The reason for this is the untimely and sometimes late appeal to a specialist. It is not uncommon for a patient to be unaware that he may have heart problems.

For this reason, an important problem is the preclinical diagnosis of possible complications of CVD by non- traditional methods, but by easier and more affordable means.

One of the simplest, most easily observed non-invasive imaging results is the retinal image obtained using optical coherence tomography (OCT) and photography of the fundus using a fundus camera.

A widely used device for optical coherence tomography is a modern method of examining the fundus, providing complete visual information of the eye tissues with complete morphological information. In simple words, this device photographs the eye at the micro level. The resulting image, if properly recognized, will provide information about the blood vessels, as well as about possible progressive heart diseases.

We will consider the pathologies leading to loss of vision if not taken properly.

Hypertensive retinopathy does not lead to loss of vision, but can affect the development of other eye diseases leading to loss. High blood pressure is the main causative agent of hypertensive retinopathy. It can have an adverse effect on the retina and contribute to the development of hypertensive retinopathy, thereby causing other eye diseases that threaten vision. Changes in the caliber of blood vessels, size, volume and thickness on the retina are the main symptoms of this disease [201]. In ophthalmological analysis, a decrease in the diameter of retinal arterioles in relation to the diameter of venules is observed.

Occlusion of a retinal artery can cause vision loss. The reaction to light of the affected eye may be weak. On the eye with occlusion, you can see a cloudy fundus with a brown-red spot on the central fossa. The thickness of the artery narrows and visually it may look like a bloodless vessel. The disease more often affected persons over 55 years of age. Symptoms of the disease can be headaches, pain in the temporal region, fatigue, or all the symptoms together. Usually, this pathology develops

against the background of hypertension, rheumatic heart disease, atherosclerosis, and diseases of the autonomic nervous system [202, 203].

Ischemic neuropathy is accompanied by ischemic convolutional neural networks performed recognition of the OCT image of the retina and the image of the fundus. To implement the collection, the system has a built-in module for storing data, controlling anomalies, receiving data from the fundus camera.

The digital health profile of patients with CVD was compiled as a result of fixing the OCT scan of the retina of the fundus photo of the patient, using the method of continuous monitoring of data from fundus cameras in real time.

To solve the problem of image recognition, a model based on the Inception 4 convolutional neural network was created, as well as an error correction method to increase the accuracy of the neural network model. The feature rejection module, with the least influence, will reduce the dimension of the matrix used. Also, to increase efficiency in time, fuzzy k-means clustering was applied. This will affect the time spent on data processing and time for recognition.

In this paper, a 4-layer hidden layer neural network is set up to predict whether one has cardiovascular disease or not, and a binary classification model with 30 variables such as gender, age, hypertension, and retinal vascularization as inputs, hidden layer nodes are set to 50, and the output layer nodes are 2. The model graph is shown in Figure 5.16:

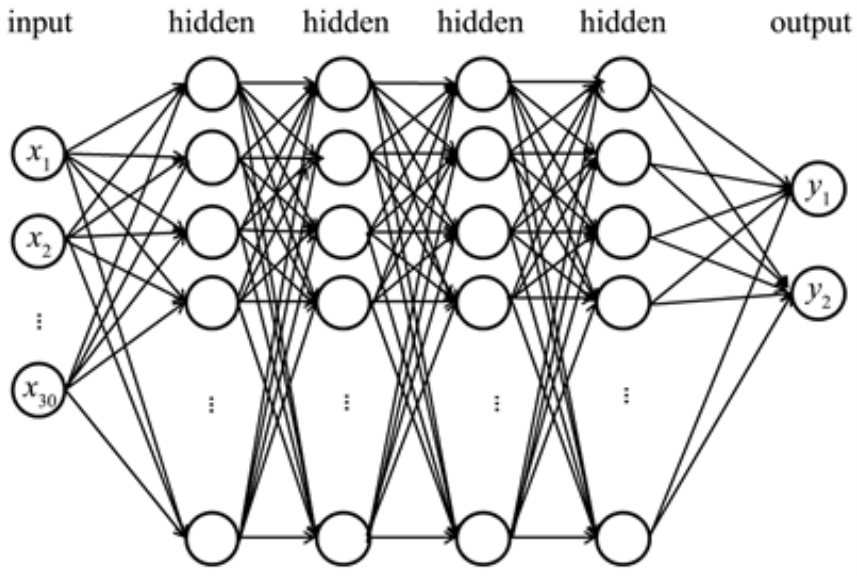

Figure 5.16. Fully connected neural network structure diagram

$$y = W^T x + b \tag{5.18}$$

$$\frac{dl}{dx} = W * \frac{dl}{dy}, \frac{dl}{dw} = x * \left(\frac{dl}{dy}\right) T \tag{5.19}$$

(Formula 1,2) where *x* as the input vector, W as the weight matrices for the respective layers, b as the bias vectors for the respective layers, y as the output vector. ℓ is the neuron of the layer. For a picture training set containing m samples, the overall cost function J can be represented mathematically as the average of the individual costs for each sample. (Formula 5.20)

$$J(W.b) = \frac{1}{2}\sum_{i=1}^{m} J(W, b, x^l, y^l) \frac{\lambda}{2} \sum_{l=1}^{nl-1} \sum_{i=1}^{sl} \sum_{j=1}^{sl+1} (W_j^l)^2 \tag{5.20}$$

Data collection and preprocessing

This stage is aimed at filtering, normalizing data. It also detects anomalies, outliers, cleansing the data and bringing them into a form suitable for use by a neural network. The choice of parameters, determining the number of layers of the neural network, the sizes of the input layers, activation functions, and exclusions are also performed at this stage [204].

This paper uses the original Cardiovascular Diseases dataset from the CDC's publicly available Behavioral Risk Factor Surveillance System (BRFSS) 2021, which has a total of 438,693 data entries and 304 feature variables. First, the training data was loaded. For the test, the RFMiD_Training_Labels.csv dataset with 47 features was used. The characteristic of this data set is represented by the following features: Diabetic retinopathy, Age-related macular degeneration, Media haze, Drusen, Myopia, Branch retinal vein occlusion, Tessellation, Epiretinal membrane, Laser scars, Macular scars, Central serous retinopathy, Optic disc cupping, Central retinal vein occlusion, Tortuous vessels, Asteroid hyalosis, Optic disc pallor, Optic disc edema, Optociliary shunt, Anterior ischemic optic neuropathy, Parafoveal telangiectasia, Retinal traction, Retinitis, Chorioretinitis, Exudation, Retinal pigment epithelium changes, Macular hole, Retinitis pigmentosa, Cotton-wool spots, Coloboma, Optic disc pit maculopathy, Preretinal hemorrhage, Myelinated nerve fibers, Hemorrhagic retinopathy, Central retinal artery occlusion, Tilted disc, Cystoid

macular edema, Posttraumatic choroidal rupture, Choroidal folds,Vitreous hemorrhage, Macroaneurysm, Vasculitis, Branch retinal artery occlusi on, Plaque, Hemorrhagic pigment epithelial detachment.

Further, the data for the test and processing were also loaded. Processing and filtering of data proceeded according to the methods presented in the works of the authors [205, 206]. The data of patients who have several types of diseases were checked. Accordingly, there is a change in the form of the table for convenience. Thus, we get a readymade table for further work. It is important to note that the ratio of patients without cardiovascular disease to patients with CVD was 23/77.

The recognition module contains a convolutional neural network named InceptionV3.

Inceptionv3 is a convolutional neural network that has a depth of 50 core layers. It was created and trained at Google [207]. A pretrained Inceptionv3 model with ImageNet weights can also classify up to 1000 objects. The input image size of this network is 299×299 pixels, which is larger than that of the VGG19 network. In 2014, at the ImageNet competition, where the tasks of detecting, classifying and localizing objects in an image were solved, the VGG19 network took second place, and the Inception network became the winner.

Based on pre-prepared data, we create a model based on InceptionV3. First, a feature extraction module was implemented based on filters according to the algorithm presented in [208, 209]. The first layer of the neural network receives pixels to apply filters to determine features, which are then used to form a feature map. Feature extraction was performed by a convolutional neural network, which is currently the most optimal in recognition and classification tasks [210, 211]. Several filters were used to preserve complexity and maintain image quality, following the example of the work of the authors.

Further, the data is transferred to the activation layer to increase the nonlinearity. A straightened linear unit has been applied. After this stage, the data merging stage passed, during which the image compression process will take place. The merging layer will save the image from unnecessary data, they are a noise, an interference, an unnecessary background information, depending on the size of the filter. The compression process involves representing the data as a vector for processing.

The last layers of the CNN perform the review and analysis of the input data, combine them into attributes according to similar features, and perform a general analysis of this data. On these layers, the process of classification and recognition will be carried out.In general, after processing the input data, it is expected to train based on a hybrid neural network architecture that combines InceptionV3 and fuzzy k-means. Recurrent neural networks will perform data storage in short-term memory cells (LSTM) and fully connected layers. As a result, regression on fully connected layers will be obtained. For example, you can analyze the process of recognizing hypertension in the following image in Figure 5.17.

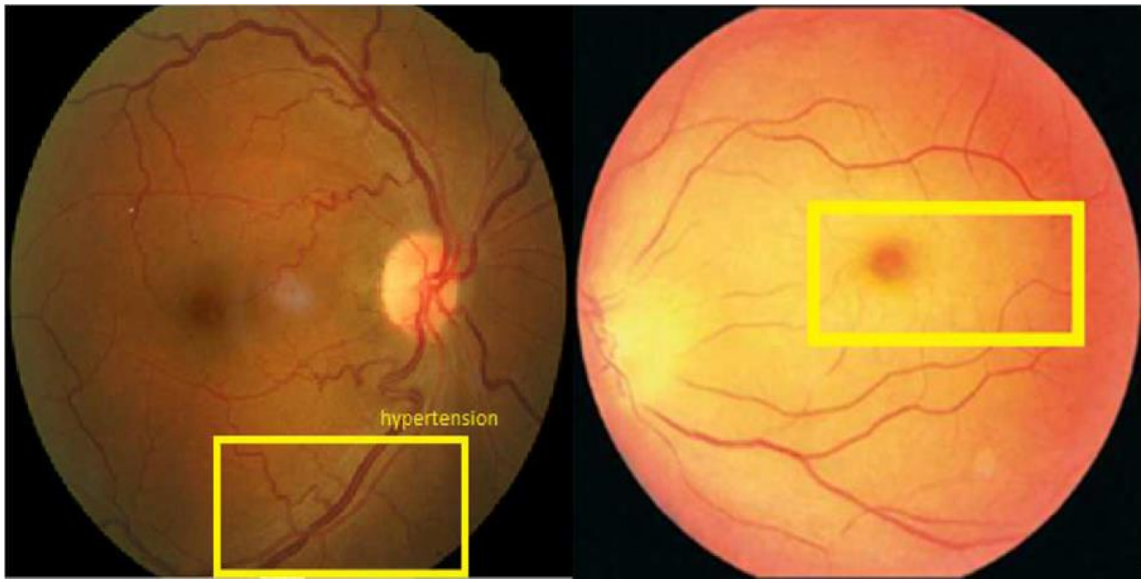

Figure 5.17. Photograph of the fundus with a sign of hypertension and Occlusion of the central retinal artery

In the lower part, you can see that the dark vein and the lighter artery, their intersection is clearly visible in the picture, and where the intersection of the vein is narrowed by the artery and this is considered a clear sign of hypertension. And the narrower the vein, the more it is compressed. That is, the greater the neglect of hypertension. For such a sign, an approach is provided to look for decussations, abnormal constrictions, or even the absence of some veins. The disease area is localized with a bounding box, thereby saving time [212, 213]. This approach is based on InceptionV3 clustering and fuzzy k-means. fuzzy k-means offers instead of processing the entire whole image, working only with the part where there are conditional features (narrowing, crossing, and others).

Using the LabelImg package, markers are placed to install bbox. Width, length, X and Y positions are stored in json files. For each snapshot, a separate data file is created for further dataset generation.

Occlusion of the central retinal artery occurs when the lumen of the central artery is closed by a thrombus, embolus, or spasm of the muscular wall of the artery in patients with hypertension, heart defects, endocarditis, atrial fibrillation, atherosclerosis, rheumatic diseases, chronic infectious diseases. On the retina is indicated by a dark spot.

Acute circulatory disorders appear with myocardial infarction, after thrombosis. The picture describes the turbidity of the retina with a red spot in the central part of the cornea. Here you need to focus on the differences in colors and shades in certain areas of the image. (Figure 5.18)

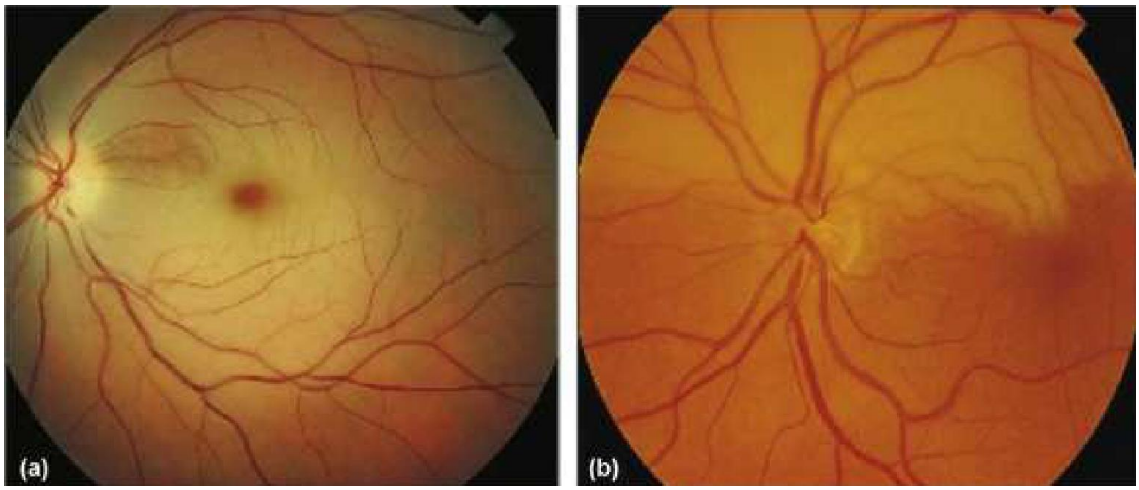

Figure 5.18. Acute circulatory disorders [10]

Training will be based on the classical algorithms used in [214, 215]. The results of the comparison will be presented in the form of an analysis.

The logic of the process of collecting information for studying the history of diseases by scanning the fundus in the medical center, preparing datasets for the application of machine learning algorithms has been developed. Recognition of the fundus image was carried out using the methods of the InceptionV3 convolutional neural network with fuzzy k-means, with the ability to localize in specific areas of the image, thereby saving time on recognition. Prediction of diagnostic parameters using artificial intelligence algorithms was carried out. Prediction of diagnostic indicators using machine learning methods was carried out on the example of several sick patients. Conducted testing

and analysis of the results. The architecture of the system based on microcontrollers with the possibility of expansion has been developed [216, 217]. The training process lasted for 12 epochs and took about 19 min. Accuracy and learning loss varied over the following ranges as illustrated on Figure 5.19:

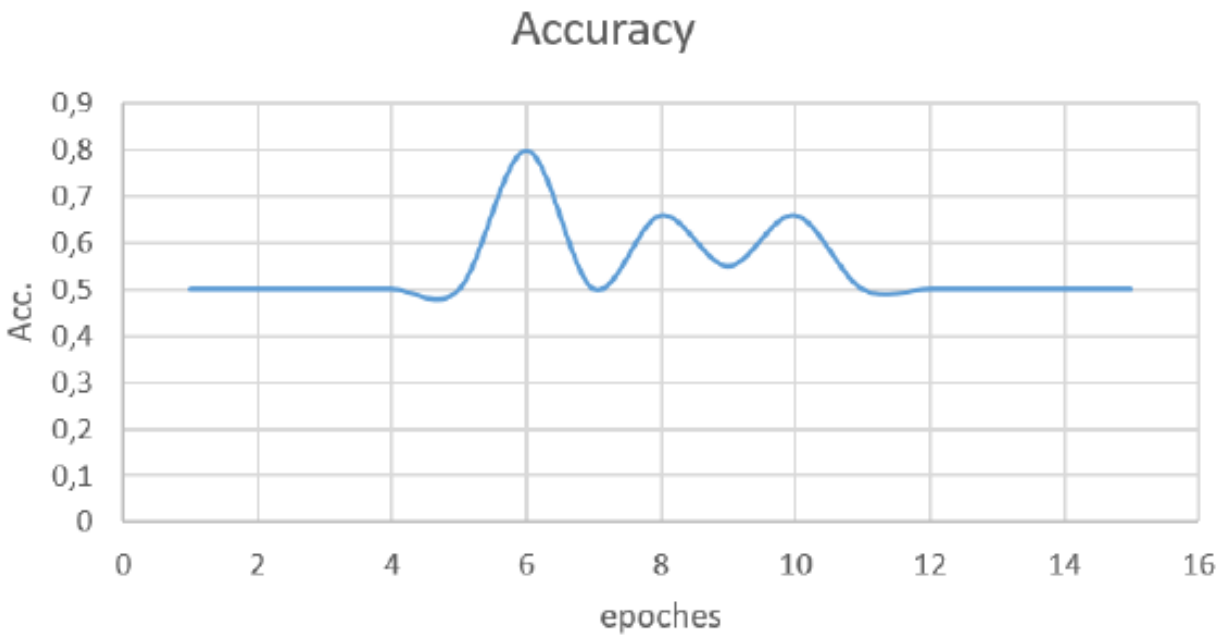

Figure 5.19. Accuracy

In test experiments, the model showed an accuracy of 92 percent. In the definition of the disease hypertension hypertension and Occlusion of the central retinal artery the accuracy is 96%, the recall is 96%, F1=94%, val_loss: 0.1636, val_accuracy: 0.6935. The 34 images of healthy patients used in the experiment, 29 images were correctly identified as healthy, 5 images were identified as pathological. The remaining 116 images with signs of the disease were correctly identified 93 images, therefore the remaining 23 were assigned to the wrong group. The obtained results are good performance indicators of the system in comparison with works [218, 219], however, there is one more improvement of the developed system. The program has advisory functionality with the ability to diagnose some complications. The presence of such a module significantly improves the demand for this system among potential patients, facilitates the work of medical personnel, partially unloading their workload, saves time for the patients themselves and the people who care about them.

Cardiovascular Diseases in the Retina, the coronary disease with the highest morbidity and mortality in the world, gives doctors a lot of

headaches and also makes doctors bear a lot of work. Identification of Cardiovascular Diseases in optical coherence tomography (OCT) images by computer aided technology can not only free doctors from complicated diagnostic tasks, but also has great significance for early detection of Cardiovascular uDiseases in the Retina and timely intervention for patients. In the experiment, study of three types of cardiovascular diseases (CVD) in the retina (hypertensive retinopathy, retinal artery occlusion, ischemic neuropathy), using the methods of neural networks, image recognition performed with the definition of the details of each disease.performed on images of 150 patients with 47 features. In this set of patients without CVD is 23% percent or 34 patients. And the results obtained on these data with a training accuracy of 96% are undoubtedly a good result compared to the work of the scientists discussed above. The experiment can shorten the diagnosis time of doctors, and can be used as the basis for assisting doctors to make further diagnosis.

4.7. Optical method of investigating eye diseases and system for diagnosing diabetic retinopathy

The proposed approach to the recognition of images of fundi is based on the use of the knowledge of specialists in the field of ophthalmology and consists of creating an expert system for the diagnosis of glaucoma. The basis of the system is a reference sample of digital images, the description of which is stored in the knowledge base. An important component of the system is the analytical subsystem, which includes many rules by which decisions are made (Figure 5.20) [9, 10, 130, 166].

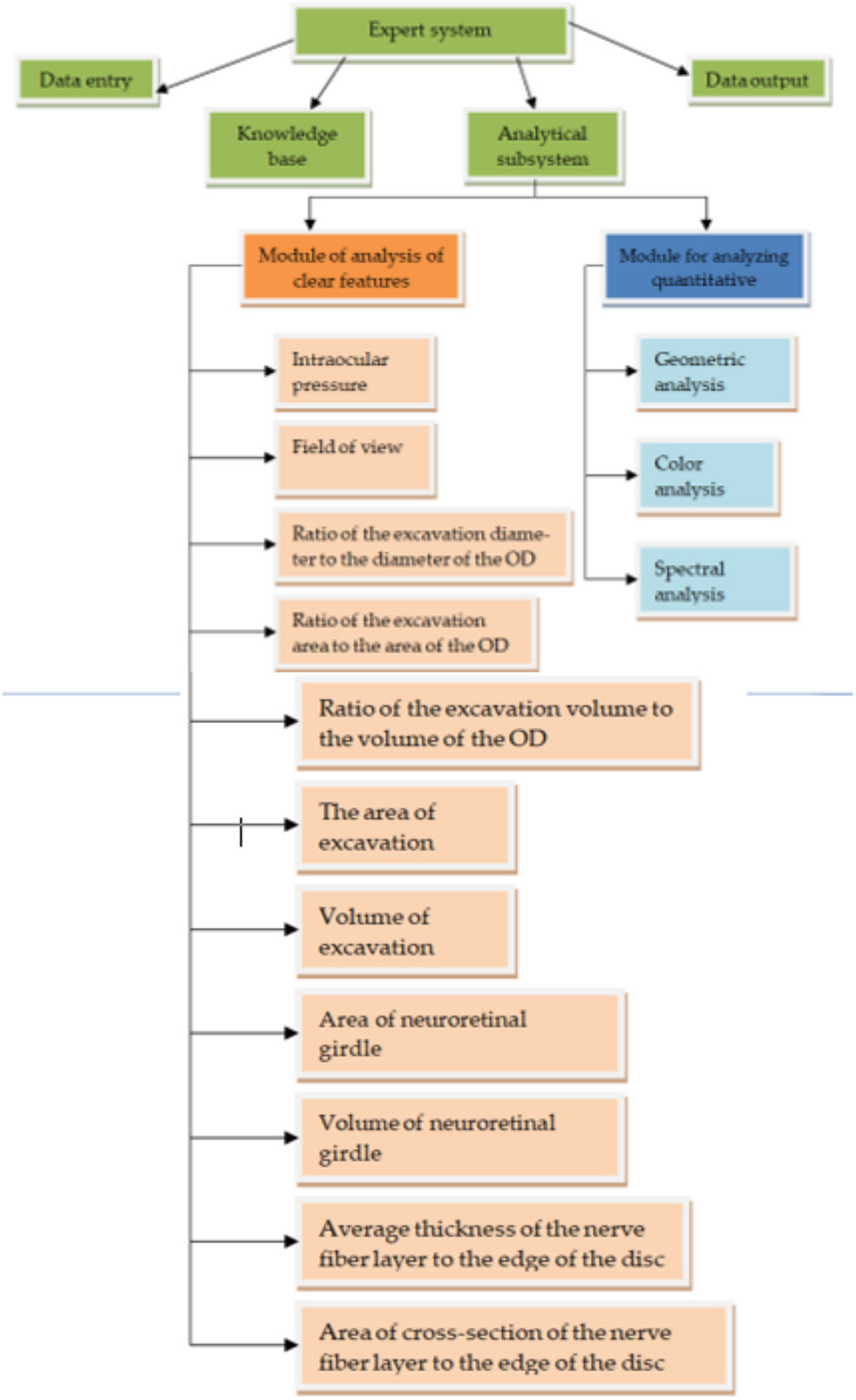

Figure 5.20. The analytical subsystem, which includes many rules, according to which decision-making is carried out.

There are factors that have a dominant influence on the correctness of image recognition. As a result of the research conducted here,

several factors that had the most significant impacts on the accuracy of the measurement results were identified, and they were divided into three groups based on the type of source (instrumental, methodical, subjective user errors).

For the considered system, instrumental factors can be classified into two groups; the first is that of factors that are due to physical processes in the equipment used, while the second is that of factors that are due to the influence of external conditions. The first group of instrumental factors includes the noise of the image sensor, color distortions of the camera, brightness distortions, diffraction effects of the optical system, uneven spectral characteristics of the illuminator in the ophthalmoscope, uneven illumination of the drug in the field of view of the camera, etc. The factors of the second group include factors determined by the external conditions of the system's application [34, 103, 173].

So, for example, an image registered in the system can be affected by factors such as the presence of bright external lighting (sunlight), which can decrease the contrast of the image. In addition, the external factors include surface vibration (this can lead to image distortion when using large exposures) [14, 15].

First, the methodological factors include the measurement model and mathematical methods of image processing that are implemented in the system software, as well as the discretization and quantization operations that are carried out when forming a digital image.

A group of factors that depend on the user is related to the setting of the ophthalmoscope (the choice of the lens, the position of the condenser, field, and aperture diaphragm, the voltage of the lamp, and light flux correction filters, position of the lens focus). Along with these, this group includes factors related to the selection of the field for research and the positioning of the research object in the field of view of the camera, as well as factors that depend on the user in the interactive mode of image processing (when the processing parameters are specified by the user when implementing the processing in the application software).

Many authors have created models for the diagnosis and classification of glaucoma using a variety of research approaches and computer programs. These methods have led to the development of several research models. Most of these models include several layers of performance analysis using deep learning. Many similarities between

retinal disease and glaucoma make it difficult to distinguish between them. The authors used such parameters as intraocular pressure, field of vision, excavation diameter to OD diameter ratio, excavation area to OD area ratio, excavation volume to OD volume ratio, excavation area, excavation volume, area neuroretinal belt, volume of the neuroretinal belt, average thickness of the nerve fiber layer along the edge of the disc, cross-sectional area of the nerve fiber layer along the edge of the disc.

In the past, glaucoma could be identified from these digital recordings of retinal images. This strategy has been used in the vast majority of clinical trials, making it the most commonly used technique.

The image classification method was used to analyze the data and organize things into categories. This project required numerical analysis of the image filled correctly. In order to finish the study on time, the information needs to be entered in different groups, such as “normal” and “glaucoma”. They used the U-Net segmentation technique to accurately identify and segment the optic cup in the retinal fundus photographs they examined.

A detailed analysis of the methods used today to diagnose glaucoma is presented in the work of the authors: Kashyap, R.; Nair, R.; Gangadharan, S.M.P.; Botto-Tobar, M.; Farooq, S.; and Rizwan [66].

It should be noted that the CNN technique for the diagnosis of glaucoma involves combining the results of two different types of measurements, namely temporal and geographical data. Because they did it this way, they could use both time and place data. Thanks to these characteristics, it was possible to make a reliable diagnosis of the condition of the eye (on the basis of a static structural system).

4.7.1 Algorithmic Software Implementation for Processing Biomedical Images

During the analysis of the characteristics of a fundus, the reliability of the final assessment of the images therein should be increased by using expert methods. The proposed approach to the recognition of images of fundi is based on the use of the knowledge of specialists in the field of ophthalmology and consists of creating an expert system for

the diagnosis of glaucoma. The basis of this system is a reference sample of digital images, the description of which is stored in a knowledge base. An important component of the system is the analytical subsystem, which includes many rules by which decisions are made.

To obtain a diagnosis with the help of an expert database, we suggest using elements of fuzzy logic. We built a model on the basis of actual data.

Using an algorithm from a processing method based on the fuzzy logic apparatus, we obtain the following.

When entering the data we obtain the following (Figure 5.22).

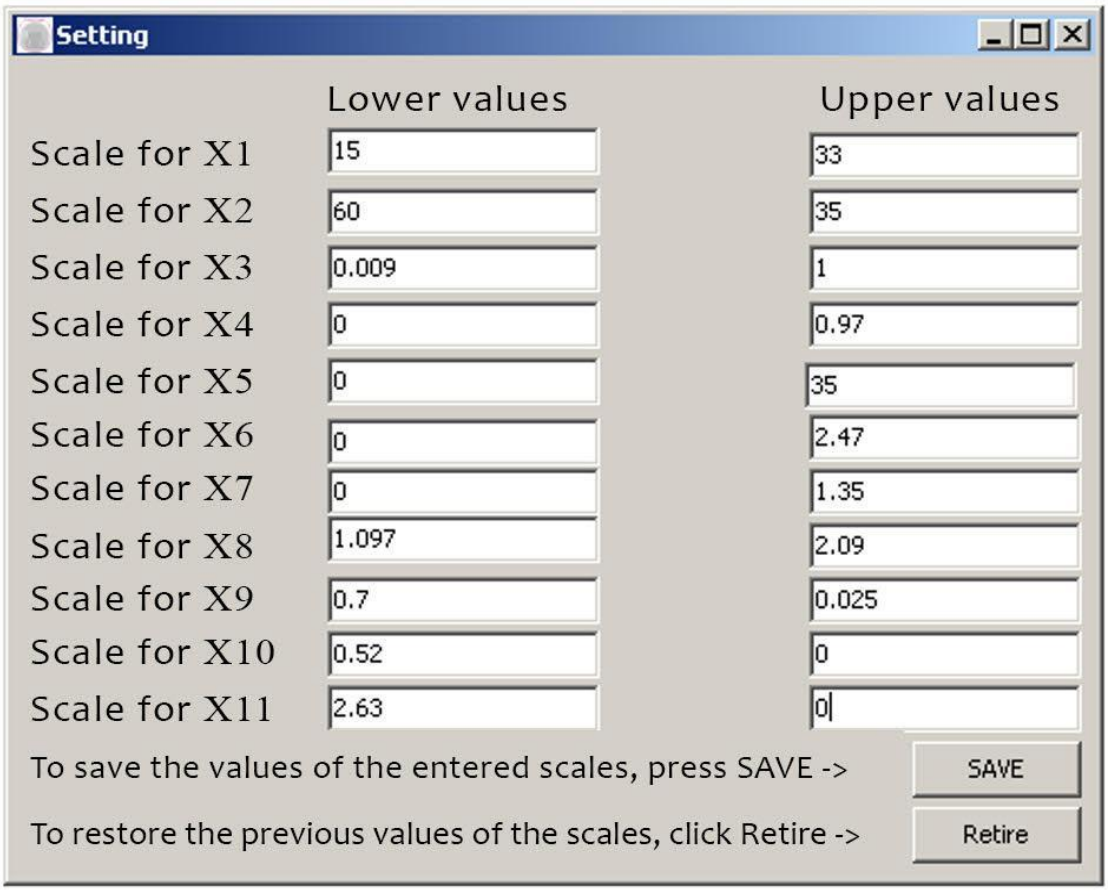

Figure 5.22. Input of initial data.

When saving the data, i.e., entering the lower and upper values, we can enter the patient's data.

Having obtained the result, we can conclude that the patient has glaucoma of the third degree (Figure 5.23).

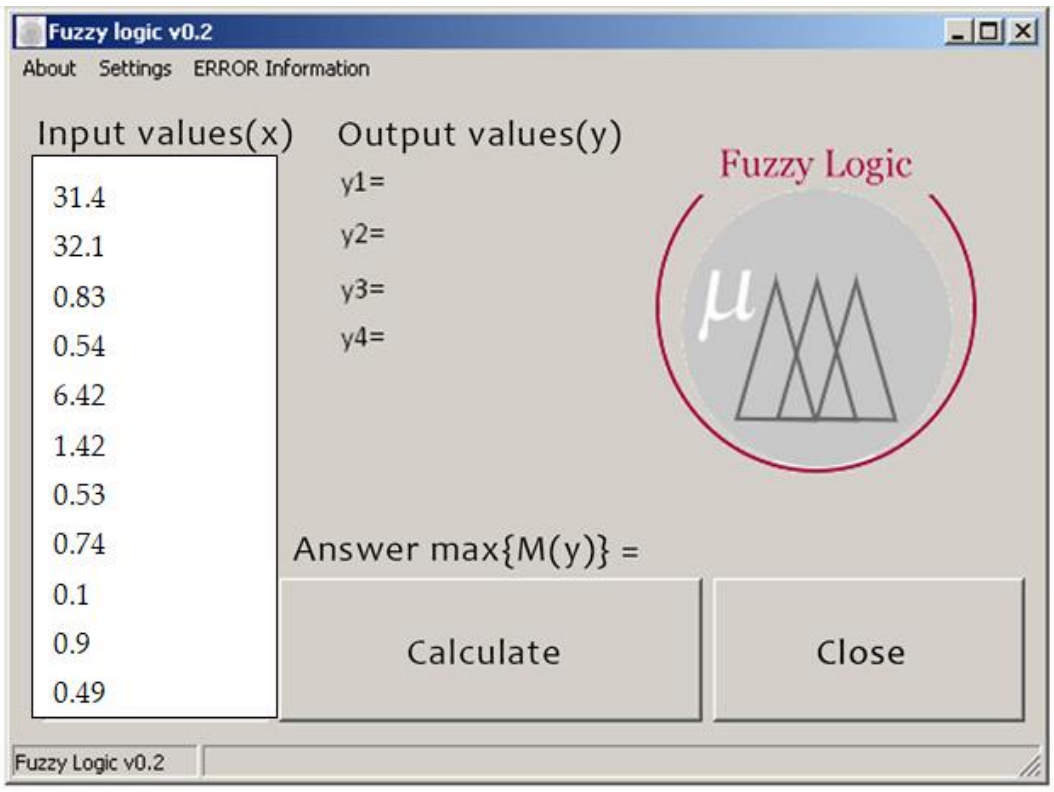

Figure 5.23. Entering the patient's input data.

4.7.2 Physical Modeling of the Optical–Electronic System for Researching Pathologies of Fundi

Physical modeling of the optical–electronic system for researching pathologies of fundi performed for the formation of an optical–electronic system for entering biomedical information.

The optical–electronic system for obtaining images of the retina of an eye is related to medicine, namely, to devices for examining fundi, and it can be used in ophthalmology to conduct medical and biological research and, specifically, to fix images of retinas. The optical channel is realized as follows.

The radiation flow coming from the radiating surface of the source to the remote illuminating surface can be calculated as follows (1):

$$\Phi = L \cdot S_{soursce} \cdot S_{sq} \cdot \frac{cos\beta_1 \cdot cos\beta_2}{l^2}, \qquad (5.21)$$

where L is the brightness of the emitting surface; S_{source} is the area of the radiating surface; S_{sq} is the area of the illuminating surface; β_1 is the angle between the direction of radiation propagation and the normal to the radiating surface; β_2 is the angle between the direction of

radiation propagation and the normal to the illuminating surface; and *l* is the distance between the surfaces.

If the lighting system directs radiation into the eye through a pupil area with an area Ssource, then this area can be considered as a light-emitting surface, the brightness of which L_{laser} due to the transition of light rays from the air to the eye is related to the brightness of the source—the LED L_{diode}—according to the following Expression (1), (2):

$$L_{laser} = n_{eye^2} \cdot L_{diode}, \quad (5.22)$$

where N_{eye} is the average refractive index of eye tissues.

Taking Expression (2) and the transmission coefficient of the optical system of the eye τ_{eye} into account, Expression (1) for the light flux falling on the retina can then be written in the following form:

$$F = \tau_{eye} \cdot n_{eye^2} \cdot L_{diode} \cdot S'_{source} \cdot S_{eye'} \cdot \frac{cos\beta_1 \cdot cos\beta_2}{l_{eye^2}}, \quad (5.23)$$

where $S_{eye'}$ is the area of the retina; and l_{eye} is the distance between the pupil and the retina.

When the light flux spreads along the optical axis of the eye, which is assumed to be perpendicular to the planes of the pupil and retina ($\beta_1 = \beta_2 = 0$), the illumination of the retina will be

$$E_{\text{ока}} = \frac{F}{S_{sq}} = \frac{\tau_{eye} \cdot n_{eye^2} \cdot L_{diode} \cdot S'_{source}}{l_{eye^2}} \quad (5.24)$$

Expression (4) is true for the illumination of a retinal point lying on the optical axis of the eye. However, since the fundus is a sphere and due to the multiple reflections of light rays inside the eye, it can be assumed that the illumination of the entire retina is uniform and is determined by Expression (4).

A uniformly illuminated retina, diffusely reflecting the light stream falling on it, represents a secondary light source, the brightness of which will be equal to

$$L_{eye} = \frac{\rho \cdot E_{eye}}{\pi} = \frac{\rho \cdot \tau_{eye} \cdot n_{eye^2} \cdot L_{diode} \cdot S'_{source}}{\pi \cdot lalignl_{eye^2}} \qquad (5.25)$$

where ρ is the diffusion reflection coefficient.

Illumination of the retinal image takes place on the photomatrix, which is built with the following optical system:

$$P = \frac{\tau_{os} \cdot \pi \cdot L_c}{4} \cdot \left(\frac{k'}{k}\right)^2 \cdot \left(\frac{D}{f'}\right)^2 \cdot \frac{\beta_p^2}{(\beta - \beta)^2} \qquad (5.26)$$

where $_{os}$ is the transmission coefficient of the optical system; *n*' is the refractive index of the medium in the image space (k' = 1); *n* is the index of refraction of the medium in the space of objects (k = noka); *D* is the diameter of the entrance pupil of the optical system; *f'* is the focal length of the optical system; β_p is the linear increase in the optical system in the pupils; and β is the linear increase in the optical system.

Substituting (5) into (6) and assuming a linear increase in the pupils β_p = 1, for the illumination of the retinal image on the photomatrix, we obtain

$$P' = \frac{\tau_{oc} \cdot \tau_{ока} \cdot \rho \cdot L_{сд} \cdot S'_{дж}}{4 \cdot l_{ока^2}} \cdot \left(\frac{D}{f'}\right)^2 \cdot \frac{1}{(1 - \beta)^2} \qquad (5.27)$$

Let us assume that τ_{eye} = 0.5, τ_{os} = 0.9, ρ = 0.2, l_{eye} = 24, and diameter = 24 mm. The maximum brightness of the light source that can be transmitted when directly observed is 7500 cd/m^2. So that patients would not feel discomfort, as an illuminator, we chose an LED; Lsd = 7000 cd/m^2. Let us also assume that the projection of the source onto the pupil of the eye occupies 50% of its area. In this case, with a pupil diameter of 6 mm, $S_{d.pup}$ = 14.13 mm. To perceive the image, we used the 6.6 Megapixel CMOS photomatrix NOII4SM6600A, the main indicators of which are as follows:

Table 5.7.

Photomatrix indicators

Dimensional capacity	2210 × 3002
Optical format, inches	1
Range of spectral sensitivity, nm, нм	400…1000
Apparent sensitivity, V/(lx/s)	2.01
Dark signal, mV/s	3.37

The required linear increase β in the optical system can be determined by the ratio that corresponds to the condition under which the retinal image occupies the largest part of the photomatrix area:

$$\beta = \frac{H_{phm}}{D_{\text{c}}}, \tag{5.28}$$

where H_{phm} is the height of the photomatrix; and D_{retina} is the diameter of the retina.

The optical matrix format of 1 inch corresponds to the size of 12.8 × 9.6 mm. The diameter of the human retina is 22 mm. Then,

$$\beta = \frac{9.6}{22} = 0.436.$$

By substituting numerical values for the definition in Expression (7), we obtain

$$E' = \frac{0.9 \cdot 0.5 \cdot 0.2 \cdot 7000 \cdot 14.13}{4 \cdot 24^2} \cdot \left(\frac{D}{f'}\right)^2 \cdot \frac{1}{(1-0.436)^2} = 12.146 \cdot \left(\frac{D}{f'}\right)^2 \tag{5.29}$$

To carry out further calculations, we will determine the illumination of the photomatrix E’ at which the value of the useful output signal will be comparable to the dark one. The minimum illumination of the image at which it is indistinguishable from the background noise is found using the sensitivity of the photomatrix and the value of the dark signal:

$$E_0 = \frac{3.37 \cdot 10^{-3}}{2.01} = 1.677 \cdot 10^{-3}(\text{Lx})$$

To obtain a good image of the retina, the illumination of the photomatrix must be at least 10 times higher than this value. Therefore,

$$E' = 0.01677(\text{Lx})$$

Then, using Expression (9) for the geometric luminous intensity of the optical system, we have

$$\left(\frac{D}{f'}\right)^2 = \frac{0.01677}{12.146} = 1.38 \cdot 10^{-3} \qquad (5.30)$$

In order to use the entire field of the optical system, the entrance pupil must be aligned with the plane of the eye pupil. In this case, the field aperture will be the frame of the photomatrix, and with the linear magnification selected in accordance with Expression (8), the image of the entire retina will be formed on the photomatrix. The diameter of the entrance pupil of the optical system D is chosen to be equal to 3 mm. As a result, the area of the entrance pupil of the optical system is equal to 7.065 mm^2, which is 25% of the area of the pupil of the eye with a pupil diameter of 6 mm. Then, from Expression (10), for the focal length of the optical system, we obtain

$$f' = \sqrt{\frac{9}{1.38 \cdot 10^{-3}}} = 80.76(\text{mm})$$

When calculating the focal length of the optical system, the linear increase in the pupils β_p was taken to be equal to 1. This corresponds to the case when the distance $-z_p$ from the front focus of the optical system to the input pupil is equal to the front focal length of the optical system:

$$-z_p = -f = -80.76(\text{mm})$$

The distance from the front focus to the retina is equal to

$$-z = -z_p - l_{\text{ока}} = -80.76 - 24 = -104.76(\text{mm})$$

The distance z’ from the back focus to the retinal image formed in the photomatrix plane is determined using the linear magnification of the optical system β:

$$z' = \beta \cdot f' = 0.436 \cdot 80.76 = 35.21(\text{mm}).$$

The results of this study can be generalized to a variety of imaging modalities. The proposed method of transfer of learning has an additional advantage, as it can be applied in various areas of medicine and biology

CONCLUSIONS

The main goal of this study is to increase the accuracy of diagnosing diabetic retinopathy using the methods of preprocessing of microscopic images followed by analysis and differentiation of pathologies using a decision support system based on neural network technologies. This system should help doctors correctly and accurately determine diabetic retinopathy even in the early stages, which will help avoid complications and save a person's vision.

The results of the dissertation research solved the urgent task of increasing the informativeness, accuracy and reliability of the classification of the information system for the diagnosis of diabetic retinopathy.

An analysis of the existing methods of diagnosing eye diseases was carried out, and it was established that in the case of early cases, diagnosis allows preventing severe stages of the disease. A comparative analysis of existing methods of medical diagnosis of gout disease is given, from which it can be seen that the reliability of diagnosing pathologies of the above-mentioned methods is significantly improved, which is possible due to the intellectualized analysis of measured images with the help of a computer decision support system. Intelligent analysis and image pre-processing to improve the informativeness of the data have expanded the capabilities of ophthalmic systems.

A number of existing methods for a decision support system were analyzed. The choice of a rule for a decision support system was justified, based on the fact that with a given number of samples and informative parameters, neural network technologies are best suited due to sufficient accuracy, simplicity of working with numerical characteristics. An analysis of existing neural network algorithms was carried out, their pros and cons were indicated.

A method of pre-processing of images of the retina in diabetic retinopathy was developed, which includes: Converting the image to grayscale, processing them using a median filter, which allowed to remove noise and defects of lighting and equipment that took images. Image compression algorithms with minimal information loss were used to save computer resources. Binarization of image features was also carried out, as well as a Sobel filter was applied to highlight image contours. The technique of removing the background lighting of the

image to improve its informative characteristics is analyzed. Selection of RGB components for further classification of the received images.

The architecture and algorithm of the method and information system for the diagnosis of fundus images were developed. A database of informative statistical indicators has been created, for further reproduction and analysis on various systems, the main characteristics are: Average value, Median, Standard deviation, Asymmetry, Mean absolute deviation, Mean squared error and others.

A decision support system based on neural networks was developed to help doctors in the process of diagnosing diseases of the fundus. The results of classification by three rules (BNN, DNN, CNN) were analyzed, their indicators were determined, and it was decided that DNN coped best with the task (Accuracy = 87.1%, Precision = 84.6%, Recall = 91.6%, Specificity = 84%).

The obtained results can be used to solve the problem of improving the quality of diagnosis and classification of diseases with the possibility of early detection and treatment of the disease.

BIBLIOGRAPHY

[1] C Dolan, R Glynn, S Griffin, C Conroy, C Loftus, PC Wiehe, ML Healy, and B Lawlor. Brain complications of diabetes mellitus: a cross-sectional study of awareness among individuals with diabetes and the general population in ireland. Diabetic Medicine, 35(7):871–879, 2018.

[2] Barbara H Bardenheier, Ji Lin, Xiaohui Zhuo, Mohammed K Ali, Theodore J Thompson, Yiling J Cheng, and Edward W Gregg. Disability-free life-years lost among adults aged 50 years with and without diabetes. Diabetes care, 39(7):1222–1229, 2016.

[3] Waleed Nazih, Ahmad O Aseeri, Osama Youssef Atallah, and Shaker El-Sappagh. Vision transformer model for predicting the severity of diabetic retinopathy in fundus photography-based retina images. IEEE Access, 11:117546–117561, 2023.

[4] Sigeru Omatu. Neuro-control and its applications to electric vehicle control. In Distributed Computing, Artificial Intelligence, Bioinformatics, Soft Computing, and Ambient Assisted Living: 10th International Work-Conference on Artificial Neural Networks, IWANN 2009 Workshops, Salamanca, Spain, June 10-12, 2009. Proceedings, Part II 10, pages 1–12. Springer, 2009.

[5] Clara I Sánchez, Meindert Niemeijer, Michael D Abràmoff, and Bram van Ginneken. Active learning for an efficient training strategy of computer-aided diagnosis systems: application to diabetic retinopathy screening. In International Conference on Medical Image Computing and Computer-Assisted Intervention, pages 603–610. Springer, 2010.

[6] Babak Ehteshami Bejnordi, Maeve Mullooly, Ruth M Pfeiffer, Shaoqi Fan, Pamela M Vacek, Donald L Weaver, Sally Herschorn, Louise A Brinton, Bram van Ginneken, Nico Karssemeijer, et al. Using deep convolutional neural networks to identify and classify tumor-associated stroma in diagnostic breast biopsies. Modern Pathology, 31(10):1502–1512, 2018.

[7] Tuow Daniel Ting and Yee Kin Ho. Molecular mechanism of gtp hydrolysis by bovine transducin: pre-steady-state kinetic analyses. Biochemistry, 30(37):8996–9007, 1991.

[8] Michael D Abràmoff, James C Folk, Dennis P Han, Jonathan D Walker, David F Williams, Stephen R Russell, Pascale Massin, Beatrice Cochener, Philippe Gain, Li Tang, et al. Automated analysis

of retinal images for detection of referable diabetic retinopathy. JAMA ophthalmology, 131(3):351–357, 2013.

[9] Rupert RA Bourne, Gretchen A Stevens, Richard A White, Jennifer L Smith, Seth R Flaxman, Holly Price, Jost B Jonas, Jill Keeffe, Janet Leasher, Kovin Naidoo, et al. Causes of vision loss worldwide, 1990–2010: a systematic analysis. The lancet global health, 1(6):e339–e349, 2013.

[10] Jerome HI Ha, Brad Bowling, and Simon DM Chen. Cystoid macular oedema following selective laser trabeculoplasty in a diabetic patient. Clinical & experimental ophthalmology, 42(2), 2014.

[11] Chongli Di, Tiejun Wang, Xiaohua Yang, and Siliang Li. An improved grassberger–procaccia algorithm for analysis of climate system complexity. Hydrology and Earth System Sciences, 22(10):5069–5079, 2018.

[12] Rishab Gargeya and Theodore Leng. Automated identification of diabetic retinopathy using deep learning. Ophthalmology, 124(7):962–969, 2017.

[13] International Diabetes Federation. Diabetes basics - international diabetes federation, June 2022. Accessed: 2022-12-08.

[14] Rahul Chakrabarti, C Alex Harper, and Jill Elizabeth Keeffe. Diabetic retinopathy management guidelines. Expert review of ophthalmology, 7(5):417–439, 2012.

[15] Nicole J Van Bergen, Rahul Chakrabarti, Evelyn C O'Neill, Jonathan G Crowston, and Ian A Trounce. Mitochondrial disorders and the eye. Eye and brain, pages 29–47, 2011.

[16] Valliappan Raman, Patrick Then, and Putra Sumari. Proposed retinal abnormality detection and classification approach: Computer aided detection for diabetic retinopathy by machine learning approaches. In 2016 8th IEEE International conference on communication software and networks (ICCSN), pages 636–641. IEEE, 2016.

[17] Neera Singh and Ramesh Chandra Tripathi. Automated early detection of diabetic retinopathy using image analysis techniques. International Journal of Computer Applications, 8(2):18–23, 2010.

[18] Meindert Niemeijer, Michael D Abramoff, and Bram Van Ginneken. Information fusion for diabetic retinopathy cad in digital color fundus photographs. IEEE transactions on medical imaging, 28(5):775–785, 2009.

[19] Deepthi K Prasad, L Vibha, and KR Venugopal. Early detection of diabetic retinopathy from digital retinal fundus images. In 2015 IEEE recent advances in intelligent computational systems (RAICS), pages 240–245. IEEE, 2015.

[20] Toufique A Soomro, Junbin Gao, Mohammad AU Khan, Tariq M Khan, and Manoranjan Paul. Role of image contrast enhancement technique for ophthalmologist as diagnostic tool for diabetic retinopathy. In 2016 International conference on digital image computing: techniques and applications (DICTA), pages 1–8. IEEE, 2016.

[21] Yitian Zhao, Yalin Zheng, Yonghuai Liu, Jian Yang, Yifan Zhao, Duan-duan Chen, and Yongtian Wang. Intensity and compactness enabled saliency estimation for leakage detection in diabetic and malarial retinopathy. IEEE transactions on medical imaging, 36(1):51–63, 2016.

[22] Xiangyu Chen, Yanwu Xu, Shuicheng Yan, Damon Wing Kee Wong, Tien Yin Wong, and Jiang Liu. Automatic feature learning for glaucoma detection based on deep learning. In Medical Image Computing and Computer-Assisted Intervention–MICCAI 2015: 18th International Conference, Munich, Germany, October 5-9, 2015, Proceedings, Part III 18, pages 669–677. Springer, 2015.

[23] Athanasios V Vasilakos, Yu Tang, Yuanzhe Yao, et al. Neural networks for computer-aided diagnosis in medicine: a review. Neurocomputing, 216:700–708, 2016.

[24] Vanitha Sankaran, Matthew J Everett, Duncan J Maitland, and Joseph T Walsh Jr. Comparison of polarized-light propagation in biological tissue and phantoms. Optics Letters, 24(15):1044–1046, 1999.

[25] Daniel SW Ting, Lily Peng, Avinash V Varadarajan, Pearse A Keane, Philippe M Burlina, Michael F Chiang, Leopold Schmetterer, Louis R Pasquale, Neil M Bressler, Dale R Webster, et al. Deep learning in ophthalmology: the technical and clinical considerations. Progress in retinal and eye research, 72:100759, 2019.

[26] Natalia I Zabolotna and Kostiantyn O Radchenko. A multifunctional automated system of 2d laser polarimetry of biological tissues. In Reflection, Scattering, and Diffraction from Surfaces IV, volume 9205, pages 239–247. SPIE, 2014.

[27] Michael Peter Milham. Open neuroscience solutions for the connectomewide association era. Neuron, 73(2):214–218, 2012.

[28] FERCHER AF. In vivo optical coherence tomography. Am J Ophthalmol, 116:113–114, 1993.

[29] David Huang and Mark Shure. Handbook of optical coherence tomography, 2003.

[30] Roy Taylor and Deborah Batey. Handbook of retinal screening in diabetes: diagnosis and management. John Wiley & Sons, 2012.

[31] N. Zabolotna, K. Radchenko, et al. Method and system of jones-matrix mapping of blood plasma films with ‘fuzzy’ analysis in differentiation of breast pathology changes. In Proceedings of SPIE, 2018.

[32] Natalia I Zabolotna, Sergei V Pavlov, Oleksandr V Karas, and Vladyslava V Sholota. Processing and analysis of images in the multifunctional classification laser polarimetry system of biological objects. In Reflection, Scattering, and Diffraction from Surfaces VI, volume 10750, pages 82–89. SPIE, 2018.

[33] NI Zabolotna, SV Pavlov, AG Ushenko, AO Karachevtsev, VO Savich, OV Sobko, and OV Olar. System of the phase tomography of optically anisotropic polycrystalline films of biological fluids. In Biosensing and Nanomedicine VII, volume 9166, pages 192–198. SPIE, 2014.

[34] Sven-Erik Bursell, Jerry D Cavallerano, Anthony A Cavallerano, Allen C Clermont, Deborah Birkmire-Peters, Lloyd Paul Aiello, Lloyd M Aiello, Joslin Vision Network Research Team, et al. Stereo nonmydriatic digital-video color retinal imaging compared with early treatment diabetic retinopathy study seven standard field 35-mm stereo color photos for determining level of diabetic retinopathy. Ophthalmology, 108(3):572–585, 2001.

[35] American Academy of Ophthalmology. Diabetic retinopathy: Causes, symptoms, treatment, October 2022. Accessed: 2023-02-03.

[36] Francesco Bandello, Marco Attilio Zarbin, Rosangela Lattanzio, and Ilaria Zucchiatti. Clinical strategies in the management of diabetic retinopathy, volume 10. Springer, 2016.

[37] L. Deng. A tutorial survey of architectures, algorithms, and applications for deep learning. APSIPA Transactions on Signal and Information Processing, 3(1):1–10, January 2014.

[38] M. Dubow et al. Classification of human retinal microaneurysms using adaptive optics scanning light ophthalmoscope

fluorescein angiography. Investigative Ophthalmology & Visual Science, 55(3):1299, March 2014.

[39] P. Scanlon, C. P. Wilkinson, S. J. Aldington, and D. R. Matthews. A Practical Manual of Diabetic Retinopathy Management. Wiley-Blackwell, 2009.

[40] G. Scotland, P. McNamee, A.D. Fleming, K.A. Goatman, S. Philip, G.J. Prescott, P.F. Sharp, and J.A. Olson. Costs and consequences of automated algorithms versus manual grading for the detection of referable diabetic retinopathy. British Journal of Ophthalmology, 94(6):712–719, 2009.

[41] C.P. Wilkinson, F.L. Ferris, R.E. Klein, P.P. Lee, C.D. Agardh, M. Davis, D. Dills, A. Kampik, R. Pararajasegaram, and J.T. Verdaguer. Proposed international clinical diabetic retinopathy and diabetic macular edema disease severity scales. Ophthalmology, 110(9):1677–1682, 2003.

[42] X. Chen and X. Lin. Big data deep learning: Challenges and perspectives. IEEE Access, 2:514–525, 2014.

[43] L. Deng. Deep learning: Methods and applications. Foundations and Trends in Signal Processing, 7(3–4):197–387, 2014.

[44] Y. Guo, Y. Liu, A. Oerlemans, S. Lao, S. Wu, and M.S. Lew. Deep learning for visual understanding: A review. Neurocomputing, 187:27–48, 2016.

[45] M.D. Abràmoff, Y. Lou, A. Erginay, W. Clarida, R. Amelon, J.C. Folk, and M. Niemeijer. Improved automated detection of diabetic retinopathy on a publicly available dataset through integration of deep learning. Investigative Ophthalmology & Visual Science, 57(13):5200, 2016.

28[46] M. Abr‘amoff, M. Garvin, and M. Sonka. Retinal imaging and image analysis. IEEE Reviews in Biomedical Engineering, 3:169–208, 2010.

[47] M. Bakator and D. Radosav. Deep learning and medical diagnosis: A review of literature. Multimodal Technologies and Interaction, 2(3):47, 2018.

[48] E. Col’as, V. Hurtado, C.I. Sánchez, and R. Hornero. Deep learning approach for diabetic retinopathy screening. Acta Ophthalmologica, 94, 2016.

[49] V. Gulshan, L. Peng, M. Coram, M.C. Stumpe, D. Wu, A. Narayanaswamy, S. Venugopalan, K. Widner, T. Madams, J. Cuadros, R. Kim, R. Raman, P.C. Nelson, J.L. Mega, and D.R. Webster.

Development and validation of a deep learning algorithm for detection of diabetic retinopathy in retinal fundus photographs. JAMA, 316(22):2402, 2016.

[50] R.J. Tapp, J.E. Shaw, C.A. Harper, M.P. de Courten, B. Balkau, D.J. McCarty, H.R. Taylor, T.A. Welborn, and P.Z. Zimmet. The prevalence of and factors associated with diabetic retinopathy in the australian population. Diabetes Care, 26(6):1731–1737, 2003.

[51] D.E. Worrall, C.M. Wilson, and G.J. Brostow. Automated retinopathy of prematurity case detection with convolutional neural networks. In Lecture Notes in Computer Science, pages 68–76. Springer, 2016.

[52] J.W. Yau, S.L. Rogers, R. Kawasaki, E.L. Lamoureux, J.W. Kowalski, T. Bek, S.J. Chen, J.M. Dekker, A. Fletcher, J. Grauslund, S. Haffner, R.F. Hamman, M.K. Ikram, T. Kayama, B.E. Klein, R. Klein, S. Krish-naiah, K. Mayurasakorn, J.P. O'Hare, T.J. Orchard, M. Porta, M. Rema, M.S. Roy, T. Sharma, J. Shaw, H. Taylor, J.M. Tielsch, R. Varma, J.J. Wang, N. Wang, S. West, L. Xu, M. Yasuda, X. Zhang, P. Mitchell, and T.Y. Wong. Global prevalence and major risk factors of diabetic retinopa- thy. Diabetes Care, 35(3):556–564, 2012.

[53] L. Guariguata, D.R. Whiting, I. Hambleton, J. Beagley, U. Linnenkamp, and J.E. Shaw. Global estimates of diabetes prevalence for 2013 and projections for 2035. Diabetes Research and Clinical Practice, 103(2):137–149, 2014.

[54] M. Niemeijer, B. Ginneken, M.J. Cree, A. Mizutani, G. Quellec, C.I. Sanchez, B. Zhang, R. Hornero, M. Lamard, C. Muramatsu, X. Wu, G. Cazuguel, J. You, A. Mayo, Q. Li, Y. Hatanaka, B. Cochener, C. Roux, F. Karray, M. Garcia, H. Fujita, and M.D. Abramoff. Retinopathy online challenge: Automatic detection of microaneurysms in digital color fundus photographs. IEEE Transactions on Medical Imaging, 29(1):185–195, 2010.

[55] L. Giancardo, F. Meriaudeau, T.P. Karnowski, Y. Li, S. Garg, K.W. To-bin Jr, and E. Chaum. Exudate-based diabetic macular edema detection in fundus images using publiclyavailable datasets. Medical Image Analysis, 16(1):216–226, 2012.

[56] M. Haloi. Improved microaneurysm detection using deep neural networks. arXiv, 2015.

[57] D. Veiga, C. Pereira, M. Ferreira, and P. Melo-Pinto. Automatic microaneurysm detection using laws texture masks and support vector machines. Computer Methods in Biomechanics and

Biomedical Engineering. Imaging & Visualization, 6(4):405–416, 2017.

[58] N. Otsu. A threshold selection method from gray-level histograms. IEEE Transactions on Systems, Man, and Cybernetics, 9(1):62–66, 1979.[59] O. Ronneberger, P. Fischer, and T. Brox. U-net: Convolutional networks for biomedical image segmentation. In Lecture Notes in Computer Science, pages 234–241. Springer, 2015.

[60] Y. LeCun, Y. Bengio, and G. Hinton. 521(7553):436–444, 2015. Deep learning.Nature,

[61] C.I. Sánchez, R. Hornero, A. Mayo, and M. García. A novel automatic image processing algorithm for detection of hard exudates based on retinal image analysis. Medical Engineering & Physics, 30(3):350–357, 2008.

[62] B. Zhang, X. Wu, J. You, Q. Li, and F. Karray. Sparse representation classifier for microaneurysm detection and retinal blood vessel extraction. Information Sciences, 200:78–90, 2012.

[63] P. Sermanet, D. Eigen, X. Zhang, M. Mathieu, R. Fergus, and Y. Le-Cun. Overfeat: Integrated recognition, localization and detection using convolutional networks. arXiv, 2014.

[64] D.H. Hubel and T.N. Wiesel. Receptive fields and functional architecture of monkey striate cortex. The Journal of Physiology, 195(1):215–243, 1968.

[65] D. Scherer, A. Müller, and S. Behnke. Evaluation of pooling operations in convolutional architectures for object recognition. In Lecture Notes in Computer Science, pages 92–101. Springer, 2010.

[66] K. Chatfield, K. Simonyan, A. Vedaldi, and A. Zisserman. Return of the devil in the details: Delving deep into convolutional nets. In Proceedings of the British Machine, 2014.

[67] P. Chudzik, S. Majumdar, F. Caliva, B. Al-Diri, and A. Hunter. Microaneurysm detection using fully convolutional neural networks. Computer Methods and Programs in Biomedicine, 158:185–192, 2018.

[68] L. Deng. Farewell editorial: Keeping up the momentum of innovations. IEEE/ACM Transactions on Audio, Speech, and Language Processing, 2014.

[69] J.I. Orlando, E. Prokofyeva, M. del Fresno, and M.B. Blaschko. An ensemble deep learning based approach for red lesion detection in fundus images. Computer Methods and Programs in Biomedicine, 153:115–127, 2018.

[70] C. Tian, Y. Fang, Y. Zheng, Y. Luo, and J. Zheng. Multi-path convolutional neural network in fundus segmentation of blood vessels. Biocybernetics and Biomedical Engineering, 40(2):583–595, 2020.

[71] K. Manogna, A.U. Bhaskar, and M.P. Raju. Analysis of cnn model based classification of diabetic retinopathy diagnosis. In 2023 4th International Conference on Electronics and Sustainable Communication Systems (ICESC), pages 129–133. IEEE, 2023.

[72] B. Ghosh, A. Roy, M. Alam, and P. Roy. Classification of multiple eye diseases using pretrained convolution neural network. In 2022 IEEE Delhi Section Conference (DELCON), pages 1–6. IEEE, 2022.

[73] R.K. Singh, A. Sharma, and A.K. Singh. Ophthalmic diseases detection using cnn: A comparative analysis of resnet and vgg architectures. In 2023 International Conference on Smart Technologies in Computing, Electrical and Electronics (ICSTCEE), pages 1–6. IEEE, 2023.

[74] M.S.P.D. Warrier and P. Krishnan. Eye disease classification using cnn and vision transformers. In 2023 2nd International Conference on Electronics and Renewable Systems (ICEARS), pages 1673–1678. IEEE, 2023.

[75] M.A. Salam and M.A.R. Ahad. Deep convolutional neural networks for automated screening and diagnosis of ophthalmic diseases. In 2022 25th International Conference on Computer and Information Technology (ICCIT), pages 1–6. IEEE, 2022.

[76] V.A. Syahira et al. Cnn based computer aided ophthalmic diagnosis systems for classifying eye conditions. In 2024 8th International Conference on Information Technology, Information Systems and Electrical Engineering (ICITISEE), pages 557–562. IEEE, 2024.

[77] E. Arora, H.S. Jolly, and A. Rehalia. Prediction of autism spectrum disorder using ann and cnn. In 2023 3rd International Conference on Technological Advancements in Computational Sciences (ICTACS), pages 457–462. IEEE, 2023.

[78] M.S.H. Shojol, M.A.I. Siddique, and F. Haque. Enhanced convolutional neural networks for early detection and classification of ophthalmic diseases. In 2023 International Conference on Information and Communication Technology for Sustainable Development (ICICT4SD), pages 209–214.IEEE, 2023.

[79] D. Gokulavani and J. Mohana. Enhancing the performance of eye tracking and pupil detection by combining variational autoencoders with u-net architecture. In Proc. Int. Conf. on Electronics and Renewable Systems (ICEARS), pages 871–878. IEEE, 2025.

[80] S. Ghosh, S. Chatterjee, and S. Ghosh. Modeling of residual u-net for retinal vessel segmentation for eye-related disease detection. In Proc. 2024 4th Int. Conf. on Computer, Communication, Control Information Technology (C3IT), pages 102–108. IEEE, 2024.

[81] A. Dhayanithi and K. Bala. Transformer-enhanced u-net with transfer learning for accurate detection of eye coloboma. In Proc. 2024 Int. Conf.on Power, Energy, Control and Transmission Systems (ICPECTS), pages 115–121. IEEE, 2024.

[82] S. Rani and V. Sharma. Diabetic retinopathy segmentation in idrid using enhanced u-net. International Journal of Engineering and Advanced Technology, 9(3):563–567, 2020.

[83] R. Kumari, P. Nanda, and B. Panda. Noise-resilient pupil segmentation in vng using ransac-enhanced u-net for improved bppv diagnosis. Procedia Computer Science, 218:1202–1207, 2023.

[84] H. Singh and M. Tiwari. Enhanced detection of eye coloboma through global attention u-net (ga-unet) for accurate ophthalmic image segmentation. Biomedical Signal Processing and Control, 80:104265, 2023.

[85] M. Sharma, R. Yadav, and S. Verma. U-net architecture for detecting glaucoma with retinal fundus images. Journal of Biomedical Engineering and Informatics, 6(2):45–52, 2023.

[86] A. Kheterpal and K.S. Gill. Next-gen ophthalmic ai: Early eye disease detection with resnet-18. In 2024 International Conference on Intelligent Computing and Emerging Communication Technologies (ICEC). IEEE, 2024.

[87] G. Kaur, N. Sharma, R. Chauhan, S. Kukreti, and R. Gupta. Eye disease classification using resnet-18 deep learning architecture. In 2023 2nd International Conference on Futuristic Technologies (INCOFT). IEEE, 2023.

[88] H. Zain, H. Haris, and A. Saleem. Identification of the diabetic retinopathy using resnet-18. International Journal of Advanced Computer Science and Applications (IJACSA), 14(3), 2023.

[89] A. Rahman, M. Akhtaruzzaman, and M.H. Kabir. Automated diagnosis of retinal diseases from oct images using resnet-18. Journal

of Imaging Science and Technology, 67(1):010403–1–010403–10, 2023.

[90] A. Patel and K.R. Mehta. Resnet-18 for automated eye disease diagnosis: A neural network solution. International Journal of Computer Applications, 185(36):1–6, 2023.

[91] G. Singh, K. Guleria, and S. Sharma. A pre-trained vgg16 model for cataract eye disease prediction. In Proceedings of the 3rd International Conference on Smart Generation Computing, Communication and Networking (SMART GENCON). IEEE, 2023.

[92] I. Vajs, A.M. Savić, V. Ković, M.M. Janković, and T. Papić. Dyslexia detection in children using eye tracking data based on vgg16 network. In 2022 30th European Signal Processing Conference (EUSIPCO). IEEE, 2022.

[93] A.A. Razi, M.M. Khan, Z. Khan, and Z.U. Sami. Ophthalmic diseases detection using cnn: A comparative analysis of resnet and vgg architectures. In Proceedings of the 16th IEEE International Conference on Computational Intelligence and Communication Networks (CICN). IEEE, 2024.

[94] S. Singla and R. Gupta. Diabetic retinopathy diagnosis using vgg-19 deep learning model. In 2024 3rd International Conference for Advancement in Technology (ICAT). IEEE, 2024.

[95] T. Malik, V. Nandal, and P. Garg. Deep learning-based classification of diabetic retinopathy: Leveraging the power of vgg-19. In 2024 International Conference on Emerging Innovations and Advanced Computing (ICIAC). IEEE, 2024.

[96] S. Parthasarathy, V. Jayaraman, and V. Vijayan. Gso-vgg-16 model for predicting diabetic retinopathy by analysing up-sampled gaussian filtered fundus images. In 2023 International Conference on Smart Systems for applications in Healthcare and Biomedical Engineering (SSSHB). IEEE, 2023.

[97] G. Kaur and N. Sharma. Cataract disease detection using vgg 19 deep learning architecture. In 2024 Second International Conference on Intelligent Cyber Physical Systems (ICPS). IEEE, 2024.

[98] R. Chen, T. Wang, E. Song, and Z. Zhou. Automatic detection of ocular surface disease on smartphone images using improved yolov5. In Proc. 2024 5th International Conference on Artificial Intelligence and Computer Engineering (ICAICE), pages 21–24. IEEE, 2024.

[99] A. Ahmed, R. Chowdhury, and A. Rahman. Enhancing choroidal nevi segmentation in fundus images using yolo. In Proceedings of the 2023 International Conference on Machine Intelligence and Emerging Technologies (MIET). IEEE, 2023.

[100] O. Mamyrbayev, A. Niyazova, A. Zhiyenbayev, K. Abdimomynov, M. Sarsenbayeva, and A. Meirmanov. Localization of eye region in infrared thermal images using deep neural network. In 2024 IEEE 18th International Conference on Application of Information and Communication Technologies (AICT), pages 1–4. IEEE, 2024.

[101] A.P. Murchison, L. Hark, L.T. Pizzi, Y. Dai, E.L. Mayro, P.P. Storey, J.A. Haller, and L.A. Hark. Non-adherence to eye care in people with diabetes. BMJ Open Diabetes Research & Care, 5(1):e000333, 2017.

[102] K. Adem. Exudate detection for diabetic retinopathy with circular hough transformation and convolutional neural networks. Expert Systems With Applications, 114:289–295, 2018.

[103] Centers for Disease Control and Prevention. United states diabetes surveillance system. Accessed 5 Feb. 2022.

[104] C. Szegedy, S. Ioffe, V. Vanhoucke, and A.A. Alemi. Inception-v4, inception-resnet and the impact of residual connections on learning. In Proceedings of the ... AAAI Conference on Artificial Intelligence, volume 31, 2017.

[105] X. Wang, Y. Lu, M. Ren, Y. Shi, J. Xiao, and Y. Jiang. Diabetic retinopathy stage classification using convolutional neural networks. In International Conference on Information Reuse and Integration for Data Science.IEEE, 2018.

[106] N. Zavhorodnia. Eye Changes in General Diseases of the Body: Educational and Methodological Manual for Intern Doctors in the Specialty ”Ophthalmology”. N/A, 2020.

[107] Centers for Disease Control and Prevention. Diabetes risk factors, Apr 2022. Accessed 6 July 2022.

[108] Centers for Disease Control and Prevention. Healthcare workers, Feb 2020. Accessed 7 Apr. 2021.

[109] I. Mendez et al. Diabetes self-management education and association with diabetes self-care and clinical preventive care practices. The Science of Diabetes Self-Management and Care, 48(1):23–34, Jan 2022.

[110] Diabetic retinopathy — national eye institute. Accessed 25 July 2021.

[111] G. Huang et al. Densely connected convolutional networks. In The IEEE Conference on Computer Vision and Pattern Recognition, July 2017.

[112] D. Kumar and J. Sivaswamy. Automatic assessment of macular edema from color retinal images. IEEE Transactions on Medical Imaging,31(3):766–776, Mar 2012.

[113] M. Rehman et al. Classification of diabetic retinopathy images based on customised cnn architecture. In Amity International Conference on Artificial Intelligence, Feb 2019.

[114] L. Vadheim et al. Telehealth delivery of the diabetes prevention program to rural communities. Translational Behavioral Medicine, 7(2):286–291,Apr 2017.

[115] E. Van Cutsem et al. Metastatic colorectal cancer: Esmo clinical practice guidelines for diagnosis, treatment and follow-up. Annals of Oncology, 25:iii1–iii9, Sept 2014.

[116] B. Harangi et al. Automatic screening of fundus images using a combination of convolutional neural network and hand-crafted features. In 2019 41st Annual International Conference of the IEEE Engineering in Medicine and Biology Society, July 2019.

[117] A. Nair et al. Spotlight on faricimab in the treatment of wet age-related macular degeneration: Design, development and place in therapy. Drug Design Development and Therapy, Volume 16:3395–3400, Sept 2022.

[118] S. Vengalil et al. Customizing cnns for blood vessel segmentation from fundus images. In International Conference on Signal Processing and Communications, June 2016.

[119] J. Villena et al. Prevalence of diabetic retinopathy in peruvian patients with type 2 diabetes: Results of a hospital-based retinal telescreening program. PubMed, 30(5):408–414, Nov 2011.

[120] H. Wang et al. Hard exudate detection based on deep model learned information and multi-feature joint representation for diabetic retinopathy screening. Computer Methods and Programs in Biomedicine, 191:105398, July 2020.

[121] L. Liu et al. Prevalence and risk factors of retinopathy in patients with or without metabolic syndrome: A population-based study in shenyang. BMJ Open, 5(12):e008855, Dec 2015.

[122] B Di. De Vos et al. 2d image classification for 3d anatomy localization: Employing deep convolutional neural networks. In Proceedings of SPIE. SPIE, Mar 2016.

[123] S. Magliah et al. The prevalence and risk factors of diabetic retinopathy in selected primary care centers during the 3-year screening intervals. Journal of Family Medicine and Primary Care, 7(5):975, Jan 2018.

[124] C. Hua et al. Retinal vessel segmentation using round-wise features aggregation on bracket-shaped convolutional neural networks. In Proceedings of the Annual International Conference of the IEEE Engineering in Medicine and Biology Society, July 2019.

[125] R. Miotto et al. Deep learning for healthcare: Review, opportunities and challenges. Briefings in Bioinformatics, 19(6):1236–1246, May 2017.

[126] H. Shin et al. Deep convolutional neural networks for computer-aided detection: Cnn architectures, dataset characteristics and transfer learning. arXiv (Cornell University), Feb 2016.

[127] C. Szegedy, W. Liu, et al. Going deeper with convolutions. In Proceedings of the IEEE Conference on Computer Vision and Pattern Recognition, June 2015.

[128] J. Song et al. Chinese text categorization based on deep belief networks. In Proceedings of the 2016 IEEE/ACIS 15th International Conference on Computer and Information Science Computer and Information Science, June 2016.

[129] N. Zavhorodnia. Anatomy of the Eye. Research Methods in Ophthalmology: Study Guide for Students of Medical Faculties. N/A, 2017.

[130] B. Bowling. Kanskis Klinische Ophthalmologie: Ein Systematischer Ansatz. N/A, 2017.

[131] Inetra Laser Eye Clinic. Diabetic retinopathy, August 2022. Accessed:2022-11-02.

[132] Kostadinka Bizheva et al. Sub-micrometer axial resolution oct for invivo imaging of the cellular structure of healthy and keratoconic human corneas. Biomedical Optics Express, 8(2):800, January 2017.

[133] Y. Sauer et al. Assessment of consumer vr-headsets' objective and subjective field of view (fov) and its feasibility for visual field testing. Virtual Reality, 26(3):1089–1101, January 2022.

[134] A. Przekoracka-Krawczyk et al. Visual therapy in open space rehabilitation of acquired visual field defect. Neuropsychiatry, 08(05), 2018.

[135] Ophthalmological center ”New Vision”. Diagnostic equipment; new vision, October 2021. Accessed: 2023-03-03.

[136] P. Kronfeld. Tonography. Archives of Ophthalmology, 48(4):393–404, October 1952.

[137] EYE-PIX. Fluorescein angiography, April 2016. Accessed: 2023-01-15.

[138] Wikipedia contributors. Optical coherence tomography, January 2023. Accessed: 2023-04-02.

[139] L. Chuang et al. Mature vessel occlusion after anti-vegf treatment in a retinal arteriovenous malformation. BMC Ophthalmology, 13(1), October 2013.

36[140] Pablo Artal. Handbook of Visual Optics, Volume Two: Instrumentation and Vision Correction. CRC Press, 2017.

[141] L. Yannuzzi et al. Fluorescein angiography complication survey. Ophthalmology, 93(5):611–617, May 1986.

[142] Medical Centre - Medical Plaza. Biomicroscopy of the eye, April 2020. Accessed: 2022-11-08.

[143] Keratoconusa. Keratotopography of the cornea of the eye, December 2022. Accessed: 2023-02-02.

[144] High Tech Instruments. Electro-retinography, January 2020. Accessed: 2023-02-02.

[145] S. Klyce. Computer-assisted corneal topography. high-resolution graphic presentation and analysis of keratoscopy. PubMed, 25(12):1426–1435, December 1984.

[146] Advanced Ophthalmology Area. What is an ocular angiography? - advanced ophthalmology area, March 2021. Accessed: 2023-03-07.

[147] V. Zablotskyi and Yu Lapchenko. Optics and Ophthalmology in MedicalInstrumentation: Study Guide for Students of Higher Educational Institutions. 2008.

[148] R. Rosen et al. Optical coherence tomographic ophthalmoscopy. In Elsevier eBooks, pages 66–80. Elsevier, 2006.

[149] Unitech Vision. Ophthalmic instruments manufacturers — non contact tonometer suppliers — india, 2023. Accessed: 2023-04-02.

[150] X. Chen, Y. Xu, D. Wong, et al. Glaucoma detection based on deep convolutional neural network. In Proceedings of the 2015 37th Annual International Conference of the IEEE Engineering in Medicine and Biology Society, August 2015.

[151] Y. Pan et al. Brain tumor grading based on neural networks and convolutional neural networks. In Proceedings of the 2015 37th Annual International Conference of the IEEE Engineering in Medicine and Biology Society, August 2015.

[152] J. Cleland et al. Caring for people with heart failure and many other medical problems through and beyond the covid-19 pandemic: The advantages of universal access to home telemonitoring. European Journal of Heart Failure, 22(6):995–998, June 2020.

[153] Y. Bar et al. Deep learning with non-medical training used for chest pathology identification. In Proceedings of SPIE. SPIE, March 2015.

[154] J. Cheng et al. Computer-aided diagnosis with deep learning architecture: Applications to breast lesions in us images and pulmonary nodules in ctscans. Scientific Reports, 6(1), April 2016.

[155] A. Masood et al. Self-supervised learning model for skin cancer diagnosis. In Proceedings of the 2015 7th International IEEE/EMBS Conference on Neural Engineering, April 2015.

[156] B. Bejnordi, M. Veta, et al. Diagnostic assessment of deep learning algorithms for detection of lymph node metastases in women with breast cancer. JAMA, 318(22):2199, December 2017.

[157] G. González et al. Disease staging and prognosis in smokers using deep learning in chest computed tomography. American Journal of Respiratory and Critical Care Medicine, 197(2):193–203, January 2018.

[158] P. Looney et al. Automatic 3d ultrasound segmentation of the first trimester placenta using deep learning. In Proceedings of the 2017 IEEE 14th International Symposium on Biomedical Imaging. Biomedical Imaging, April 2017.

[159] LLC Eyenuk. Home - eyenuk, inc. artificial intelligence eye screening, October 2022. Accessed: 2022-12-04.

[160] N. Bayramoglu et al. Deep learning for magnification independent breast cancer histopathology image classification. In Proceedings of the 2016 23rd International Conference on Pattern Recognition, December 2016.

[161] R. Samala et al. Deep-learning convolution neural network for computeraided detection of microcalcifications in digital breast tomosynthesis. In Proceedings of SPIE. SPIE, March 2016.

[162] O. Karas. Optical electronic system for analysis of blood plasma films polarization maps. Journal of Science. Lyon, 17:28–32, 2020.

[163] J. Bezdek. Pattern Recognition With Fuzzy Objective Function Algorithms. Springer eBooks, 1981.

[164] A. Rotshtein. Intelligent Identification Technologies: Fuzzy Sets, Genetic Algorithms, Neural Networks. Universe, 1998.

[165] Z. Xiao et al. The trapezoidal fuzzy soft set and its application in mcdm. Applied Mathematical Modelling, 36(12):5844–5855, December 2012.

[166] L. Breiman. Classification and regression trees. Biometrics, 40(3):874,1984.

[167] R. Arunkumar and P. Karthigaikumar. Multi-retinal disease classification by reduced deep learning features. Neural Computing and Applications, 28(2):329–334, 2015.

[168] A. Ng. Ai is the new electricity, 2018.

[169] C. Valverde et al. Automated detection of diabetic retinopathy in retinal images. Indian Journal of Ophthalmology, 64(1):26, January 2016.

[170] T. Walter et al. A contribution of image processing to the diagnosis of diabetic retinopathy-detection of exudates in color fundus images of the human retina. IEEE Transactions on Medical Imaging, 21(10):1236–1243,October 2002.

[171] X. Zhou et al. Application of deep learning in object detection. In Proceedings of the 2017 IEEE/ACIS 16th International Conference on Computer and Information Science, May 2017.

[172] D. Hawkins and G. McLachlan. Discriminant analysis and statistical pattern recognition. Journal of the American Statistical Association, 88(422):695, June 1993.

[173] J. Brownlee. Machine Learning Mastery With Python: Understand Your Data, Create Accurate Models, and Work Projects End-to-End. Machine Learning Mastery, 2016.

[174] T. Hastie. An introduction to statistical learning: With applications in r by gareth james, huang, jianhua, robert tibshirani, daniela witten. Journal of Agricultural Biological and Environmental Statistics, 19(4):556–557, November 2014.

[175] B. Kamiński et al. A framework for sensitivity analysis of decision trees.Central European Journal of Operations Research, 26(1):135–159, May 2017.

[176] J. Quinlan. Induction of decision trees. Machine Learning, 1(1):81–106, March 1986.

[177] Lucidspark. Decision tree template, 2023. Accessed: 4 May 2023.

[178] S. Das et al. Medical diagnosis with the aid of using fuzzy logic and intuitionistic fuzzy logic. Applied Intelligence, 45(3):850–867, May 2016.

[179] A. Rotshtein. Medical Diagnosis Based on Fuzzy Logic. Contingent, Vinnytsia, Ukraine, 1996.

[180] N. Zabolotna et al. Support for decision-making in the system of polarization imaging diagnostics of histological sections based on the analysis of their anisotropy parameters. Optical-electronic Information and Energy Technologies, 2:29–40, 2019.

[181] M. Hansen et al. Results of automated retinal image analysis for detection of diabetic retinopathy from the nakuru study, kenya. PLOS ONE, 10(10):e0139148, October 2015.

[182] M. Javidi et al. Vessel segmentation and microaneurysm detection using discriminative dictionary learning and sparse representation. Computer Methods and Programs in Biomedicine, 139:93–108, February 2017.

[183] A. Tufail et al. An observational study to assess if automated diabetic retinopathy image assessment software can replace one or more steps of manual imaging grading and to determine their cost-effectiveness. Health Technology Assessment, 20(92):1–72, December 2016.

[184] Wikibooks contributors. Artificial neural networks/neural network basics,2023. Accessed: 2 Jan. 2023.

[185] E. Decencière et al. Teleophta: Machine learning and image processing methods for teleophthalmology. Irbm, 34(2):196–203, April 2013.

[186] R. Srivastava et al. Detecting retinal microaneurysms and hemorrhages with robustness to the presence of blood vessels. Computer Methods and Programs in Biomedicine, 138:83–91, January 2017.

[187] N. Tajbakhsh et al. Convolutional neural networks for medical image analysis: Full training or fine tuning? IEEE Transactions on Medical Imaging, 35(5):1299–1312, May 2016.

[188] C. Di et al. A four-stage hybrid model for hydrological time series forecasting. PLOS ONE, 9(8):e104663, August 2014.

[189] S. Pavlov and O. Karas. Analysis of the results of the jones matrix mapping system of biological tissues. In XLVIII Scientific and Technical Conference of the Faculty of Information Communications, Radio Electronics and Nanosystems, 2018.

[190] I. Goodfellow et al. Deep Learning. MIT Press, 2016.

[191] R. Pires et al. Assessing the need for referral in automatic diabetic retinopathy detection. IEEE Transactions on Biomedical Engineering, 60(12):3391–3398, December 2013.

[192] A. Razavian et al. Cnn features off-the-shelf: An astounding baseline for recognition. In Proceedings of the IEEE Conference on Computer Vision and Pattern Recognition Workshops, June 2014.

[193] L. Monnier. Diabétologie. 2010.

[194] Kaggle. Diabetic retinopathy detection. https://www.kaggle.com/c/diabetic-retinopathy-detection, 2015. Accessed: 16 Sept. 2022.

[195] J. Banfield and A. Raftery. Model-based gaussian and non-gaussian clustering. Biometrics, 49(3):803, September 1993.

[196] J. Hilbe. Logistic Regression Models. Chapman and Hall/CRC, 2009.

[197] W. Wojcik. Expert Systems: Study Guide. League-Pres, 2006.

[198] H. Lee et al. Deep learning framework for wireless systems: Applications to optical wireless communications. IEEE Communications Magazine, 57(3):35–41, March 2019.

[199] R. Ramo. Detection and diagnosis of skin diseases by using snake algorithm and neural networks. Technium, 4(10):104–114, December 2022.

[200] J. S. Wolffsohn and P. G. Hurcomb. Hypertension and the eye. Current Science Inc, 4:471–476, 2002.

[201] C. Y. Cheung, V. Biousse, P. A. Keane, E. L. Schiffrin, and T. Y. Wong. Hypertensive eye disease. Nature Reviews Disease Primers, 8(1):14, March 2022.

[202] S. S. Hayreh. Central retinal artery occlusion. In Springer, editor, Ocular Vascular Occlusive Disorders. Springer, 2015.

[203] M. Agarwal, C. Gupta, A. Jain, et al. Branch retinal artery occlusion as a presenting sign of acute retinal necrosis: a rare association. Journal of Ophthalmic Inflammation and Infection, 10, 2020.

[204] Sohan Singh Hayreh. Management of ischemic optic neuropathies. Indian Journal of Ophthalmology, 59(2):123–136, Mar–Apr 2011.

[205] G. Balakayeva and D. Darkenbayev. The solution to the problem of processing big data using the example of assessing the solvency of borrowers. Journal of Theoretical and Applied Information Technology, 98(13):2659–2670, 2020.

[206] G.T. Balakayeva, C. Phillips, D.K. Darkenbayev, and M. Turdaliyev. Using nosql for processing unstructured big data. News of the National Academy of Sciences of the Republic of Kazakhstan, Series of Geology and Technical Sciences, 6(438):12–21, 2019.

[207] A. Zhuparova, R. Sagiyeva, and D. Zhaisanova. Analysis of india ecosystem for startup with using data mining: Settlement of big data. In Proceedings of the 32nd International Business Information Management Association Conference, IBIMA 2018 - Vision 2020: Sustainable Economic Development and Application of Innovation Management from Regional expansion to Global Growth, pages 2176–2183, 2018.

[208] W. Forum. Google has developed a way to predict your risk of a heart attack just by scanning your eye.https://www.weforum.org/agenda/2018/02/google-has-developed-away-to-predict-your-risk-of-a-heart-attack-just-by-scanning-your-eye/,2018. Accessed: 2022-05-29.

[209] Y. Amirgaliyev, V. Berikov, L.S. Cherikbayeva, K. Latuta, and K. Bekturgan. Group approach to solving the tasks of recognition. Yugoslav Journal of Operations Research, 29(2):177–192, 2019.

[210] T.Z. Mazakov, S.A. Jomartova, T.S. Shormanov, G.Z. Ziyatbekova, B.S. Amirkhanov, and P. Kisala. The image processing algorithms for biometric identification by fingerprints. News of the National Academy of Sciences of the Republic of Kazakhstan, Series of Geology and Technical Sciences, 1(439):14–22, 2020.

[211] T. Sarsembayeva, N. Zholdas, M. Mansurova, M. Sarsembayev, and A. Urykkaliyev. Study of non-invasive methods of measuring glucose for patients with diabetes mellitus. In 2022 International Conference on Smart Information Systems and Technologies (SIST), pages 1–6, 2022.

[212] OSTRYE NARUŠENIJA KROVOOBRAŽENIJA V SOSUDAH SETČATKI. Ostrye narušenija krovoobraženiya v sosudah

setčatki. https://legeartis-don.ru/media/blog/info/ostryenarusenia-krovoobrasenia-v-sosudah-setcatki.html, 2022. Accessed: 2022-05-29.

[213] Symbat Kabdrakhova and Lyailya Zhapsarbayeva. On algorithm of finding solutions of semiperiodical boundary value problem for linear hyperbolic equation and its convergence. Applied Mathematical Sciences, 9(22):4585–4607, 2015.

[214] S.S. Kabdrakhova. On algorithm of finding solutions of semiperiodical boundary value problem for systems of nonlinear hyperbolic equations.2017.

[215] Linda McManus and Richard Mitchell. Pathobiology of Human Disease: A Dynamic Encyclopedia of Disease Mechanisms. Elsevier, 1st edition, 2014.

[216] Reena Mukamal. Early signs of heart disease appear in the eyes. https://www.aao.org/eye-health/news/eye-stroke-heartdisease-vision-exam-retina-oct, 2022. Accessed: 2022-05-29.

[217] J. Wang, J. Jiang, Y. Zhang, Y.W. Qian, J.F. Zhang, and Z.L. Wang. Retinal and choroidal vascular changes in coronary heart disease: An optical coherence tomography angiography study. Journal of Biomedical Optics Express, 10(4), 2019.

[218] Christopher P. Longa, Alison X. Chana, Christine Y. Bakhoum, Samantha Madalaa Toomey, K. Anupam, William R. Garga, Michael H. Freeman, Anthony N. Goldbaum, Mathieu F. De Maria, and Christopher B. Bakhoum. Prevalence of subclinical retinal ischemia in patients with cardiovascular disease – a hypothesis driven study. EClinical Medicine, 33:100775, 2021.

[219] A. Diaz-Pinto, N. Ravikumar, R. Attar, et al. Predicting myocardial infarction through retinal scans and minimal personal information. Nature Machine Intelligence, 4:55–61, 2022.

Appendixes

A. Block diagram of the multilayer perceptron learning algorithm

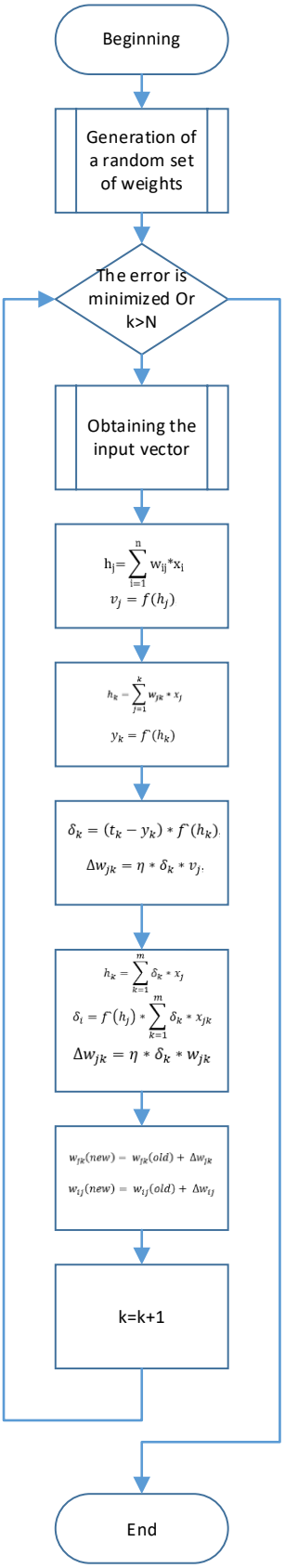

B. Deep neural network structure

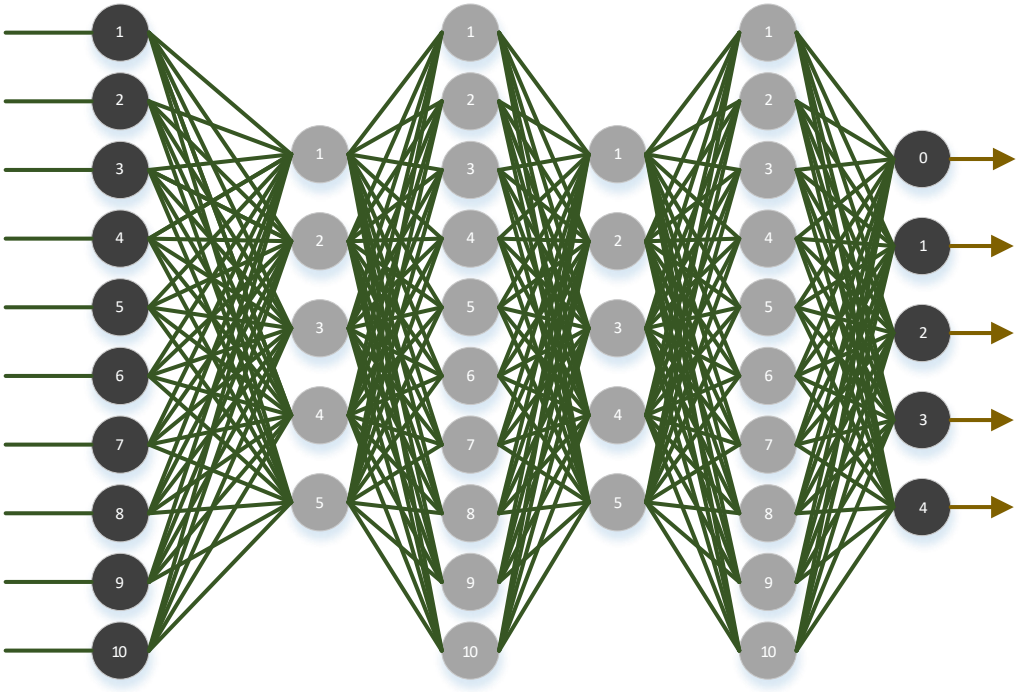

C. Statistical indicators for neural network training

Informative indicators

Belonging to a group

mean	SD	SC	MAD	...	RMSE		
2.6621	2.9678	0.9645	0.3390	...	1.9277	0	1
1.9996	5.4878	0.1129	1.4434	...	2.8996	1	0
2.3036	4.5537	0.0935	1.7041	...	2.9948	0	1
1.1455	4.9820	0.9668	1.0513	...	2.4657	0	1
1.7377	0.9514	0.1562	0.6448	...	0.3812	1	0
1.8286	5.4660	0.1378	0.7666	...	0.8150	1	0
1.5772	2.6932	0.7972	0.1790	...	2.9526	1	0
2.5380	3.8917	0.6173	0.5633	...	0.7642	0	1
0.1597	2.5805	0.4997	0.8059	...	2.0776	0	1
1.1633	0.5482	0.8039	0.2552	...	2.4087	1	0
2.4961	3.5985	0.8322	1.9461	...	2.2903	1	0
0.2421	5.9532	0.7680	1.4771	...	0.6060	0	1
2.2630	2.3886	0.7280	0.3782	...	0.3178	1	0
0.6062	0.6568	0.6661	1.2940	...	0.4412	1	0
1.1915	5.4037	0.8013	0.3159	...	0.1702	1	0
2.4639	4.4435	0.6629	0.1740	...	2.6552	0	1
0.1104	1.6741	0.7813	0.2686	...	1.2717	0	1
2.8780	2.8132	0.5317	1.5375	...	2.2853	0	1
1.3434	1.7810	0.3997	1.6764	...	2.7709	1	0
0.6298	3.5738	0.9144	1.7643	...	1.7796	1	0
1.9582	0.3736	0.2618	1.6938	...	2.4680	0	1
2.9428	2.2135	0.8144	0.8585	...	2.7553	1	0
1.6101	2.4840	0.7513	1.7105	...	1.5798	1	0
0.1500	1.1499	0.2829	0.0414	...	0.7007	0	1
1.3535	5.5586	0.6664	0.3218	...	1.1305	1	0
1.2059	4.2386	0.7386	0.9970	...	2.8946	0	1
0.1813	3.7545	0.7075	1.3532	...	2.3962	1	0
0.3290	3.7727	0.1136	1.9665	...	1.2565	0	1
1.4103	6.9344	0.4796	1.2800	...	1.2678	1	0
2.8647	5.9246	0.1760	0.9499	...	2.4520	0	1
0.6898	0.6203	0.2832	1.3749	...	0.0268	0	1
1.8079	5.0143	0.2279	1.0647	...	2.6320	1	0
2.8067	1.5907	0.5753	0.4121	...	2.9511	0	1
1.0875	6.2732	0.6385	0.3729	...	1.4276	0	1
1.3945	6.7255	0.8539	1.7651	...	1.9601	1	0
1.0921	2.1302	0.9636	0.1432	...	1.0841	0	1
0.6909	6.9719	0.7128	1.5703	...	0.6445	1	0
2.1847	3.0657	0.7918	1.6658	...	2.0140	1	0
0.0249	1.2191	0.4132	1.1564	...	0.2332	0	1
2.0311	2.9382	0.1067	0.8082	...	1.5693	1	0
0.6797	2.8971	0.1599	1.7518	...	0.0558	1	0
2.4509	1.4337	0.3456	0.2540	...	0.6498	1	0
0.8075	3.0386	0.6293	0.1422	...	2.1196	0	1
...	...	...	...	...	...	...	...
1.4200	3.4447	0.0055	1.5222	...	1.4158	0	1

Sample #1, 2, 3, ... n

D. An example of generated and processed retinal images for neural network training

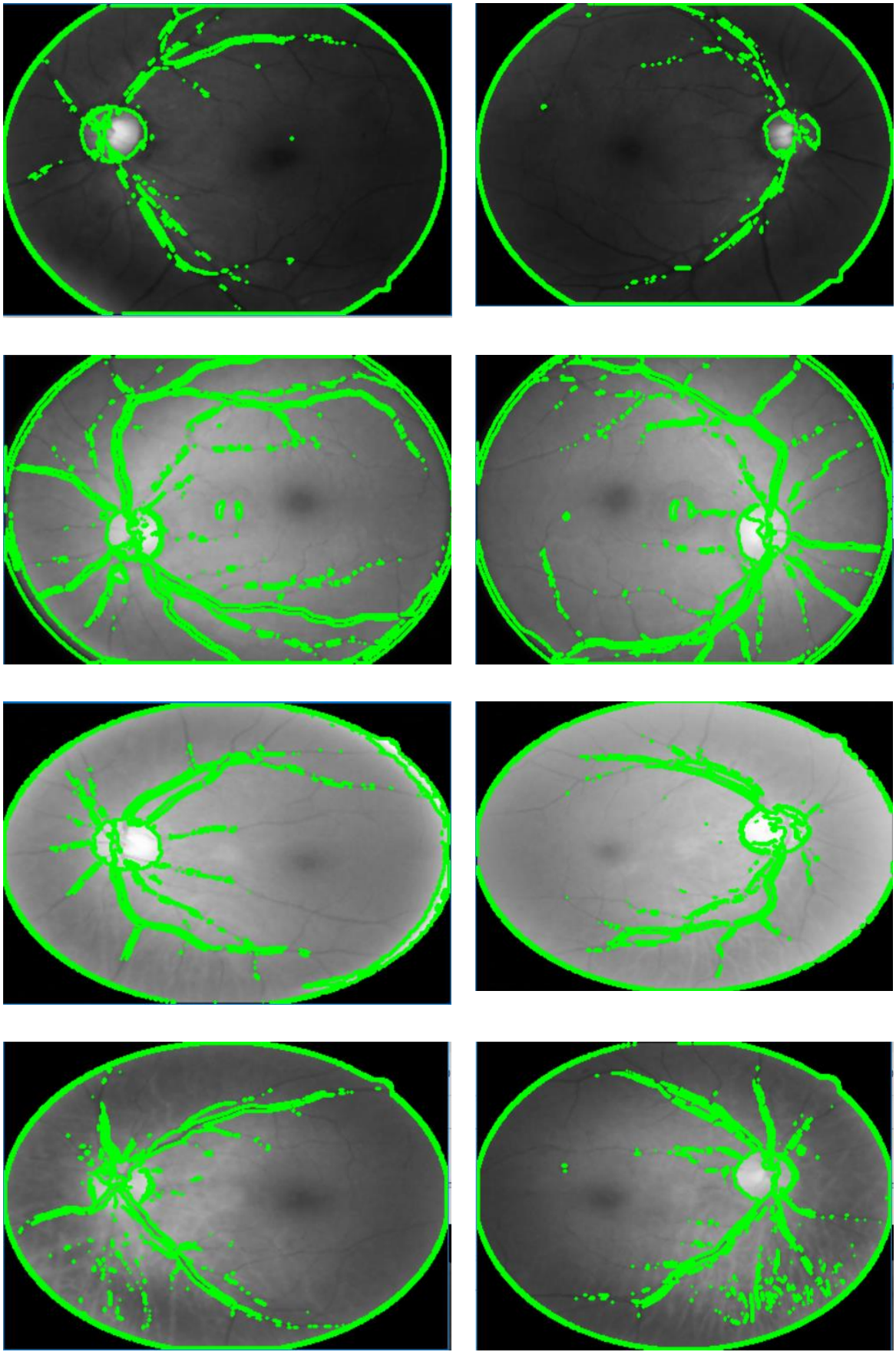

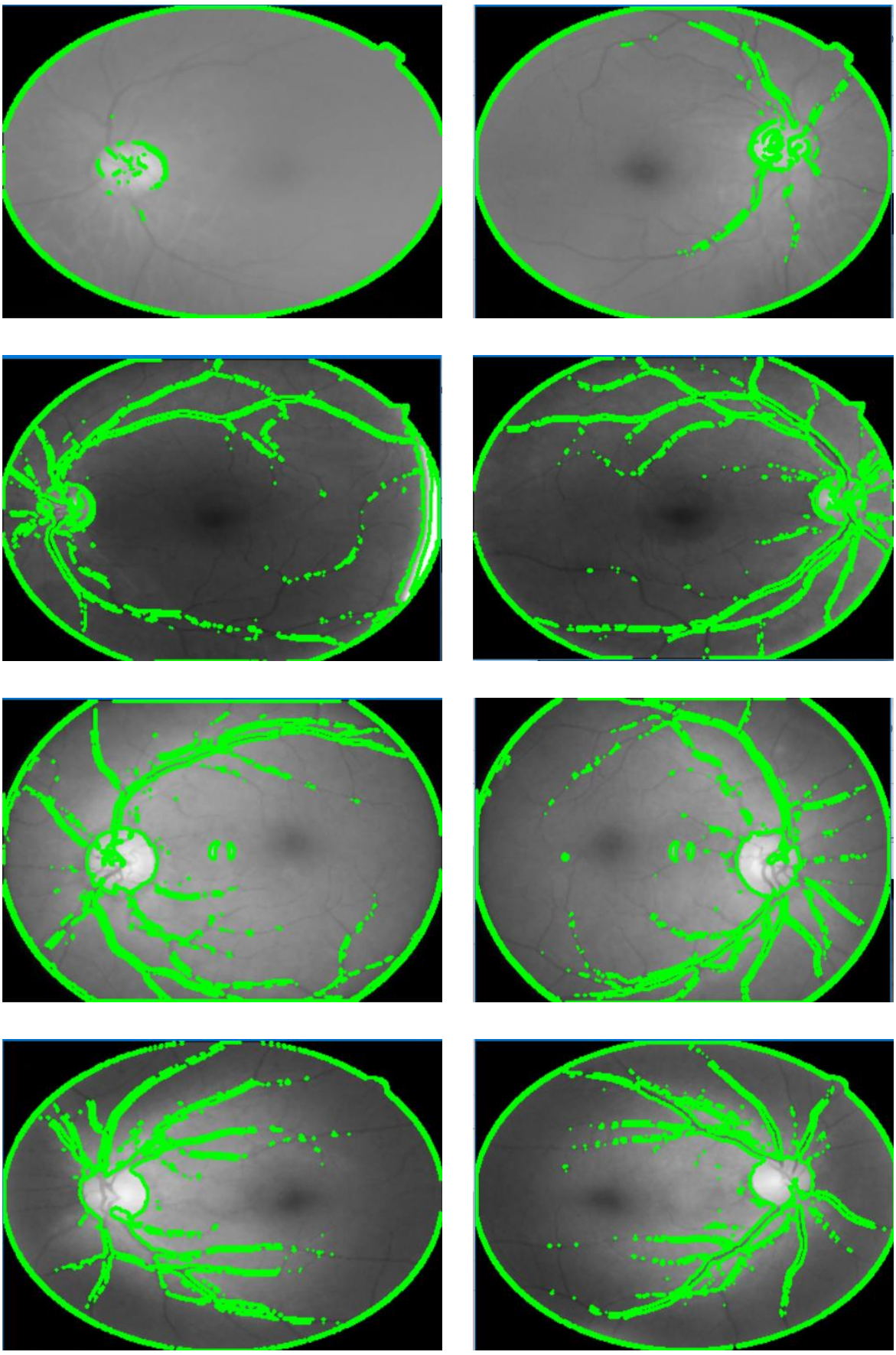

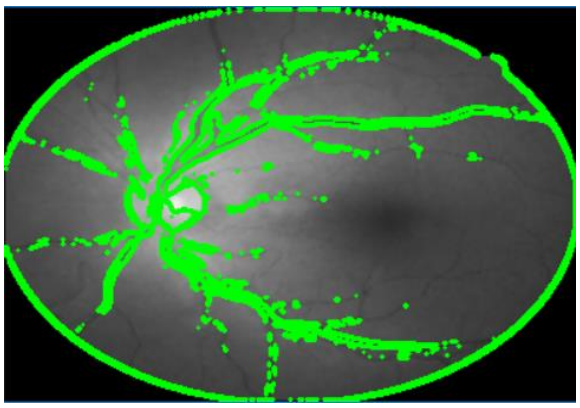

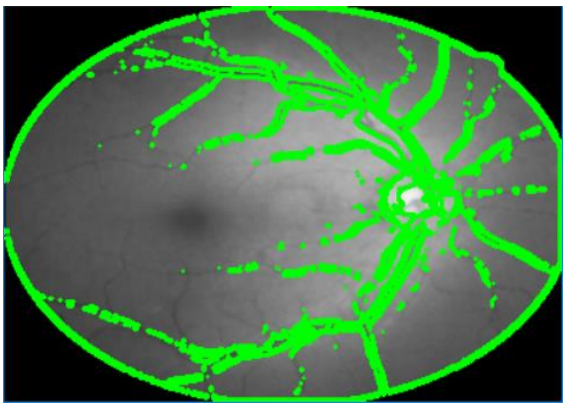

E. Exemplary listing of the graphic user interface code

```
import tkinter as tk
from tkinter import ttk, filedialog
from PIL import Image, ImageTk

class DiseaseDiagnosisApp(tk.Tk):
    def __init__(self):
        super().__init__()

        self.title("Diagnosis of fundus diseases")
        self.geometry("800x600")

        self.image1_block1 = None
        self.image2_block1 = None
        self.image3_block1 = None

        self.image1_block2 = None
        self.image2_block2 = None
        self.image3_block2 = None

        self.create_widgets()

    def create_widgets(self):
        # Block 1: Select image and output 3 images
        block1 = tk.Frame(self)
        block1.pack(side=tk.TOP, padx=10, pady=10)

        self.image_label1_block1 = tk.Label(block1)
        self.image_label1_block1.pack(side=tk.LEFT, padx=10,
pady=10)
```

```
        self.image_label2_block1 = tk.Label(block1)
        self.image_label2_block1.pack(side=tk.LEFT, padx=10,
pady=10)

        self.image_label3_block1 = tk.Label(block1)
        self.image_label3_block1.pack(side=tk.LEFT, padx=10,
pady=10)

        select_image_button_block1 = tk.Button(block1,
text="Choose an image", command=self.load_image_block1)
        select_image_button_block1.pack(side=tk.LEFT, padx=10,
pady=10)

        # Dividing line
        separator1 = ttk.Separator(self, orient=tk.HORIZONTAL)
        separator1.pack(fill=tk.X, padx=10, pady=10)

        # Block 2: Select image and output 3 images
        block2 = tk.Frame(self)
        block2.pack(side=tk.TOP, padx=10, pady=10)

        self.image_label1_block2 = tk.Label(block2)
        self.image_label1_block2.pack(side=tk.LEFT, padx=10,
pady=10)

        self.image_label2_block2 = tk.Label(block2)
        self.image_label2_block2.pack(side=tk.LEFT, padx=10,
pady=10)

        self.image_label3_block2 = tk.Label(block2)
        self.image_label3_block2.pack(side=tk.LEFT, padx=10,
pady=10)

        select_image_button_block2 = tk.Button(block2,
text="Обрати зображення", command=self.load_image_block2)
        select_image_button_block2.pack(side=tk.LEFT, padx=10,
pady=10)
```

```
            # Dividing line
            separator2 = ttk.Separator(self, orient=tk.HORIZONTAL)
            separator2.pack(fill=tk.X, padx=10, pady=10)

            def calculate_histogram(self, image):
            # Convert the image to black and white
            gray_image = image.convert("L")
            # Calculation of the histogram
            hist_array, _ = np.histogram(gray_image, bins=256,
range=(0, 256))
            return hist_array

            def plot_histogram(self, hist_array, label_widget):
            plt.clf()
            plt.bar(range(len(hist_array)), hist_array)
            plt.xlabel("Pixel values")
            plt.ylabel("Frequency")
            plt.tight_layout()

            # We convert the graph into a Tkinter image
            plt_img =
Image.fromarray(np.uint8(plt.gcf().canvas.renderer._renderer), 'RGB')
            plt_tk = ImageTk.PhotoImage(plt_img)

            label_widget.config(image=plt_tk)
            label_widget.image = plt_tk
            # Unit 3: Entering patient data and buttons
            block3 = tk.Frame(self)
            block3.pack(side=tk.TOP, padx=10, pady=10)

            tk.Label(block3, text="Name:").grid(row=0, column=0,
sticky=tk.W)
            self.full_name_entry = tk.Entry(block3)
            self.full_name_entry.grid(row=0, column=1, padx=10,
pady=5)

            tk.Label(block3, text="Gender:").grid(row=1, column=0,
sticky=tk.W)
            self.gender_entry = tk.Entry(block3)
```

```
            self.gender_entry.grid(row=1, column=1, padx=10, pady=5)

            tk.Label(block3, text="Date of birth:").grid(row=2,
column=0, sticky=tk.W)
            self.birth_date_entry = tk.Entry(block3)
            self.birth_date_entry.grid(row=2, column=1, padx=10,
pady=5)

            tk.Label(block3, text="Address:").grid(row=3, column=0,
sticky=tk.W)
            self.address_entry = tk.Entry(block3)
            self.address_entry.grid(row=3, column=1, padx=10, pady=5)

            select_patient_button = tk.Button(block3, text="Select a
patient", command=self.select_patient)
            select_patient_button.grid(row=4, column=0, padx=10,
pady=10)

            show_history_button = tk.Button(block3, text="Display
research history", command=self.show_history)
            show_history_button.grid(row=4, column=1, padx=10,
pady=10)

            decision_support_button = tk.Button(block3, text="Decision
support system", command=self.decision_support)
            decision_support_button.grid(row=5, column=0,
columnspan=2, padx=10, pady=10)

        def load_image_block1(self):
            file_path = filedialog.askopenfilename(filetypes=[("Image",
"*.png;*.jpg;*.jpeg;*.bmp")])
            if file_path:
                image = Image.open(file_path)
                image.thumbnail((200, 200))
                image_tk = ImageTk.PhotoImage(image)

                if not self.image1_block1:
                    self.image1_block1 = image_tk
```

```
self.image_label1_block1.config(image=self.image1_block1)
                elif not self.image2_block1:
                    self.image2_block1 = image_tk

self.image_label2_block1.config(image=self.image2_block1)
                elif not self.image3_block1:
                    self.image3_block1 = image_tk

self.image_label3_block1.config(image=self.image3_block1)
                else:
                    self.image1_block1 = image_tk

self.image_label1_block1.config(image=self.image1_block1)

        def load_image_block2(self):
            file_path = filedialog.askopenfilename(filetypes=[("Image",
"*.png;*.jpg;*.jpeg;*.bmp")])
            if file_path:
                image = Image.open(file_path)
                image.thumbnail((200, 200))
                image_tk = ImageTk.PhotoImage(image)

                if not self.image1_block2:
                    self.image1_block2 = image_tk

self.image_label1_block2.config(image=self.image1_block2)
                elif not self.image2_block2:
                    self.image2_block2 = image_tk

self.image_label2_block2.config(image=self.image2_block2)
                elif not self.image3_block2:
                    self.image3_block2 = image_tk

self.image_label3_block2.config(image=self.image3_block2)
                else:
                    self.image1_block2 = image_tk

self.image_label1_block2.config(image=self.image1_block2)
```

```
    def create_tables(self):
        # Create the patients table, if it does not already exist
        cursor = self.conn.cursor()
        cursor.execute('''
            CREATE TABLE IF NOT EXISTS patients (
                id INTEGER PRIMARY KEY AUTOINCREMENT,
                full_name TEXT,
                gender TEXT,
                birth_date TEXT,
                address TEXT
            )
        ''')

        # Create the research_history table, if it does not exist yet
        cursor.execute('''
            CREATE TABLE IF NOT EXISTS research_history (
                id INTEGER PRIMARY KEY AUTOINCREMENT,
                patient_id INTEGER,
                image BLOB,
                hist_array TEXT,
                FOREIGN KEY (patient_id) REFERENCES patients
(id)
            )
        ''')
        self.conn.commit()

    def create_widgets(self):
        ...

    def load_image_block1(self):
        ...

    def load_image_block2(self):
        ...

    def calculate_histogram(self, image):
        ...
```

```
        def plot_histogram(self, hist_array, label_widget):
            ...

        def select_patient(self):
            # Save the patient's data to the database
            full_name = self.full_name_entry.get()
            gender = self.gender_entry.get()
            birth_date = self.birth_date_entry.get()
            address = self.address_entry.get()

            cursor = self.conn.cursor()
            cursor.execute('INSERT INTO patients (full_name, gender,
birth_date, address) VALUES (?, ?, ?, ?)',
                           (full_name, gender, birth_date, address))
            self.conn.commit()

        def save_image_and_hist_to_db(self, image, hist_array,
patient_id):
            # Save the image and histogram to the database
            cursor = self.conn.cursor()
            cursor.execute('INSERT INTO research_history (patient_id,
image, hist_array) VALUES (?, ?, ?)',
                           (patient_id, sqlite3.Binary(image.tobytes()),
str(hist_array.tolist())))
            self.conn.commit()

        def show_history(self):
            ...

        def decision_support(self):
            ...

        def __del__(self):
            # We close the connection to the database when closing the
program
            self.conn.close()
        def select_patient(self):
            # logic for processing patient data
            full_name = self.full_name_entry.get()
```

```
        gender = self.gender_entry.get()
        birth_date = self.birth_date_entry.get()
        address = self.address_entry.get()
        ...

        # An example of outputting patient data
        print("ПІБ:", full_name)
        print("Стать:", gender)
        print("Дата народження:", birth_date)
        print("Адреса:", address)

    def show_history(self):
        ...
        print("History of the patient's studies")

    def decision_support(self):
        #decision support system
        ...
        print("decision support system")

if __name__ == "__main__":
    app = DiseaseDiagnosisApp()
    app.mainloop()
```

Mamyrbayev O.,
Pavlov S.,
Momynzhanova K.,
Zhanegizov A.

METHODS AND SYSTEMS FOR DIAGNOSING DIABETIC RETINOPATHY AND GLAUCOMA

Monography

Editor-in-chief: Kambarova K.M.
Managing Editor: Ukenova L.N.
Layout & Design: Slamova A.B.

LLP «Publishing house «Alash Book»
Almaty city, st. Zheltoksan, 96/98, of. 224
Tel: +7 777 880 08 05, +7 778 977 08 08
e-mail: info@alashbook.kz

Signed to print 16.05.2025
Format 60x84 1/16. Volume 10 p. sh.